Master's thesis

NTNU
Norwegian University of Science and Technology
Faculty of Engineering
Department of Structural Engineering

Metathip Sihaklang

Microproportioning modelling, with measurements of the maximum particle packing in filler-modified cement paste and the viscosity of paste fluid

TKT4925 Concrete Technology, Master's thesis

Master's thesis in Civil Engineering
Supervisor: Stefan Jacobsen
June 2019

NTNU
Kunnskap for en bedre verden

Metathip Sihaklang

Microproportioning modelling, with measurements of the maximum particle packing in filler-modified cement paste and the viscosity of paste fluid

TKT4925 Concrete Technology, Master's thesis

Master's thesis in Civil Engineering
Supervisor: Stefan Jacobsen
June 2019

Norwegian University of Science and Technology
Faculty of Engineering
Department of Structural Engineering

NTNU
Norwegian University of
Science and Technology

Department of Structural Engineering
Faculty of Engineering
NTNU- Norwegian University of Science and Technology

ACCESSIBILITY

OPEN

MASTER THESIS 2019

SUBJECT AREA:	DATE:	NO. OF PAGES:
Concrete Technology	**11.06.2019**	**130 (Incl. appendices)**

TITLE:

(English)
Microproportioning modelling, with measurements of the maximum particle packing in filler-modified cement paste and the viscosity of paste fluid
(Norsk)
Mikroproporsjoneringsmodellering med måling av maksimum partikkelpakning i fillermodifisert pasta og viskositet på pastavæske

BY:

Metathip Sihaklang

SUMMARY:
This work is a finalization of a master's degree in the course TKT4925 Concrete Technology, Master's Thesis. The thesis describes laboratory work performed during summer 2018, autumn 2018 and spring 2019. The thesis is based on to two concrete-proportioning rheology models: the particle-matrix model and the Bingham fluid model. It explores five micro-proportioning approaches: the empirical model from Ernst Mørtsell, the Krieger-Dougherty equation, the Chong's relative viscosity, the relative concentration of solids, and the suspension parameters called liquid thickness. This thesis's purpose is to investigate how well the five micro-proportioning approaches predict the rheology of filler modified pastes: mini slump flow, flow resistance, plastic viscosity, and yield stress. The materials and methods that were used and investigated in this project, such as the mixing procedure, centrifugation and viscosity measurements are described in detail. In addition, the results are presented in detail in tables and analyzed through a regression analysis. The results demonstrated that the five micro-proportioning approaches gave accurate and reasonable predictions for the rheology of filler modified pastes, with the exception of the pastes that contained silica fume or biotite and small-series.

RESPONSIBLE TEACHER/SUPERVISOR: **Stefan Jacobsen, Professor at the Department of Structural Engineering at NTNU**

OTHER PROFESSIONAL CONTACTS: **Ph.D. candidate Elisabeth Leite Skare and postdoctoral researcher Rolands Cepuritis**

CARRIED OUT AT: **The Department of Structural Engineering at NTNU**

Preface

This thesis is written as a finalization of the master's degree, Civil Engineering offered by NTNU, under the course TKT4925 Concrete Technology, Master's Thesis. The work took place in the spring of 2019.

This master's thesis is about the laboratory work I performed in the summer of 2018 with David Nicolas from The Mines d'Alès School, and from autumn 2018 to spring 2019 with Tone Nilsen, an engineer from concrete lab at the Department of Structural Engineering. The work is part of an ongoing project at NTNU called The MiKS project. The thesis is a continuation from the project report that I wrote in autumn 2018 for the course TKT4530 Concrete Technology, Specialization Project.

This thesis studies the five different micro-proportioning approaches: the Krieger-Dougherty model [1], the relative viscosity by Chong et al. [2], the relative concentration of solids (ϕ/ϕ_{max}) [2-5], the liquid thickness based on Powers, 1968 [6], and the empirical model of Mørtsell [7], with the main focus on quantifying the effect of crushed aggregate fines on the rheology of filler modified paste and concrete. This thesis is associated with the Elisabeth Leite Skare's doctoral thesis. Therefore, a lot of information in this thesis was taken from previous work of the doctoral thesis from the MiKS project. The details and results from this master's thesis will be used as part of the research for the doctoral thesis of Elisabeth Leite Skare.

Some of the details in the chapter on methods in this thesis has also been used as part of my term report about the chapter on the evaluation of methods, which is associated with the subject TBA4128 Project Management Advanced Course. The subject took place in the autumn of 2018.

I hope that this project report is useful, and potentially provides helpful information for others who wish to study the same area.

Trondheim, 11. June 2019

Metathip Sihaklan

Acknowledgements

I would like to thank the contributors who have helped to make this master thesis possible. Firstly and the most importantly, I wish to thank my supervisor, Professor Stefan Jacobsen for giving me the opportunity to work and be a part of the MiKS project. I am grateful for his extensive knowledge about concrete technology, his patience, his ability, and the time he took to help and advise me through the laboratory work, project report, and master thesis. I am endlessly grateful to him.

Secondly, I would also like to thank my other professional contacts, Ph.D. candidate Elisabeth Leite Skare and postdoctoral researcher Rolands Cepuritis at the Department of Structural Engineering, NTNU. I am grateful for their helpfulness, time, advice, proofreading, and the knowledge they had of the MiKS project. I thank them very much.

Thirdly, I would like to thank David Nicolas from The Mines d'Alès School, for his co-operation in the laboratory work and his friendship during the summer of 2018. I would also like to express my appreciation to Tone Nilsen from the concrete lab at the Department of Structural Engineering, NTNU, for her co-operation in the laboratory work, and her help and advice in the chemical lab.

Fourthly, I would like to acknowledge Alisa Machner at the Department of Structural Engineering, NTNU, for the instruction and her help in the chemical lab during the summer 2018, and Steinar Seehuus from the concrete lab at the Department of Structural Engineering, NTNU, for his practical help in the concrete lab.

I also wish to acknowledge my boyfriend Eric Andreas Bjørklund, who has proofread and spell-checked my report, and for his support and encouragement.

Last, but not least, I wish to thank my wonderful parents Pathama and Gunnar Birkebekk, for always believing in me and being there for me from the start.

Summary

There are three main methods that were studied: measuring maximum particle packing (ϕ_{max}) by centrifugation, extraction of Excess Fluid (EF) in fresh paste and measuring viscosity of EF. These methods were investigated on different test series of 200 ml – 400 ml replica cement paste mixes.

The results were used to investigate the four different micro-proportioning approaches that describe the rheology of matrices: the Krieger-Dougherty model [1], the relative viscosity by Chong et al. [2], the relative concentration of solids (ϕ /ϕ_{max}) [2-5] and the liquid thickness based on Powers, 1968 [6], in order to study the usefulness of these models and suspension parameters. In addition, another micro-proportioning model, called the empirical model by Mørtsell [7], was studied and compared to the first four micro-proportioning approaches. The five micro-proportioning approaches were analyzed by regression analysis against the rheological parameters that were measured in the previous laboratory work by Ph.D. student Elisabeth Leite Skare: mini slump flow, flow resistance ratio (λ_Q), plastic viscosity (η) and yield stress (τ_0). The best models and parameters were determined by high correlation coefficients (close to one) from the regression analysis and how accurate the five micro-proportioning approaches described the rheology in fresh concrete as the graphic plots.

Through the results, the laboratory methods were precise and provided accurate measured values. The results demonstrated that the five micro-proportioning approaches provided high correlations for the rheology, and the rheological parameters were described well by the models/parameters. While the plastic viscosities and apparent viscosity of EF were not found to be one-to-one relationships by the Krieger-Dougherty model [1] and the relative viscosity by Chong et al. [2]. The filler-modified pastes containing either silica fume or biotite and small-series, were observed to provide low correlation coefficients for all the five micro-proportioning approaches with unclear relationships to rheology.

Sammendrag

Det er tre hovedmetoder som ble undersøkt: måling av maksimum partikkelpakning (ϕ_{max}) ved sentrifugering, ekstraksjon av overflødig væske (EF) i fersk sementpasta og måling av viskositet av EF. Disse metodene ble utført i forskjellige testserier med volum av 200 ml. – 400 ml. replika sementpasta blandinger. I tillegg ble måling av nøyaktigheten av EF volumet og faststoffinnholdet i EF undersøkt.

Resultatene fra de utviklede metodene ble brukt til å undersøke fire forskjellige mikroproporsjoneringsmetoder som beskriver matriksens reologi: den Krieger-Dougherty modellen [1], den relative viskositet av Chong et al. [2], den relative konsentrasjonen av faststoffer (ϕ/ϕ_{max}) [2-5] og væsketykkelsene (LT1 og LT2) basert på Powers, 1968 [6], for å studere deres brukbarhet. I tillegg ble en annen mikroproporsjoneringsmodell kalt «den empiriske modellen» studert og sammenlignet med de fire første mikroproporsjoneringsmetoder. De fem mikroproporsjoneringsmodellene ble analysert ved hjelp av regresjonsanalyse mot de reologi parameterne i fersk sementpasta som ble målt i laboratoriearbeidet til doktorgradsstudent Elisabeth Leite Skare. Disse parameterne er synkutbredelse, flytmotstand (λ_Q), plastiske viskositet (η) og flyteskjærspenning (τ_0). De beste modellene og parameterne ble definert basert på hvor høy korrelasjonskoeffisienter er (nærmest 1) fra regresjonsanalysen, og hvor nøyaktige de fem mikroproporsjoneringsmetoder beskrev de fire reologiske parameterne som grafiske plotter.

Resultatene viste at laboratoriemetodene var presise og ga nøyaktige målte verdier. I tillegg viste resultatene at de fem mikroproporsjoneringsmetoder ga høye korrelasjonskoeffisienter som kan estimere verdiene til reologiene, og de fire reologiske parameterne ble godt beskrevet av mikroproporsjoneringsmodellene/parameterne. Mens den Krieger-Dougherty modellen [1], den relative viskositet av Chong et al. [2] ga ikke en-til-en relasjon til de plastiske viskositetene som ble målt av Skare fra laboratoriet. De fillermodifiserte pastaene som inneholder enten silikastøv eller glimmer og små serier, ble observert for å gi lave korrelasjonskoeffisienter samt uklare relasjoner som grafiske plotter.

Table of contents

List of figures

List of Tables

List of Symbols

ϕ	solid fraction.
ϕ_{max}	maximum packing.
η_c	pore fluid viscosity.
η	apparent viscosity
μ	plastic viscosity.
$[\eta]$	intrinsic viscosity.
ν	kinematic viscosity.
η_{pore_fluid}	dynamic viscosity.
λ_Q	flow resistance.
τ	shear stress.
τ_0	yield stress.
$\dot{\gamma}$	shear rate.
fi/c, f/c	filler-to-cement ratio (in mass-ratio).
fi/b	filler-to-binder ratio (in mass-ratio).
fa/c	fly ash-to-cement ratio (in mass-ratio).
fa/b	fly ash-to-binder ratio (in mass-ratio).
s/c	silica-to-cement ratio (in mass-ratio).
w/c	water-to-cement ratio (in mass-ratio).
w/p	water-to-powder ratio (in mass-ratio).
w/b	water-to-binder ratio (in mass-ratio).
ϕ/ϕ_{max}	relative concentration of solids.
k_s	correlation factor of silica.
k_c	correlation factor of cement.
k_f	correlation factor of filler.
k_{sp}	correlation factor of superplasticizer.
k_{fa}	correlation factor of fly ash.

Acronyms, Initialisms and Term

ASTM	American Society for Testing Materials.
COIN	Concrete Innovation Centre.
EF	Excess Fluid.
FA	Fly Ash.
MiKS	Mikroproporsjonering i Knust Sand project (Micro proportioning with crushed sand).
NTNU	Norwegian University of Science and Technology.
powder	(cement + filler).
PSD	Particle Size Distribution.
RPM	Rounds Per Minute.
SINTEF	Stiftelsen for Industriell og Teknisk Forskning (The Foundation for Scientific and Industrial Research)
SSA	Specific Surface Area.
VSI	Vertical Shaft Impact.
SP	Superplasticizer.
LT	Liquid thickness.
VFF	Void filling fluid.
SSE	Sum of squared errors.
SSTO	The total sum of squares.
NS-EN	Norwegian Standard.
Ph.D.	Doctor of Philosophy.

1. Introduction

1.1. Background

Sources of natural sand for use as aggregates in concrete production are becoming less available as natural sand is dredged from the sea and rivers, but dredging has been prohibited due to concerns over the erosion of the river bed and coastal areas, and other environmental concerns [8]. This has increased the concrete producers' interest in the use of crushed sand, which are made of crushed rocks and/or gravel [8]. The demand for high quality crushed aggregate materials has grown over the past decade [9]. A previous study in [10] on the production of crushed sand demonstrated that the manufactured sand particles have higher angularity, and the particles are much finer than natural sand due to the blasting and crushing process [10]. Natural sand contains little fine material with particles size less than 0.063 mm, while manufactured sand has a substantially finer material content [11].
Wigum and Danielsen [12] have found that concrete proportioned with fine material from manufactured sand had increased water requirements, which decreased the concrete's workability. In addition, Cepuritis [8] has found that using crushed fine aggregates in a cement paste will require a higher distribution of cement in the concrete. This poses a problem because of the high cost of cement and high CO_2 emissions from cement production. For this reason, the study on the effect of crushed fine aggregates on the rheology of cement paste is important for the concrete industry.

The study of filler-modified pastes on the rheological parameters of cement has been studied as part of the "micropropotioning with crushed sand" project (MiKS project) in Elisabeth Leite Skare's ongoing doctoral thesis. It was also studied in the Cepuritis's doctoral thesis [8], where it was found that the effect of crushed fine aggregates on the cement paste can be predicted by adjusting the particle size distribution (PSD) and the volume of the aggregates, when the crushed sand is produced by Vertical Shaft Impact (VSI) [10]. Skare's doctoral thesis investigated the rheology of filler-modified pastes when considering measurable parameters such as solid fraction (ϕ), maximum packing of particles (ϕ_{max}), and viscosity of pore fluid. One of the main purposes of Skare's doctoral thesis is to find a micro-proportioning model that can predict matrix rheology from matrix composition, by investigating 5 different approaches: the Krieger-Dougherty model [1],

the relative viscosity by Chong et al. [2], the relative concentration of solids (ϕ /ϕ_{max}) [2-5], the liquid thickness based on Powers, 1968 [6], and the empirical model of Mørtsell [7]. This thesis will carry out a laboratory study of the viscosity of suspensions, the maximum packing on the rheology of cement paste with crushed fine aggregates, and a limited analysis of the latter 5 approaches.

1.2. The MiKS project

The MiKS (microproportioning with crushed sand) project is a project that should take five years to complete; it started in 2016 and is projected to end in 2021. It was started by the Research Council of Norway together with the partners of the project: NTNU, SINTEF, NIST (National Institute of Standards and Technology), DTU (Danmarks Tekniske Universitet), Skanska Norge As, Feiring Bruk and Norcem-Heidelberg AS. In addition, one postdoctoral researcher, Rolands Cepuritis (NTNU/Norcem), and one Ph.D. candidate, Elisabeth Leite Skare (NTNU/DTU) are working on and conducting research in the project. More information about the MiKS Project can be found in [13], and more questions about the MiKS project can be directly sent to Stefan Jacobsen, a professor at the Department of Structural Engineering at NTNU.

1.3. Scope

The scope of this report is to describe the details of a limited laboratory program that took place from July to August in 2018 with an intern, David Nicolas from the Mines d'Alès School. From September 2018 to Mars 2019, the program continued with Tone Nilsen, an engineer from the construction department at NTNU.

This thesis therefore makes and investigates matrix replicas of a major matrix rheology test for Skare's Ph.D. laboratory work in the MiKS-project (see section 1.2 and [13]), in order to measure maximum packing (ϕ_{max}) and pore fluid viscosity on small mixes of filler-modified cement pastes as inputs to the five micro-proportioning approaches: the Krieger-Dougherty model [1], the relative viscosity by Chong et al. [2], the relative concentration of solids (ϕ /ϕ_{max}) [2-5], the liquid thickness based on Powers, 1968 [6], and the empirical model of Mørtsell [7].

The mixes were replicated from a large series of pastes made for rheology measurements as an empirical database (see Appendix B), in order to develop a micro-proportioning model with the main focus on quantifying the effect of crushed fine aggregates on the rheology of filler-modified paste and concrete. The results were analyzed through a regression analysis and described in detail in order to evaluate the methods from laboratory work and their accuracy, along with usefulness of the five microproportioning approaches.

2. Models, Parameters and Methods

2.1. Models and parameters

The micro-proportioning principle investigates the effect of crushed fine aggregates on concrete rheology. Its main purpose is to achieve the desired properties of fresh concrete made of crushed sand. However, it is difficult to construct micro-proportioning models based on input parameters from the concrete constituents, due to the time-dependent property of the rheological parameters in the fresh concrete, called thixotropy, see Jacobsen et al. [6]. The phenomenon of thixotropy is observed in concrete as the viscous behavior of the fresh concrete decreases with the rate of shear, and is re-established after the concrete has started to set [6]. The following sections are short descriptions of the particle-matrix model which is used for the proportioning of concrete, the Bingham fluid model which describes a fluid in fresh concrete, and the five micro-proportioning approaches that describe the rheology of the matrix: the Krieger-Dougherty model [1], the relative viscosity by Chong et al. [2], the relative concentration of solids (ϕ /ϕ_{max}) [2-5], the liquid thickness based on Powers, 1968 [6], and the empirical model of Mørtsell [7]. The feasibility of these micro-proportioning approaches is investigated in the MiKS project.

2.1.1. The particle-matrix model

The following section is a short description of the basic principles of the particle-matrix model. More details and information can be found in [6-8].

The particle-matrix model is a model used to simplify how the workability of concrete can be controlled, based on the different ingoing materials in the concrete mix. The model was developed by Ernst Mørtsell in 1996 [7]. The particle sizes in this section are defined by the mass fraction of particles that passes a sieve with square openings of minimum edge length 0.125 mm. The model's idea is to consider the concrete composition as a two-phase system: the matrix phase and the particle phase.

The matrix phase consists of all the materials with particles of size less than 0.125 mm. This means that all the fluids, that is free water and additives, and all the solid materials such as binder, filler, and fine aggregates are included in the matrix phase. The matrix phase is a flowable component with heavy and viscous fluid and can therefore be characterized as a liquid phase.

The particle phase contains the parts that are remaining from the matrix phase, whichmeans all the particles of size less than 0.125 mm. The particle phase is characterized as a frictional material, since it only consists of dry materials, which also include the absorbed water in the aggregates. This increases its density.

These two phases are based on a different parameter characterization each, with the matrix phase characterized by the flow resistance ratio (λ_Q), and the particle phase characterized by the air voids modulus [8]. The flow resistance ratio (λ_Q) describes a matrix or concrete according to how liquid and viscous it is, and it can be measured by FlowCyl-measurements [9]. The air voids modulus describes the content of the air voids and the particle packing of the particle phase.

The flow resistance of the matrix phase (λ_Q), the air voids modulus of the particle phase, and the volume fraction of the matrix are defined by the slump-flow test, which characterizes the workability of the concrete.

2.1.2. The Bingham fluid model

A Bingham fluid model characterizes a fluid as a relationship between shear stress (τ) and yield shear value (τ_0), plastic viscosity (η or μ), and rate of shear ($\dot{\gamma}$) [6]:

$$\tau = \tau_0 + \eta\dot{\gamma} \quad (1)$$

Bingham's model describes the mobility of a fresh concrete, which indicates that the material will start to flow when the material is loaded up to a specific yield shear value (τ_0) [6].

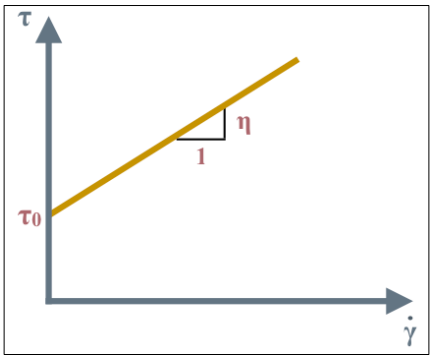

Figure 1: Bingham's model

Figure 1 illustrates the relationship between the shear stress (τ) and the rate of shear ($\dot{\gamma}$) as a linear relation, where the plastic viscosity (η) is defined as the rate between the increase in the shear stress and the rate of shear [6]. The figure is adapted from Jacobsen et al.'s compendium [6]. More information about the Bingham fluid model can be found in Jacobsen et al. [6].

2.1.3. The empirical model

The empirical model or the linear factor model is developed in Ernst Mørtsell's doctoral thesis [7], Chapter 5. The model investigates the rheological properties of the different types and amount of filler in the different filler-modified pastes, as well as the silica fume, cement and water, described by the flow resistance (λ_Q).

The model simplifies a relationship between flow resistance (λ_Q) and the water-to-cement ratio (w/c), silica-to-cement ratio (s/c), and filler-to-cement ratio (f/c) through the following function [7]:

$$\lambda_Q = f(x) \; ; \; \text{where } x = k_c * \frac{1}{\frac{w}{c}} + k_s * \frac{s}{c} + k_f * \frac{f}{c} \qquad (2)$$

where the constants k_c, k_s and k_f are the correlation factors of cement, silica, and filler respectively.

In order to find a solution for the constants (k_c, k_s and k_f) in the empirical model (eq.*(2)*), Mørtsell [7] plotted the values of λ_Q from the FlowCyl measurement on the y-axis, against the calculated values of x, by using the "trendline function" in Excel to find the maximum R-squared values (R^2). The R^2 value is described further in Section 2.1.7. The regression line of these values resulted in a function, which demonstrated the relationship between the x and y values [7]. In Mørtsell's study [7], the regression line was defined as a function of $y = kx^n$, where Mørtsell [7] used the value of k to calculate the values for k_c, k_s, and k_f by using equation *(2)*. More details about Mørtsell's study can be found in [7].

Cepuritis [9] found that the rheology of the cement paste is affected by the specific surface area (SSA) of the crushed fine aggregates (more details about the measurement of specific surface area can be found in Section 2.2.1.), and the amount of superplasticizer (SP) in the paste. However, Mørtsell's first empirical model [7] did not include the SSA of crushed fine aggregates, and the SP dosage was constant in Mørtsell's study. Consequently, the SP dosage was not included in his model. In addition, fly-ash (FA) was not used in his study. Therefore, a more suitable model has been developed by Rolands Cepuritis, which includes the SSA for FA and the filler (SSA_{fa} and SSA_f), the fly-ash-to-cement ratio (fa/c), correlation factor of fly-ash (k_{fa}), correlation factor of SP (k_{sp}) ,and superplasticizer-to-cement ratio (sp/c).

The new empirical model is defined by the following equation:

$$\lambda_Q = f(x) \;;\; \text{where } x = k_c * \frac{1}{\frac{w}{c}} + k_{fa} * \frac{fa}{c} + k_s * \frac{s}{c} + k_f * SSA_f * \frac{f}{c} + k_{SP} * \frac{SP}{c} \qquad (3)$$

In this study, the constants k_c, k_s, k_{fa}, k_{sp} and k_f were determined by "Solver", which is a Microsoft Excel add-in program. The Solver is described in further detail in Sections 2.1.7 and 2.2.7.

The empirical model can also be modified by adding and deleting parameters. Section 3.8 describes the analysis of the calculated λ_Q from equation *(3)*, see Appendix A, plotted against the measured values of λ_Q from Ph.D candidate Elisabeth Leite Skare and former Ph.D candidate Evgeny Ramenskriv. Skare and Ramenskriv measured the values of λ_Q in the laboratory, with the batch size of 2.05 liters for each mix (see Appendix B).

The constants k_c, k_s, $k_{fa,}$ $k_{sp,}$ and k_f were determined by "Solver", as described in Sections 2.1.7 and 2.2.7 (see also Section 3.8 for the values of the constants).

2.1.4. Maximum packing and the relative concentration of solids

The studies by Chong et al. [2] and Krieger and Dougherty [1] have found that the viscosity of a suspension can be described as a function of ϕ/ϕ_m (see section 2.1.5), where ϕ is the volume fraction of solid particles and ϕ_m is the maximum packing of the suspension (by volume). In this study, ϕ/ϕ_m is called the relative concentration of solids.

In order to determine the relative concentration of solids (ϕ/ϕ_m), the maximum packing of suspension needs to be measured. The maximum packing of a cement paste is illustrated in the figures next page.

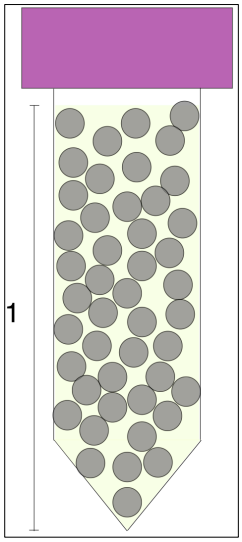

Figure 2: The paste before centrifugation

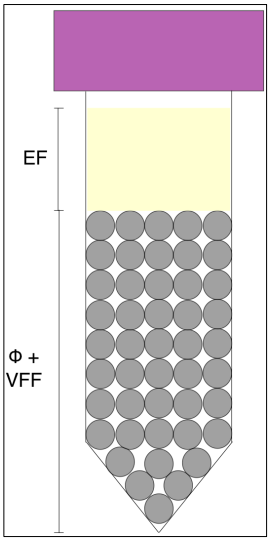

Figure 3: The paste after the centrifugation

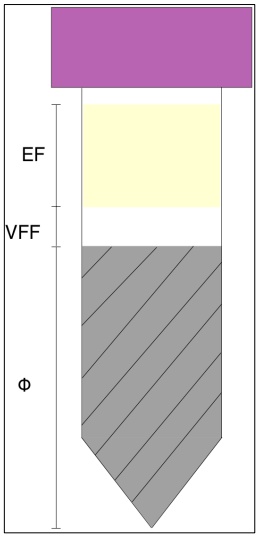

Figure 4: Illustration of a layout of solid fraction

Figure 2 illustrates that when the cement paste is newly mixed, the particles are dispersed randomly in the paste. Figure 3 describes the paste after the centrifugation, where the liquid phase called excess fluid (EF) is extracted from the paste. Figure 4 is the illustration of the layout of a solid fraction, if the air voids (void filling fluid or VFF) are extracted out of the paste.

The total volume of the paste is assumed to be equal to 1, which is determined by the following equation:

$$1 = \text{VFF} + \text{EF} + \phi + \text{air} \tag{4}$$

where VFF is void filling fluid, EF is excess fluid and determined as a volume fraction, ϕ is the volume fraction of solid particles and air is assumed to be negligible. The EF fraction is defined as follows:

$$EF\ fraction = \frac{W_{tot,EF}\ (g)}{W_{tot,paste}(g)} * \rho_{paste} \tag{5}$$

where $W_{tot,EF}$ is the total weight of the EF, $W_{tot,paste}$ is the total weight of the paste, and ρ_{paste} is the theoretical density of the paste calculated by an excel calculation sheet "Matrice Weight Calculation.xlsx", attached in Appendix C. EF fraction, $W_{tot,EF}$, $W_{tot,paste}$ and ρ_{paste} are attached in Appendix F.

The maximum packing (ϕ_m) is the solid fraction of the paste when a volume of 1 is considered, and where all the particles are in the same phase after the centrifugation. The maximum packing is defined as follows:

$$\phi_m = \frac{\phi}{1 - EF} \tag{6}$$

Therefore, the relative concentration of solids is given by the following equation:

$$\frac{\phi}{\phi_m} = 1 - EF \tag{7}$$

The centrifugation method is described in detail in Section 2.2.4. The results for the maximum packing are summarized and described in Section 3.2.
In Section 3.4, the relative concentration of solids is analyzed and plotted against four different rheological parameters: measured flow resistance (λ_Q), yield stress (τ_0), average mini slump flow, and measured plastic viscosity (η). The four rheological parameters were previously determined and listed in Appendix B by Skare.

2.1.5. The Krieger-Dougherty equation and the Chong's relative viscosity

In this study, two of the models that are related to the viscosity of suspension to the relative concentration of solids (ϕ/ϕ_m) were evaluated. The two models are the Krieger-Dougherty equation [1] and the Chong's relative viscosity [2].

The Krieger-Dougherty equation

The Krieger-Dougherty equation [1] was applied in the studies in [3-5] to study the flow behavior of filler-modified cement paste (matrix) based on characteristics of the constituents of the mix, that is the particle size distribution, and the particles' shape and volume fractions. The equation describes the flow behavior of a dispersion as the relationship between viscosity, particle volume fraction, and maximum packing [4].

The Krieger-Dougherty equation is defined as follows:

$$\frac{\eta}{\eta_c} = \left(1 - \frac{\phi}{\phi_m}\right)^{-[\eta]\phi_m} \tag{8}$$

where η is the apparent viscosity of the suspension, η_c is the viscosity of the continuous phase (or liquid phase), ϕ is the volume fraction of solid particles, ϕ_m is the maximum packing (by volume), and $[\eta]$ is the intrinsic viscosity which is a measure of the effect of the solute particles on the viscosity [4]. For cement-based materials, the intrinsic viscosity has a value closer to 6, according to [3, 4].

In this study $[\eta]$ was determined by using the Microsoft Excel add-in program, "Solver" (more about the Solver in Sections 2.1.7 and 2.2.7.). The values of $[\eta]$ are summarized in Section 3.5, Table 9, and Table 10.

The original equation of $[\eta]$ is defined as follows:

$$[\eta] = \lim_{\phi \to 0} \frac{\frac{\eta}{\eta_c} - 1}{\phi} \tag{9}$$

In this study, the maximum packing (ϕ_m) was determined by using a centrifuge machine, which is further described in Sections 2.1.4 and 2.2.4. The results of ϕ_m are explained in Section 3.2. The viscosity of the continuous phase (η_c) was determined by performing a viscosity measurement of a liquid phase called excess fluid (EF), which is further described in Sections 2.1.4 and 2.2.4 to 2.2.5. The volume fraction of solid particles (ϕ) for each investigated mix had been previously determined by Ph.D. candidate Elisabeth Leite Skare, further details of which can be found in Appendix B. The apparent viscosity (η) calculated by the Krieger-Dougherty equation is analyzed and plotted against the measured plastic viscosity (η) in Section 3.5. The plastic viscosity (η) had been measured by rheometers in the previous laboratory work by Skare, with the batch size of 2.05L. (see Appendix B).

The Chong's relative viscosity

Chong et al. [2] studied the relationship between the relative viscosity of suspensions on particle volume fraction (solid fraction) and maximum packing. Similar to the Krieger-Dougherty equation [1], the Chong's equation also describes the flow behavior of a concentrated suspension as the relationship between viscosity and the relative concentration of solids (ϕ/ϕ_m), where the equation is described in following manner:

$$\frac{\eta}{\eta_0} = \left(1 + 0.75 * \left(\frac{\frac{\phi}{\phi_\infty}}{1 - \frac{\phi}{\phi_\infty}}\right)\right)^2 \quad (10)$$

where η is the apparent viscosity of the suspension, η_0 is the viscosity of the continuous phase (or liquid phase), ϕ is the volume fraction of solid particles, and ϕ_∞ (also use ϕ_m) is the maximum packing (by volume). The value of ϕ and ϕ_m for each mix were obtained from the same methods that were applied for the Krieger-Dougherty equation.

The apparent viscosity (η) calculated by the Chong's equation (Appendix I) is analyzed and plotted against the measured plastic viscosity (η) in Section 3.6. The measured plastic viscosity (η) were also measured by rheometers in the previous laboratory work by Skare with the batch size of 2.05L. (see Appendix B).

2.1.6. The liquid thicknesses

Powers (1968) described the continuous matrix phase as the volume of the matrix that fills up voids and also contains the excess matrix, which is a thin wall of matrix that prevents particles from having direct contact with each other [6]. A new parameter adapted from Powers (1968) has been developed for the MiKS project, which is based on the same idea. The model is called "the liquid thickness" and is illustrated in Figure 5 (adapted from Powers [6]), which describes the paste consisting of the water film coating each of the solid particles.

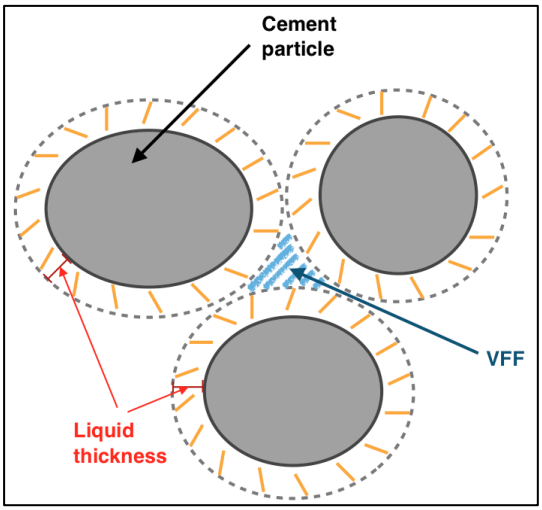

Figure 5: Illustration of the liquid thickness

The first version of liquid thickness (LT1) is defined by the following equation:

$$\mathrm{LT1} = \frac{1 - \phi}{\mathrm{SSA}} \tag{11}$$

where LT is the liquid thickness, ϕ is the volume fraction of solid particles, EF is excess fluid, and SSA is the specific surface area (more details provided in Section 2.2.1). The values for LT1 were previously calculated by Skare and are provided in Appendix B.

As displayed in Figure 5, there is the minimum void-space (1-ϕ) between the particles, which can be filled with VFF. Professor Stefan Jacobsen developed a new version of liquid thickness by excluding VFF from the first version of liquid thickness (LT1). The second version of liquid thickness (LT2) provided a smaller amount of fluid covering the surface of the particles, in comparison with the LT1 (eq.*(11)*). This second version of liquid thickness (LT2) is defined by the following equation:

$$\mathrm{LT2} = \frac{1 - \phi - \mathrm{VFF}}{\mathrm{SSA}} = \frac{\mathrm{EF}}{\mathrm{SSA}} \tag{12}$$

The results for LT2 are summarized in Appendix J. In Section 3.7, both models are analyzed and plotted against four different rheological parameters: measured flow resistance (λ_Q), yield stress (τ_0), average mini slump flow, and measured plastic viscosity (η). The four rheological parameters were previously determined and listed in Appendix B by Skare.

2.1.7. Excel's Solver

As mentioned in Sections 2.1.3 and 2.1.5, the constants in the empirical model (eq.*(3)*): k_c, k_s, k_{fa}, k_{sp} and k_f, and [η] in the Krieger-Dougherty model (eq.*(8)*) are determined by regression analysis (Appendix A and Appendix H), using a Microsoft Excel add-in program called Solver. Solver can adjust parameters in an equation by minimizing the sum of the squared errors (SSE). Solver was used to maximize the R-squared (R^2) value, which is a number between 0 and 1. The R^2 value shows how close the calculated values are to the fitted regression line, where $R^2 = 1$ is the best value representing a perfect fit (or one-to-one relation),

R^2-value is determined by the following equations [14]:

$$R^2 = 1 - \frac{SSE}{SSTO} \tag{13}$$

$$\text{SSE} = \sum_{i=1}^{n}(y_i - \hat{y})^2 \tag{14}$$

$$\text{SSTO} = \sum_{i=1}^{n}(y_i - \bar{y})^2 \tag{15}$$

where SSE is the error of sum of squares, SSTO is the total sum of squares, y_i is the measured value at point i, $\hat{y}$ is the estimated/predicted regression line, and $\bar{y}$ is the average value of y_i determined by $\bar{y} = \frac{1}{n} * \sum_{i=1}^{n} y_i$. The Solver is described further in Section 2.2.7.

2.2. Methods

2.2.1. Particles size distribution and specific surface area

The main parameters that are used to describe fine aggregates are the PSD and the SSA. A PSD is defined as a grading curve that contains a size distribution of fine to coarse grains. For fine particles, it determines the mass fraction of particles that passes a sieve with square openings of minimum edge length 0.063 mm [11]. In order to determine the SSAs, one can use the SediGraph [15] to obtain the particle size distribution. There are other methods for measuring the SSA for particles. However, the SediGraph [15] was chosen for this project because it is considered to be the best method for measuring the size distribution for crushed fine aggregates (≤ 63 μm), according to Cepuritis et al. [11]. The SSA of all dry materials was obtained by using the SediGraph [15]. The Sedigraph [15] measured the average diameter of the particle (1/mm), and multiplied the average diameter with the summarized volume ratio for each of the materials in mass percentages to obtain the SSA. The exception was the SSA for silica fumes, where the SSA was calculated from Jacobsen et al.'s compendium [6]. Each constituent's SSA value had been previously measured and calculated by Skare (see Appendix B).

The SSA can also be determined by the Blaine method or the air permeability method, which is commonly applied to cement according to NS-EN 196-6:2010 [16]. The Blaine method measures SSA by comparing the sieved fine aggregates (on standard sieves) of cement with a reference sample of cement that has a known specific surface, as explained in [16]. More information and details about the Blaine method can be found in [16].

2.2.2. Mix composition and proportioning of matrix

Mix composition and proportioning

In the MiKS project, seven different test series have been conducted and they consist of 129 mixes (see Appendix B), with variations in the solid fraction, admixture dosage, w/c, w/b, fi/b, w/p, and powder types. The recipes contain two different cement types, industry cement and standard FA, and two types of pozzolans (fly-ash and condensed silica fume). They also contain different types of fillers from Velde (fine, intermediate, and coarse particle size distribution, which are crushed fillers from one type of rock), one type of filler from Feiring (intermediate), and biotite. All of the fillers were sieved through a standard sieve with diameter of size 0.125 mm, which means that the fillers' sizes were less than 0.125 mm.

The seven series were denoted series A, B, C, D, E, F and G, and the details about the mixes are presented in Table 1 and Table 2. The parameters of the mixes are the results from Skare's previous work (see Appendix B).

As mentioned above, there are 129 mixes in this project, but only 125 mixes were measurable mixes. There are four mixes from the E-series that were difficult to mix because the mixes had the lowest w/b of all the mixes in this project, see Appendix B.

Table 1: Overview of materials used in the different series

Series	A	B	C	D	E	F	G
Filler type							
Velde Fine	●		●	●			
Velde Intermediate	●	●			●		●
Velde Coarse	●						
Feiring Intermediate						●	
Biotite							●
Cement type							
Norcem standard FA	●	●			●	●	●
Norcem Industri			●	●	●	●	
Pozzolans							
Norcem Fly Ash			●	●	●	●	
Elkem Undensified Microsilica					●	●	
Admixtures							
Dynamon SR-N (Superplasticizer)	●	●	●	●	●	●	●

Table 2: Overview of variables and constants in all of the series

Series	SP-dosage	fi/b	w/b	Solid volume fraction	FA/b
A	◆	●	●	●	▬
B	●	●	●	●	▬
C	◆	●	◆ *	●	●
D	◆	●	●	◆	●
E	●	●	●	●	●
F	◆	●	●	●	●
G	◆	●	◆	◆	▬

◆ = constant ● = varies ▬ = not added

* with two exceptions (see Appendix)

The mixes were proportioned by using an excel calculation sheet from Cepuritis, called "Matrice Weight Calculation.xlsx" (see Appendix C). The volume of each mix was determined in advance and keyed into the calculation sheet. The parameters of each mix, that is w/b, s/c, fa/c, f/c, and SP/c, were also filled in as inputs in the calculation sheet.
It was important to ensure that there was sufficient volume of the EF (at least 10 ml. from each mix was required for the experiment). The volume of EF depends on several factors including the solid fraction, particle type and size distribution, and w/c in the mix. For this study, it was found that the mix's w/c determined its volume, which also determined the EF's volume, such that a paste volume of 400 ml was needed when w/c < 0.5 and a volume of 200 ml was needed when w/c > 0.5.

2.2.3. Mixing procedure

A previous study from [17] proved that in order to improve flow properties and achieve a well-dispersed paste (fewer lumps), high shear mixing with a moderate speed is required. A proper procedure and set-up for mixing was inspired by Serina Ng et al. [18]. However, the method from [18] was designed for a matrix mix with the size of 2.05L, while the mixes in this study had a volume between 0.2 and 0.4L. Therefore, the mixing procedure from COIN [19] was also applied, in order to design a proper replica mixing procedure for the project.

As the pre-mix of dry powders is optional [18], all the fillers and cements were premixed by hand for 10 seconds. The wet-mixing was followed by the method from COIN [19], using a hand-blender by Phillips ProMix Hand blender (model no. HR1673) with its steel blade, and a cylindrical plastic container (see Figure 6). Table 3 illustrates all the individual steps of the replica mixing procedure.

Figure 6 The equipment: a metal blow for dry particles, falcon tubes, a beaker glass, a cup, a glass bottle and the hand blender with its steel blade and plastic container.

Table 3: Mixing procedure

Mixing step	Time	Procedure
		Pre-mix (dry)
1	10 seconds	All fillers and cements were premixed by hand in a metal blow for 10 seconds.
2		Water and admixture were pre-mixed together in the cylindrical plastic container.
		Wet mixing
3	10 seconds	Dry powders from step 1 added to the cylindrical plastic container.
4	30 seconds	Mixing at the high speed of the hand-blander.
5	5 min	Rest
6	1 min	Mixing at the high speed again to avoid false set.
7		The prepared paste was transferred into 4 (or 8, depending on the volume of the mix) 45 ml falcon tubes.
Total time	6 min 50 seconds	*only for mixing

Directly after the mixing was performed, the prepared paste was transferred into 4 (or 8, depending on the volume of the mix) falcon tubes with a volume of 45ml, and the tubes were then closed with lids. After all the tubes were filled with the paste, they were weighed on a two-digits balance. The total weight of each tube had to be approximately the same, since they would be placed in a centrifugation machine, where the balance could be affected by an unbalanced weight.

2.2.4. Centrifugation for maximum packing and excess fluid

Figure 7 Centrifugation machine [20]

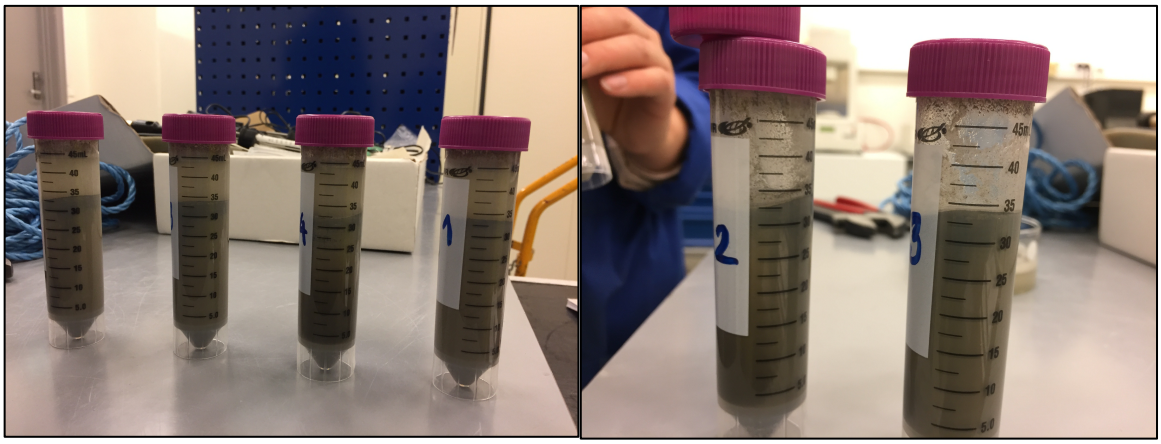

Figure 8 Example of falcon tubes filled with cement paste after the centrifugation, left: with excess fluid and right: after extracted excess fluid

To measure the maximum packing for each mix (as described in Section 2.1.4), the pastes were centrifuged (by centrifugation machine Hettich Universal 320, Figure 7) immediately after the paste was filled in all the tubes. The centrifugation procedure was previously used by Ng S. [21] in her study on the kinematic viscosity of filler pore solution. The prepared mixes were centrifuged at 4000 RPM (rounds per minute) for 5 minutes [21], where it resulted in the well packed particles, and the cement paste was stiff (see Figure 8), with the exception of some of the mixes in the B-series (see section 3.2.2, Figure 11).

The fluid that was extracted from the paste after centrifugation was called the EF (see section 2.1.4, Figure 3). The EF volume of each mix was essential for calculating the EF fraction, the maximum packing (ϕ_{max}) (eq. *(6)*), and the relative concentration of solids (ϕ /ϕ_{max}) (equation *(7)*). The calculation of the EF fraction has been previously described in Section 2.1.4. The results of the amount of EF from the centrifugation can be found in Appendix F.

To investigate if the centrifugation procedure was suitable, a test was performed by Skare and David Nicolas. They tested the procedure with a mix, where the centrifugation was run for 10 minutes. There was no difference in the amount of EF when the mix was centrifuged for 5 or 10 minutes. Therefore, in this experiment, centrifugation was performed for 5 minutes for every mix, so that the laboratory could be operated the most efficiently.

2.2.5. Viscosity measurement of excess fluid

The viscosity measurement of the EF was performed immediately after the centrifugation. In this project, two different viscometers were used, with two different methods for preparing the EF for viscosity measurement. These methods are described in detail in the sections below.

2.2.5.1. The trial and error test

The trial and error test was performed in order to investigate the appropriate methods of handling a sample after centrifugation, that would contribute to the most accurate measurement of volume and solid content in EF and the most time-effective way to perform the experiment.

The procedure for the trial and error test is described in detail in Table 4.

Table 4 The procedure for trial and error test

1. Proportioning of a mix by using the calculation sheet in Appendix C. 2. Mixing with the same procedure described in Section 2.2.3 3. Centrifugation of the mix with the same procedure described in Section 2.2.4	
Method 1	Method 2
4. Use a syringe to extract the EF from falcon tube	4. Pour the EF into a beaker glass directly from the falcon tube
5. Weigh the EF (syringe was already weighed)	5. Weigh the EF (the beaker glass was already weighed)
6. Weigh a small piece of paper towel	6. Weigh a small piece of paper towel
7. Use the paper towel to absorb the rest of the EF in the falcon tube and put the paper towel in an oven for evaporation	7. Use the paper towel to absorb the rest of the EF in the falcon tube and put the paper towel in an oven for evaporation
8. Weigh the paper towel after the evaporation was finished	8. Weigh the paper towel after the evaporation was finished
9. Weigh a filter (size 0.45 μm)	
10. Filter all the EF in falcon tube through the filter, then put the filter in an oven for evaporation	
11. Weigh the dry filter and the syringe	

The aims of the test were to investigate the following matters:

- After the centrifugation, what was the difference (in %) of the amount of the solid particles that was left in the falcon tubes, when the EF was poured directly from the falcon tubes compared to when the EF was extracted by a syringe.
- To examine the quantity of the solid particles that disappeared in the filtration of the centrifuged pore fluid.

The results from the trial and error test are in summarized in Section 3.1.1, with the detailed calculations in Appendix D.

2.2.5.2. Preparation of samples for viscosity measurements for the A-, C-, D- and G-series

Following the method from Section 2.2.5.1, after the centrifugation was completed, the EF was poured directly out of the falcon tubes into a beaker glass. By following the procedure from Ng S.[21], the viscometer with size no. 50 was used for the A-, C-, D- and G-series, and the EF was filtered with a syringe-filter with a 0.45 μm pore size. After the filtration, in order to avoid/reduce the evaporation, the top of the beaker glass was covered by a plastic wrap.

2.2.5.3. Preparation of samples for viscosity measurements for the B-, E- and F-series

For the B-, E-, and F- series, the EF for some of the mixes could not be filtered through a filter with a size of 0.45 μm. This was due to the high amount of small solid particles in the EF.

The problem was discussed with Professor Stefan Jacobsen, Cepuritis, and Skare, and it was concluded that the problem was caused by the high SP dosage in the mixes in the B -series, and some of the mixes in the E- and F-series, considering that the SP makes the paste more flowable by dispersing the flocculated particles.

It was tested if the EF from some of the B- and E-series were able to flow through the viscometer (ASTM D2515 size no. 50) without the filtration. It appeared that they could flow through, but they exceeded the maximum range of the viscometer's flow time. Therefore, these series needed a different procedure.

There is a special type of viscometer for opaque liquid. However, in order to be able to analyze and compare the results for the B-, E- and F-series with the results for the A-, C-, D- and G-series, the procedures should be as similar as possible. Therefore, a new ASTM D2515 viscometer with size no. 75 (one size bigger) was selected for the B-, E- and F-series. The purpose of the new viscometer was to perform the viscometer measurements of the B-, E- and F-series without the filtration of the EF. The new viscometer is tested, and the result demonstrated that the unfiltered EF could flow through the viscometer, and the flow time was in the range of the viscometer's flow time.

2.2.5.4. The viscometer procedure

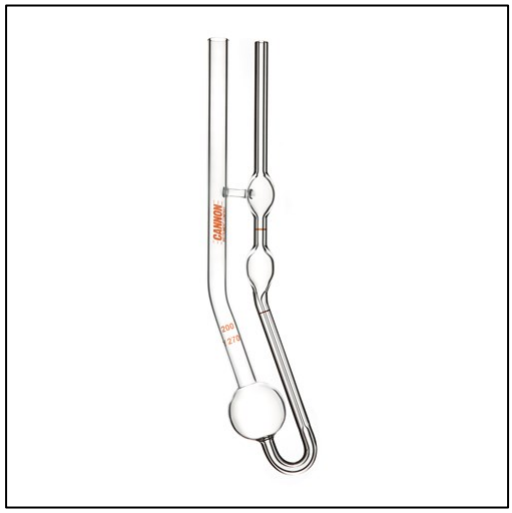

Figure 9 Cannon-Fenske Routine Viscometer for Transparent liquids [22]

The kinematic glass viscometer for transparent liquids ASTM D2515, Cannon-Fenske Routine Viscometer (see Figure 9), with size no. 50 and 75, were used to measure the kinematic viscosity of the mixes according to ASTM D2515-66 [23]. The viscosity measurement was performed immediately after the filtration was finished. In this study, the viscosity measurements were performed three times consecutively for each mix. The set-up and procedure for the viscometer was obtained from Ng S. [21].

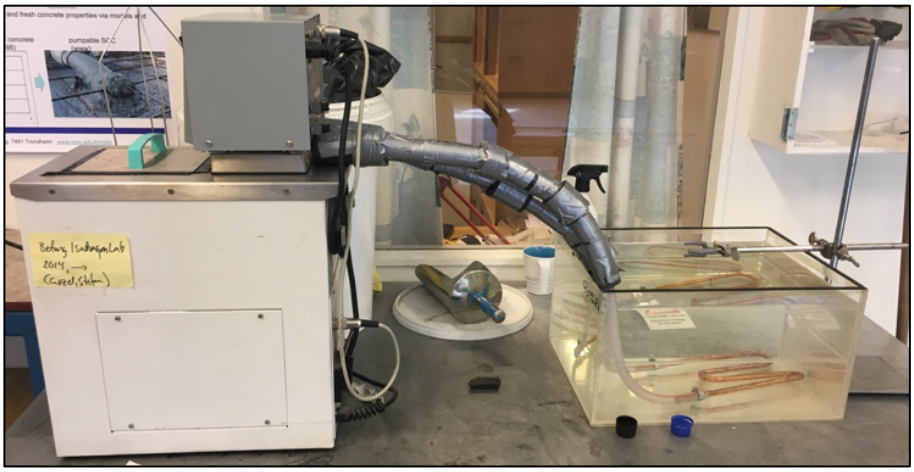

Figure 10 The set up for Julabo and water bath

The viscometer procedure

1. Turn on the Julabo (the temperature controller) and adjust the temperature to 20 degrees Celsius.
2. Use an external thermometer to measure the temperature in the water bath, then adjust the temperature in the bath by filling in hot or cold water, until the temperature is 20 degrees Celsius.
3. Wait approximately 20 to 30 minutes to ensure that the temperature in the water bath is stable.
4. Put the viscometer into the water bath and use the metal bar (see Figure 10) to fasten the viscometer in the water bath
5. Put a funnel on the largest tube (venting tube, see Appendix E) of the viscometer and pour the EF into the tube (needs approximately 10 ml. of EF).
6. Put the hand aspirator on the smallest tube (tube with capillary, see Appendix E) of the viscometer and extract the EF until it flows over the upper timing mark M1 (see Appendix E).
7. Wait at least 10 minutes for the temperature of the EF to be at the same temperature as the water in the bath.
8. Take of the hand aspirator and start measuring immediately at the time when the EF's meniscus passes the upper timing mark M1, and stop immediately at the time when the EF's meniscus passes the lower timing mark M2 (see Appendix E).
9. Repeat steps 6, 8 and 9 for 2 more times.

The flow times measured from the experiment can be found in Appendix F.

2.2.5.5. Calculations of dynamic viscosity and kinematic viscosity

The average flow time was calculated from the measured flow times from the viscometer (see Appendix F), which were applied in the table of the kinetic energy correction (also called the Hagenbach correction), see Appendix E. The average flow time was also used to calculate the kinematic viscosity (ν) and dynamic viscosity (η_{pore_fluid}), which are described below.

Kinematic viscosity (ν) [21] is calculated by the formula:

$$\nu = K(t - \vartheta) \tag{16}$$

where K is the constant determined by ASTM D2515-66 [23], t is the average flow time of viscometer, and ϑ is the Hagenbach correction. The full information about the kinematic viscosity can be found in Appendix E.

Dynamic viscosity (η_{pore_fluid}) is calculated with the formula:

$$\eta_{pore\_fluid} = \nu * \rho \tag{17}$$

where ρ is the density of the fluid used in the measurement, which is the filtered EF for the A-, C-, D- and G-series, and the unfiltered EF for the B-, E- and F-series. The calculation of ρ is described in Section 2.2.6.

The dynamic viscosity was applied in the Krieger-Dougherty equation *(8)* (see Section 3.5) and the Chong's equation *(10)* (see Section 3.6), in order to find the apparent viscosity (η).

2.2.6. Solids content and density of excess fluid

In order to find the density of the EF (for filtered EF and unfiltered EF), the EF was evaporated. After filling the viscometer with the filtered EF, the rest of the EF was used in an evaporation test. Approximately 1 gram of EF was poured in to a petri dish on the three-digits balance. Thereafter, the petri dish was placed in an oven at 40 degrees for approximately 30 minutes. The results from the evaporation are summarized in Appendix F in Table F1 to Table F7.

The calculation of the EF's density is defined by the following equations:

$$\frac{2.7+1}{2} * V_{solid,EF} + 0.998 * (1 - V_{solid,EF}) \quad (18)$$

$$1.85 * V_{solid,EF} + 0.998 * (1 - V_{solid,EF}) \quad (19)$$

where 1.85 is the average theoretical density of particles ($\delta_{porefluid}$ = 2.7 and $\delta_{polymer}$ =1), 0.998 is the density of water at 20°C, and $V_{solid,EF}$ is the volume fraction of solid in EF, which was found from the evaporation. $V_{solid,EF}$ is the solid fraction of fluid (%), divided by the average theoretical density of the pastes. The densities of EF for each of the mixes are summarized in Table F1 to Table F7 in Appendix F.

It was also possible to use a small volumetric flask for accurate measurements of the fluid density. However, this method was not used in this study since it was subsequently discovered that there was a need for the values of fluid density. In addition, some of the fluids were opaque fluids with high solids concentration, which could have led to uncertainty if they were read through a volumetric flask.

2.2.7. Use of Solver and Trendline function

In order to find the minimized values for the sum of the squares (R^2 =1) of the constants (k_c, k_s, k_{fa}, k_{sp} and k_f) in the new empirical model (eq. *(3)*), and the intrinsic viscosity [η] in the Krieger-Dougherty equation (eq.*(8)*), the Excel's solver was used. The principle of the Solver was previously mentioned in Section 2.1.7. The first step is to find the difference between the measured values and the predicted values of the output. The next step is to summarize the squared values of the differences, and then use the Solver to adjust the values of the constants.

In this study, the outputs were λ_Q and η. For λ_Q, the parameters and constants (k_c, k_s, k_{fa}, k_{sp} and k_f) were entered into an excel spreadsheet, together with the equation's formula. The values of the constants were first assumed to be 1. Then, the predicted values were determined in Excel by solving the equation with parameters and constants. The differences between the measured values of λ_Q and the predicted values of λ_Q were then calculated. The differences were calculated to be squared-values and then summarized in a cell called "SSE" (sum of squared errors, eq. *(14)*). The Solver was used to calculate new values of SSE, by adjusting the constants k_c, k_s, k_{fa}, k_{sp}, and k_f to obtain the minimized values of the SSE.

Thereafter, the measured values of λ_Q were plotted against the predicted values of λ_Q, and the function "trendline" was used to plot the regression line. The option to "show R-square value in the diagram" was chosen. The total sum of squares, SSTO, (eq. *(15)*) and R^2 values ware automatically calculated by Microsoft Excel.
The same method was applied for the Krieger-Dougherty equation (eq.*(8)*), in order to find the value(s) of [η] and R^2.

The results from the Solver and trendline function are summarized in Table 14 and Table 15 for the empirical model (k_c, k_s, k_{fa} k_{sp}, k_f, and R^2), and in Table 9 and Table 10 for the Krieger-Dougherty's apparent viscosity ([η] and R^2). The detailed instructions for the Solver can be found in [24], and the full detailed calculations can be found in Appendix A and Appendix H.

The trendline function was also used to calculate the R^2 values of the relationship between rheology and relative concentration of solids (Section 3.4), the Krieger-Dougherty's apparent viscosity (Section 3.5), liquid thicknesses (Section 3.7), and the Chong's relative viscosity (Section 3.6).

2.2.8. Repeatability and precision of the methods

Repeatability and precision of A6, B22, E39 and E47
To investigate the accuracy of the methods, the maximum packing and viscosity measurements, four different mixes were repeated with the same recipes and methods. These mixes are mix no. A6, B22, E39 and E47. All the details of these mixes can be found in Appendix M.
They will also be described further in Sections 3.2.1, 3.3.1 and 3.3.2.2

Repeatability and precision of viscosity of water
In order to examine the viscosity of water and the accuracy of both Cannon-Fenske Routine viscometers (see Section 2.2.5.4 for the viscometers), the viscosity measurements were performed on de-ionized water from the de-ionizing tank (VWR Puranity TU12) in the concrete lab at NTNU. The same procedure in Section 2.2.5.4 was used, with measurements conducted five times. The water measurements were performed after the experiments on all the mixes were completed.

The de-ionizing water was measured for both viscometers at 10, 20, and 30 degrees Celsius, and compared to the standard dynamic viscosity of water from Kestin et al. [25]. This measurement is described further in Sections 3.3.2.2 and 3.3.2.3.
All the details of this measurement can be found in Appendix G.

2.2.9. The range of correlation coefficients

In this study the models and parameters were evaluated based on how accurate the correlation coefficients from regression analysis were and how well the five micro-proportioning approaches described the rheology as the graphic plots.

In Chapter 3, Sections 3.4 to 3.8, the range of correlation coefficients are divided into seven colors. The R^2 values between 0.90 and 1.00 are considered to be the best correlation coefficients that provide the ideal or (almost) one-to-one relationships, and presented as bright green ( ), in accordance with Skare and Professor Jacobsen. The R^2 values of 0.70 to 0.89 (presented as grey-green ( ) and light yellow ( ) color) are considered to be a “reasonable prediction”, according to the study by Bentz et al. [5]. The correlation coefficients below 0.70 were considered to be poor values in this study, since they would not give a relationship closed to a one-to-one relationship.

3. Results and discussion

3.1. Excess fluid (EF) from the centrifugation

This section presents the results from the trial and error test described in 2.2.5.1. It also discusses the EF's volume and characterization of the opacity and transparency of the EF. Finally, it presents the solids content in the EF.

3.1.1. Accuracy of the measurement of volume and solid content in excess fluid

Table 5 demonstrates the solids content determined from the trial and error test described in Section 2.2.5.1. In method 1 a syringe was used to extract the EF before filtering, and in method 2 the EF was poured out directly from the falcon tubes.

Table 5: The measurements of solids content from the trial and error test

Method	EF (g)	Average solid content left in papers (g)	ϕ_{max}	VFF	Solid content in syringe (g)	Solid content in filter (g)
1. Syringe + filter	40.87	0.16	0.510	0.374	1.02	0.74
2. Pouring directly	41.74	0.10	0.514	0.369	÷	÷
Difference	0.87 g. (more in method 2)	0.06 g. (more in method 1)	0.004 (higher in method 2)	0.005 (higher in method 1)		

The results in Table 5 demonstrate that method 2 resulted in the highest amount of EF, and the solids that were left in the syringe and the filter were small enough to be neglected. The results from this test led to the method/procedure that was used and described in Section 2.2.5. The detailed calculation and measurements can be found in Appendix D.

3.1.2. Volume and characterization of excess fluid

Volume of excess fluid

Sections 2.1.4 and 2.2.4 respectively described how to calculate the EF by volume and the method for obtaining the EF. The EF fraction of all the series are summarized in Table F1 to Table F7 and the full calculation can be found in Appendix F.

As indicated in Table F1 to Table F7 the amount/volume of the EF that could be extracted from a paste after centrifugation depended on the w/b ratio of each mix. The mixes with a lower w/b-ratio had a tendency to receive a lower value of EF fraction, while the mixes with a higher w/b-ratio often had a higher value of EF fraction.

Transparent and opaque fluid

As mentioned in Sections 2.2.5.2 and 2.2.5.3, different methods were used to prepare the EF before the viscosity measurements. As the EF from the A-, C-, D- and G-series were filtered through a filter with a 0.45 μm pore size, all the EF from these series were transparent liquids (see the online file in Appendix L). However, the EF from the B-, E- and F-series were not filtered through a filter, and therefore the EF from those series were either transparent or opaque liquids. The characterization of all the EF from the B-, E- and F-series are summarized in Table L1 in Appendix L, where it indicates which mixes were opaque and which mixes were transparent.

In Appendix L, Table L1 it seems that the opacity and transparency of the EF depended on the SP dosage, FA content, and silica content. When considering the B-series, no FA and silica fume were added in the mixes, while the SP dosage for the mixes were high, ranging between 1% to 1.75% of the cement content (see Appendix B). The high content of SP dosage caused a high dispersion in the flocculated particles and made all the EF in the B-series opaque. For the E- and F-series, the SP dosage varied between 0.75% to 1.5% of the cement content, and almost all of the mixes in these series had FA and/or silica added to them (see Appendix B), which seem to be the reasons for the opacity of the E- and F-series.

3.1.3. Solids content in excess fluid

In order to calculate the EF's density, the solids content in the EF for each mix had to be measured (see Section 2.2.6). As mentioned in Sections 2.2.5.2 and 2.2.5.3, the EF from the A-, C-, D- and G-series were filtered through a filter before the viscosity measurements were performed, while the EF from the B-, E- and F-series were unfiltered. Practically, one would predict that the solid content in the EF from the A-, C-, D- and G-series should be lower than in the B-, E- and F-series. However, Table F1 to Table F7 demonstrate that the solids content (from evaporation method) of the EF in each mix were mostly unpredictable. As can be seen in Table F1 to Table F7, the solids content in many of the mixes in the A-, C-, D- and G-series were in the same range as the mixes in the B-, E- and F-series. Based on the knowledge of the SP's constituents (see Appendix K), the size of the fillers (see Sections 2.2.1 and 2.2.2), and pozzolans (see Appendix B), it can be predicted that the solids content in the EF are polymer from the SP, and/or some small particles from fillers, and/or pozzolans. However, given some of practical limitations to this study, the proportion of each material that was in the EF is unclear. Section 3.2.2.1 describes how the solids content affected the viscosity of EF in more detail.

3.2. The maximum packing of the particles

Maximum packing is one of the important parameters for this project, and therefore had to be investigated and analyzed. The maximum packing was described in Section 2.1.4. In Appendix F, Table F1 to Table F7, all values of the maximum packing of each of the mixes are summarized and calculated using equation *(6)*.

3.2.1. Accuracy of the maximum packing

To investigate the accuracy of the measurements, four different mixes were repeated with the same recipes and methods, as mentioned in Section 2.2.8. All the details can be found in Appendix M.

Table 6 displays the accuracy of the maximum packing in mixes no. A6, B22, E39 and E47, which were obtained by repeating the mixes with the same recipes and methods. The highest difference was found in mix no. B22, where the paste was not well packed after centrifugation. This is described further in Section 3.2.2.

Table 6 Accuracy of the maximum packing on A6, B22, E39 and E47

Mix no.	ϕ_{max}	Difference
A6 original	0.551	0.003
A6 repeated	0.548	
B22 original	0.543	0.005*
B22 repeated	0.538	
E39 original	0.560	0.002
E39 repeated	0.558	
E47 original	0.553	0.001
E47 repeated	0.554	

*The paste of B22 was not well packed after centrifugation, see section 3.2.2.

The results from Table 6 demonstrate that the uncertainties from maximum packing were minimal, which meant that the values of maximum packing from the experiment were highly accurate and can be trusted and further applied in the equations in this study.

3.2.2. The effect of superplasticizer on maximum packing

It should be noted that the centrifugation method (as mentioned in Section 2.2.4) could not measure the maximum packing of all the mixes. In this study, some of the mixes in the B-series had pastes which could not be packed, where their pastes were not stiff after the centrifugation (see example in Figure 11). These mixes are B22, B23 and B24, where the mixes contained the highest amount of SP dosage used in this project, that is 1.75% SP dosage of the cement content (see Appendix B). This indicates that an excessive quantity of SP dosage would make a paste highly flowable, and the particles could not be packed together by the centrifugation method. This means that the paste has reached its saturation point and would not be able to absorb more of the SP. This is explained further in Section 3.3.2.3.

Figure 11 provides an example of mix no. B24, where the paste was not packed after centrifugation. Figure 11 demonstrates that the paste could still be poured from the falcon tube. The full details and pictures from mix no. B22, B23 and B24 are attached in the online file in Appendix F.

Figure 11 The unpacked paste after centrifugation from mix no. B24

3.3. Viscosity measurements

This section presents the EF's flow time measurements. It also discusses the viscosity measurements on de-ionized water for both viscometers (mentioned in section 2.2.8) at 10, 20 and 30 degrees Celsius, along with the kinematic and dynamic viscosity of the EF's accuracy. Finally, it presents the effect of SP dosage on dynamic viscosity.

3.3.1. Flow times of viscosity measurements and their precisions

As mentioned in Section 2.2.5.4, the viscosity measurements were performed three times continually for each mix (the same pore water sample centrifuged for one mix). The flow times can be found in Appendix F, and the average flow time for each mix can be found in Table F8 to Table F14. In addition, four mixes were repeated to examine the precision of the method (see below).

All of the mixes gave a highly accurate set of time (by seconds) from three measurements, with some uncertainties of 2-3 seconds for some mixes. This meant that the time measurements were performed precisely, were accurate, and could be trusted.
In order to investigate the viscometers' accuracy, four different mixes (A6, B22, E39, E47 – also mentioned in Section 2.2.8) were repeated with the same recipes and methods. It appears that the mixes still gave an accurate set of time from the three measurements, but the results were different from their original mixes by 5-11 seconds (see Table 7, Figure 14 and Appendix M). The reason for these differences is unclear, which meant the results of the time measurements could not be fully trusted. However, the average flow time of each mix had to be applied in equation *(16)* to calculate the kinematic viscosity, in order to calculate the dynamic viscosity (eq. *(17)*). The uncertainties of kinematic viscosity and dynamic viscosity determined the effect of the uncertainties of time measurements between the original mixes and the repeated mixes. This is described further in Section 3.3.2.2.

Table 7 demonstrates the flow time measurements of mix no. A6, B22, E39 and E47 with their original and repeated time measurements. It indicates that each of the mixes gave a highly accurate set of time (three times for each mix), with a difference of 5-11 seconds between the original and repeated mixes.

Table 7 Flow time measurements of the original and repeated mixes, A6, B22, E39 and E47

	Flow time measurements (sec.)				
Mix no.	**1**	**2**	**3**	**Average**	**Difference**
A6 original	306	303	306	305	11
A6 repeated	293	294	294	294	
B22 original	176	176	177	176	5
B22 repeated	183	181	181	182	
E39 original	164	164	164	163	9
E39 repeated	175	172	172	174	
E47 original	163	163	163	305	11
E47 repeated	174	174	174	294	

3.3.2. Viscosity of the pore fluids and water

3.3.2.1. Viscosity of water from the concrete lab at 10, 20 and 30C degrees.

The water's viscosity was measured in order to examine the accuracy of the viscometers, after the experiments on all the mixes were conducted (mentioned in Section 2.2.8)

Figure 12 illustrates the variations of the water's viscosity, as measured by the Cannon-Fenske Routine viscometer no. 50 and no. 75 (see Section 2.2.5.4) at 10, 20, and 30 degrees Celsius, compared to the standard dynamic viscosity of water from Kestin et al. [25]. As displayed in Figure 12, the laboratory's water had a tendency to have a higher dynamic viscosity than the standard dynamic viscosity of water as measured by Kestin et al. [25].

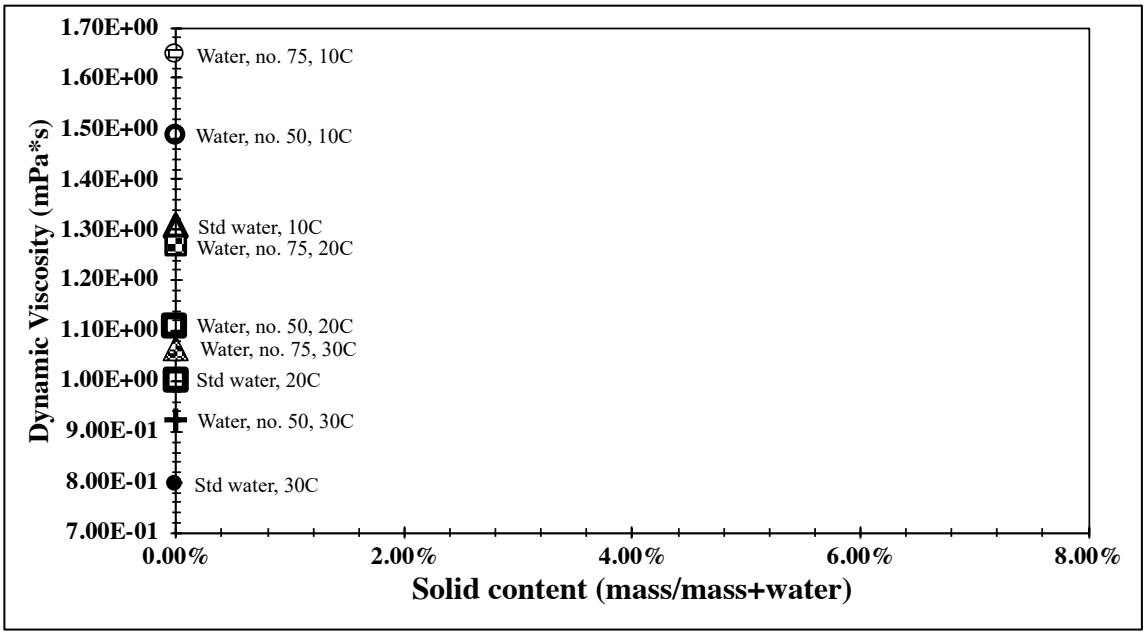

Figure 12 The dynamic viscosity of water measured in the laboratory using Cannon-Fenske Routine viscometer no. 50 and no. 75, with different temperature of 10, 20, and 30 degrees Celsius.

The calculation of the measured viscosity of water (see Appendix G) demonstrated that the dynamic viscosity of water as measured in the laboratory was different from the standard dynamic viscosity, with a range between 11% to 16% of standard dynamic viscosity for viscometer no. 50, and 26% to 34% of standard dynamic viscosity for viscometer no.75. This meant that the mixes that used viscometer no. 75 with no filtration were less accurate than the mixes that used viscometer no. 50 with filtration.

3.3.2.2. Kinematic viscosity, dynamic viscosity and their accuracies

As described in Section 2.2.5.5, the mix's kinematic viscosity is directly related to its average flow time, while the dynamic viscosity depends on the kinematic viscosity and density of EF of the mix, where the EF's density is directly related to its solids content in EF. Table F8 to Table F14 in Appendix F summarize all of the calculated kinematic viscosity (eq.(16)) and dynamic viscosity (eq.(17)) for each mix.

Figure 13 (a) illustrates the variations of the kinematic viscosity from all of the mixes, plotted against the solids content from each mix, and Figure 13 (b) illustrates the dynamic viscosity from all of the mixes, and the dynamic viscosity of water at 20 degrees Celsius (see section 2.2.8) plotted against the solids content from each mix. Figure 13 (a) and (b) indicate that the solids content in EF has minimal effect on the kinematic viscosity and the dynamic viscosity, which means that the kinematic viscosity and dynamic viscosity were not substantially affected by the possible inaccuracy of the EF's density.

The EF's dynamic viscosity for all the mixes seem to be in the same range as the measured viscosity from the laboratory, but they are all higher than the standard dynamic viscosity measured by Kestin J. et al. [25]. The higher dynamic viscosity from the laboratory may be due to the inaccuracy of viscometers found in Section 3.3.2.1.

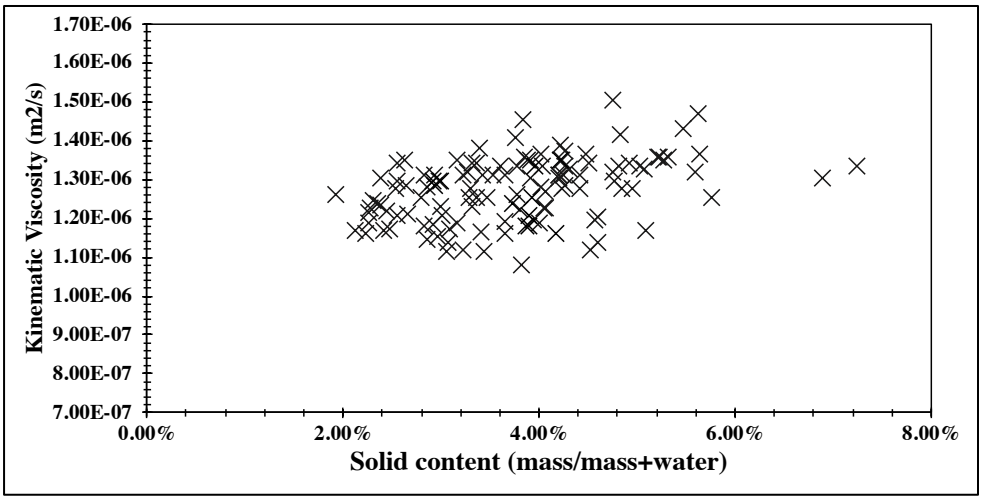

(a)

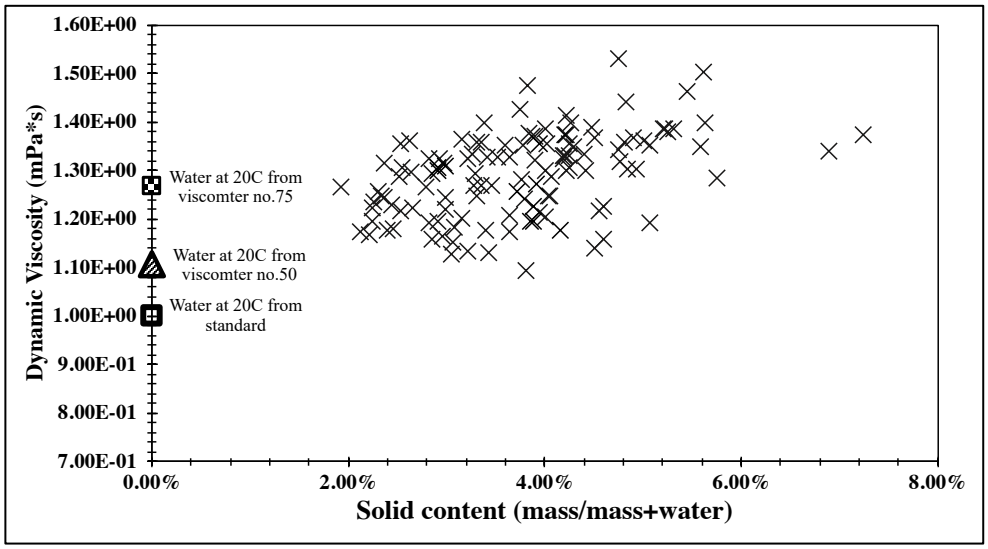

(b)

Figure 13 Solid content by mass of solids/(mass of solids+mass of water) plotted against (a) kinematic viscosity and (b) dynamic viscosity from all mixes and water

To examine the effect of the inaccuracy of time measurements on the pore fluid viscosity (as mentioned in Section 3.3.1), four different mixes were repeated with the same recipes and methods (see section 2.2.8 and Appendix M).

Figure 14 (a) and (b) illustrate the variations of the kinematic viscosity and dynamic viscosity on solids content from four different mixes (A6, B22, E39 and E47) that were repeated with the same recipes and methods, as compared to the corresponding original mixes. Figure 14 (a) and (b) demonstrate that the original and repeated mixes on kinematic viscosity and dynamic viscosity seem to differ by 10 seconds, as mentioned in Section 3.3.1. Calculating the differences between the original mixes and repeated mixes, it was found that the differences were in the range of 4% to 7% of the original mixes. The full calculations and detail can be found in Appendix M.

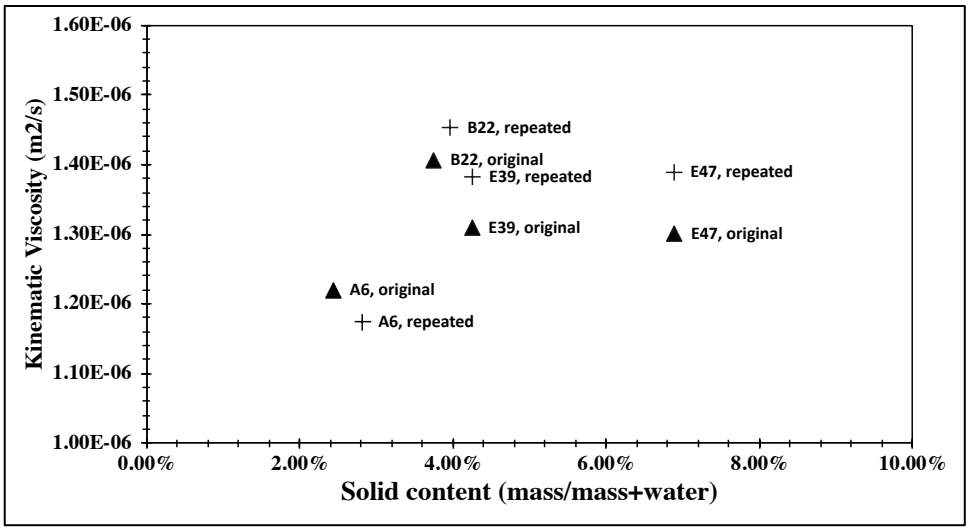

(a)

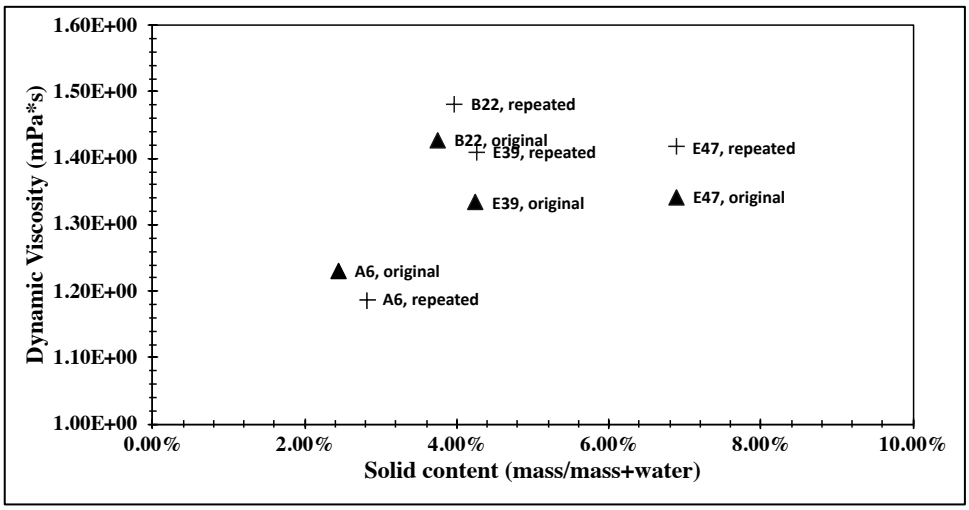

(b)

Figure 14 Repeated and original mixes no. A6, B22, E39 and E47 on (a) kinematic viscosity and (b) dynamic viscosity against solids content by mass of solids/mass of solids+mass of water.

3.3.2.3. The effect of superplasticizer on viscosity

Figure 15 illustrates the relationships between the dynamic viscosity and the SP dosage (in % of the cement content), where the mixes in the graph have the same values in terms of the parameters, that is the w/c, w/b, fi/b, w/p, FA/b, s/b, and solid fraction, with variations in SP dosage.

Figure 15 demonstrates that the general trend is that the dynamic viscosity increases with increasing SP dosage. At the point where SP dosage = 1.50, it appears as if the cement pastes reached their saturation point, according to the drastic changes in the curves in Figure 15. This means that the pastes could not absorb more of the SP dosage into the mix when the dosage reached 1.5% of cement.

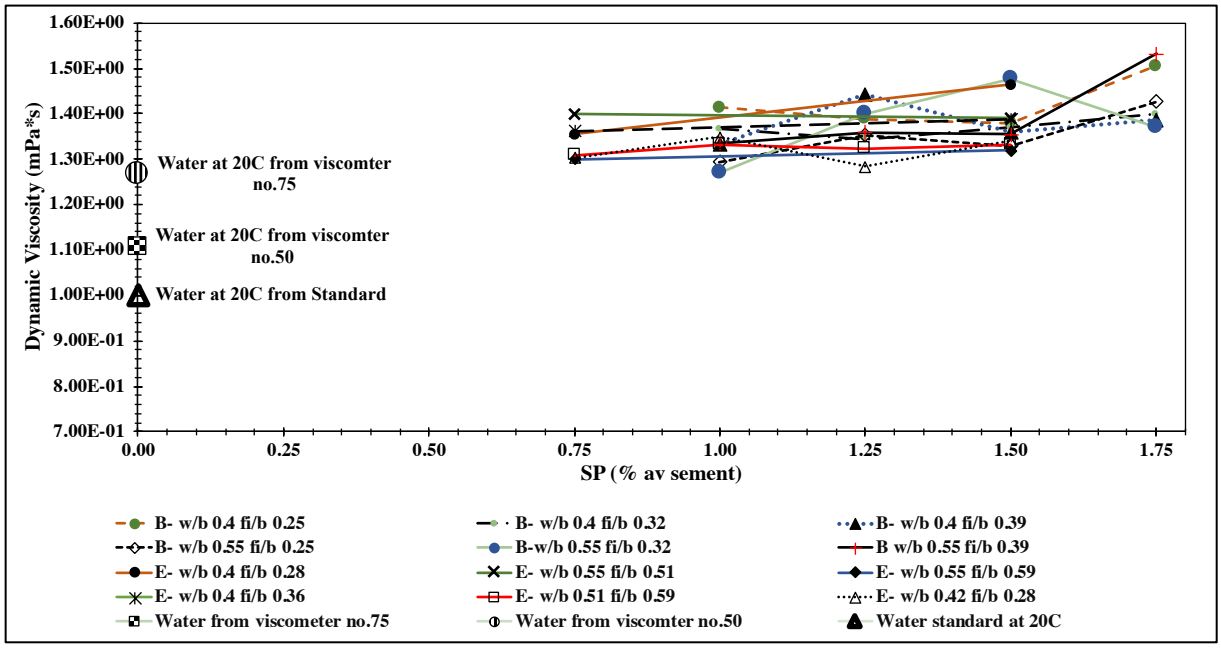

Figure 15 The effect of SP dosage on the dynamic viscosity from the mixes with the same values of parameters but varying SP dosage

Figure 16 illustrates the relationships between the dynamic viscosity and the SP dosage (in % of the cement content) for all of the mixes, where the series/mixes with higher SP dosage seem to provide a higher dynamic viscosity of EF.

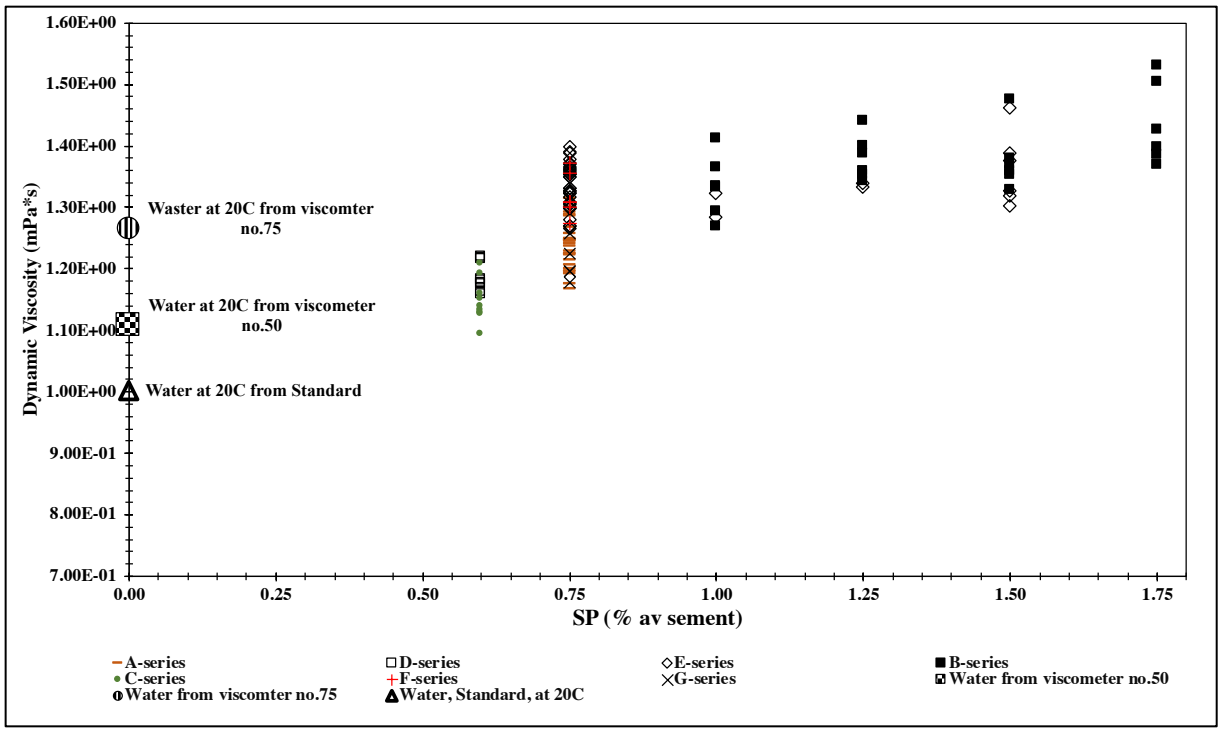

Figure 16 The effect of SP dosage on the dynamic viscosity all of the mixes from each series and dynamic viscosity of water.

The full details of the plots in this section can be found in the online link in Appendix F.

3.4. Rheology and the relative concentration of solids

The relative concentration of solids (ϕ/ϕ_m) was mentioned in Section 2.1.4, and the full calculations and analysis are attached in the online file in Appendix F. This section presents and discusses the relationships between ϕ/ϕ_m and rheology (mini slump flow, flow resistance ratio (λ_Q), plastic viscosity (μ) and yield stress (τ_0)), based on the theoretical behavior of a cement paste from Jacobsen et al. [6] and the Bingham fluid model described in Section 2.1.2.

The four rheological parameters (mini slump flow, λ_Q, μ, and τ) that are presented in this section were previously measured in the laboratory on matrices with the batch size of 2.05L by Skare (see Appendix B). The trendline function described in Section 2.2.7 was used to calculate the correlation coefficients (R^2 values).

3.4.1. The R^2 values of the relationships between relative concentration of solids and rheological parameters

Table 8 presents the summarized R^2 values from all of the relationships between the relative concentration of solids and the four rheological parameters: average mini slump flow, the flow resistance ratio (λ_Q), the measured plastic viscosity (μ), and yield stress (τ_0) (see Appendix B for the rheology values). The values of all ϕ/ϕ_m are summarized in Table F15 in Appendix F.

Table 8 The R^2 values from the relationships between rheology and the relative concentration of solids.

	R^2 values from the relative concentration of solids								
	Series	A	B	C	D	E	E - no silica	F	G
Parameter	Flow resistance ratio	0.90	0.97	0.81	0.79	0.16	0.51	0.09	0.11
	Mini slump flow	0.82	0.75	0.81	0.88	0.02	0.22	0.01	0.15
	Yield stress	0.86	0.56	0.82	0.90	0.17	0.03	0.08	0.18
	Plastic viscosity	0.89	0.93	0.85	0.77	0.26	0.46	0.22	0.23

0.00-0.09	**0.10-0.49**	**0.50-0.59**	**0.60-0.69**	**0.70-0.79**	**0.80-0.89**	**0.90-1.00**

Table 8 demonstrates that the best R^2 values between ϕ/ϕ_m and rheology are from the A-, B-, C- and D-series, while the E-, F- and G-series had poor correlation coefficients. As demonstrated in Table 8, the E-series was also analyzed by excluding the mixes that contained silica fume (Appendix B). It appears as if silica fume had an effect on the correlation coefficients in the E-series, as can be seen from the improvement of the R^2 values (except for yield stress) in Table 8. The same method was used for the F-series, in which some of the mixes also contained silica fume (Appendix B). However, the results of the F-series with no silica could not be discussed, because there were only six mixes in the F-series and only two mixes did not contain silica fume, which means that R^2 value would always be 1 and the correlation coefficient would not be representative of the series.

3.4.2. The graphic plots of relative concentration of solids versus rheological parameters

Figure 18 illustrates the relative concentration of solids, ϕ/ϕ_{max}, (Table F15 in Appendix F), plotted against the measured flow resistance ratio, λ_Q, (Appendix B) for the series with the best R^2 values.

Figure 18 illustrates the relative concentration of solids, ϕ/ϕ_{max}, (Table F 15 in Appendix F) plotted against the plastic viscosity, μ, (Appendix B), for the series with the best R^2 values.

Figure 17 and Figure 18 provide some examples from the graphic plots of the relationships between the relative concentration of solids and rheology, with the best R^2 values from Table 8. All the plots of the relationships between ϕ/ϕ_m and rheology can be found in Appendix F, Figure F1 to Figure F4.

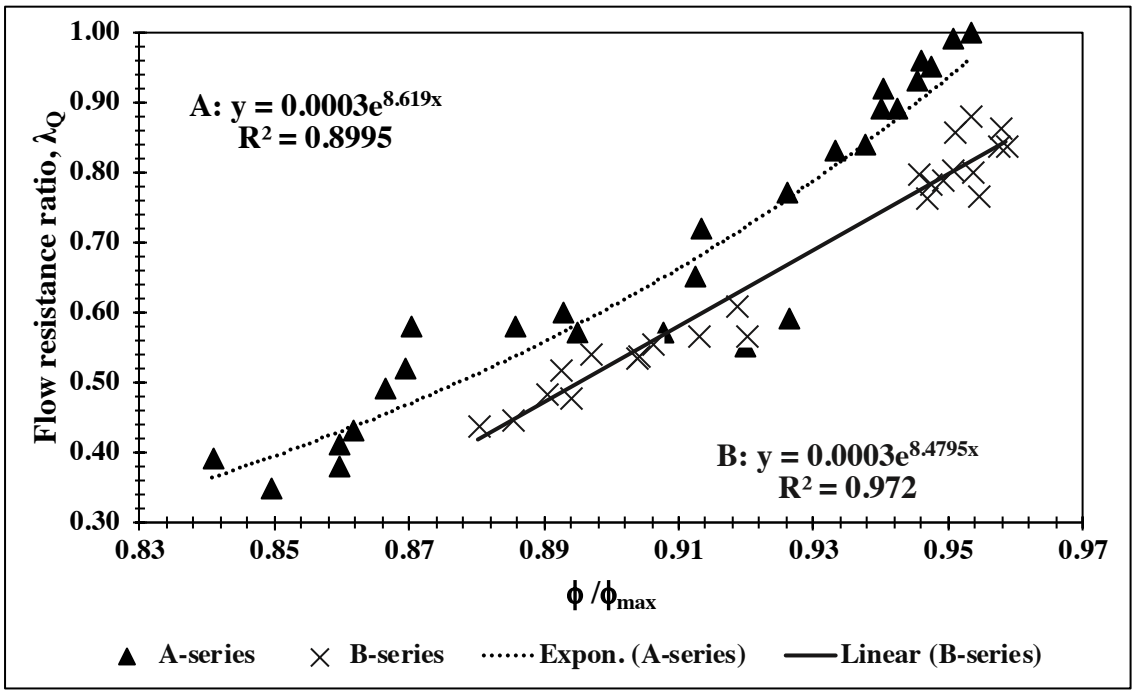

Figure 17 The relationships between relative concentration of solids (ϕ/ϕ_{max}) on flow resistance ratio (λ_Q) from the series with the best R^2 values.

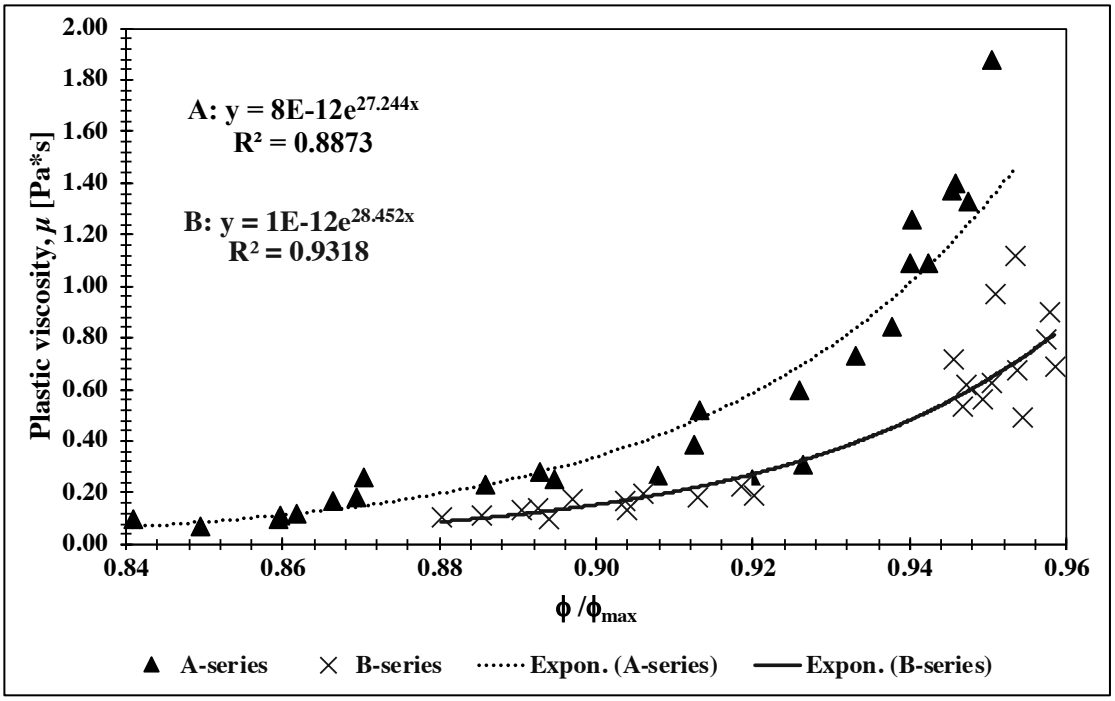

Figure 18 The relationships between relative concentration of solids (ϕ/ϕ_{max}) on plastic viscosity (μ) from the series with the best R^2 values.

The relationships in Figure 17 imply that flow resistance (λ_Q) increases with increasing ϕ/ϕ_{max}. From Jacobsen et al. [6], it is well known that a paste with a higher solid fraction is denser and has a thicker consistency. For the same reason, average mini slump flow decreases with increasing ϕ/ϕ_{max} (see Figure F1 in Appendix F). Figure 18 demonstrates that a higher ϕ/ϕ_{max} leads to a higher plastic viscosity (μ), with the same relationship for yield stress (τ_0) (see Figure F 4, Appendix F). The behavior of τ_0 is also clearly described by the Bingham fluid model about the mobility of fresh concrete, as previously mentioned in Section 2.1.2.

Figure 18 also demonstrates a mix in the A-series that has the highest value of measured plastic viscosity (μ). This filler-modified paste is mix no. A21 (see Appendix B). This is discussed further in Section 3.9.1.

However, it must be noted that when considering all the mixes in the E- and F-series, it demonstrates the opposite results for ϕ/ϕ_{max} versus mini-slump flow and yield stress (see Figure F1 (b) and Figure F4 (b) in Appendix F), where ϕ/ϕ_{max} increases with increasing mini slump flow and decreasing yield stress (τ_0). If only the mixes without silica fume in the E- and F-series are considered, the relationships behave in the same way as the other series (Figure F1 (c) and Figure F4 (c), Appendix F). This clearly indicates that silica fume has an effect on the mixes, and the methods used in this experiment were not suitable for the mixes that contained silica fume. This should be studied further in the MiKS project.

The high correlation coefficients from this section means that the relative concentration of solids (ϕ/ϕ_{max}) is a suspension parameter, that can be used to predict the rheology of a cement paste with the same conditions as the mixes with highest R^2 values in the A-, B-, C- and D-series from Table 8.

3.5. The Krieger-Dougherty equation

The Krieger-Dougherty equation (eq.*(8)*) was described in Section 2.1.5, and the full calculations and values of the Krieger-Dougherty's apparent viscosity (η) can be found in Appendix H. This section presents the summarized values of intrinsic viscosity ([η]) and their correlation coefficients (R^2 values). In addition, the relationships between the apparent viscosity of pore fluid from the Krieger-Dougherty equation, and the plastic viscosity (μ) measured in the laboratory, are introduced as graphic plots in this section.

The plastic viscosity (μ) in this section had been measured in the laboratory on matrices with the batch size of 2.05L by Skare (see Appendix B).

3.5.1. Intrinsic viscosity and R-squared values

Intrinsic viscosity ([η]) is one of the parameters required for the Krieger-Dougherty equation (eq.*(8)*), and it was described in Section 2.1.5. The Microsoft Excel add-in program "Solver" was used as the analysis tool to calculate the values of [η], and the trendline function in Microsoft Excel was used to calculate the R^2 values (also mentioned in Sections 2.1.7 and 2.2.7). The detailed calculations of regression analysis by Solver, trendline function, and values of the Krieger-Dougherty's apparent viscosity of pore fluid can be found in Appendix H.

Table 9 presents the intrinsic viscosity and R^2 values calculated by the regression analysis of the Krieger-Dougherty's apparent viscosity of pore fluid (eq.*(8)*), compared to the plastic viscosity measured in the laboratory (Appendix B). The values of [η] in Table 9 were calculated to fit the regression line for each of the series individually (see Appendix H).

Table 9 Intrinsic viscosity and R^2 values from the regression analysis of the Krieger-Dougherty's apparent viscosity compared to the measured plastic viscosity with varying intrinsic viscosity for each series

	The Krieger-Dougherty with varying intrinsic viscosity [η]											
	Series	**A**	**B**	**C**	**D**	**E**	**E - no silica**	**F**	**F - no silica**	**G**	**All**	**All - no silica**
Parameter	[η]	4.34	3.63	6.20	6.41	4.34	4.36	4.55	4.55	4.39	-	-
	R^2 values											
	Plastic viscosity	0.87	0.79	0.40	0.88	0.32	0.59	0.09	-	0.16	0.67	0.78

0.00-0.09	**0.10-0.49**	**0.50-0.59**	**0.60-0.69**	**0.70-0.79**	**0.80-0.89**	**0.90-1.00**

Table 9 implies that the A- and D-series present the best R^2 values of all the series, while the C-, E-, F- and G-series had the poorest correlation coefficients of all the series. As mentioned in Section 2.2.2 and Appendix B, the E- and F-series are the only series with mixes that contained silica fume. However, by excluding the mixes that contained silica fume from the E- and F-series, the correlation coefficients of the E-series and "All series" are improved. The blank space for R^2 value in the F-series exists for the same reason as described in Section 3.4.1, that is there are only two mixes without silica fume in the F-series and the R^2 value will always be 1.

Table 10 displays the intrinsic viscosity and R^2 values, calculated by the regression analysis of the Krieger-Dougherty's apparent viscosity of pore fluid (eq.(*8*)), compared to the plastic viscosity measured in the laboratory (Appendix B). The values of [η] in Table 10 were calculated to fit the regression line for all series ([η] constant for all series) (see Appendix H).

Table 10 Intrinsic viscosity and R^2 values from the regression analysis of the Krieger-Dougherty's apparent viscosity compared to the measured plastic viscosity with constant intrinsic viscosity for all series

	The Krieger-Dougherty with constant intrinsic viscosity [η]											
	Series	**A**	**B**	**C**	**D**	**E**	**E - no silica**	**F**	**F - no silica**	**G**	**All**	**All - no silica**
Parameter	[η]	-	-	-	-	-	-	-	-	-	4.01	3.99
	R^2 values											
	Plastic viscosity	0.87	0.78	0.42	0.86	0.32	0.45	0.10	-	0.15	0.31	0.34

0.00-0.09	**0.10-0.49**	**0.50-0.59**	**0.60-0.69**	**0.70-0.79**	**0.80-0.89**	**0.90-1.00**

Table 10 demonstrates that the A- and D-series had the best R^2 values of all the series, while the poorest correlation coefficients were in the C-, E-, F- and G-series. The mixes with silica fume in the E- and F-series (Appendix B) were also excluded from the analysis, in order to examine the effect of silica fume on the correlation coefficients. As with Table 9, the R^2 values of the E-series and "All series" improved when silica fume was excluded, and the R^2 value of the F-series was not calculated because the correlation from two mixes would always result in an R^2 value of 1 (also mentioned in Section 3.4.1).
It must be noted that the change in [η] from 4.01 (with silica) to 3.99 (without silica) also affected the R^2 values of the A-, B-, C-, D- and G-series, but the changes were so minimal that if the numbers were reduced to 2 decimal places, they would be the same.

When comparing the results in Table 9 to the results in Table 10 it appears that using Solver to calculate the intrinsic viscosity ([η]) for each series, provides a better correlation for each series than using a constant [η] for all series. This was not unexpected since calculating for constant [η] means calculating an average value to fit all the series, which will clearly give a lower correlation.

On the other hand, comparing the correlations in Table 9 and Table 10to the correlations of measured plastic viscosity of matrices (μ) in Table 8, the relative concentration of solids, ϕ/ϕ_{max}, (see section 2.1.4) provide a better correlation for the A-, B- and C-series. This means that for a matrix under the same conditions as the A-, B- and C-series, the relative concentration of solids (ϕ/ϕ_{max}) is a more suitable suspension parameter to use for the prediction of plastic viscosity, while the Krieger-Dougherty equation (eq.(*8*)) is only suitable for the A- and D-series.

3.5.2. The graphic plots of relationships between the Krieger-Dougherty's apparent viscosity of pore fluid and measured plastic viscosity of matrices

Figure 19 and Figure 20 provide some examples of graphic plots with linear regression from the apparent viscosity of pore fluid (η) predicted by applying the Krieger-Dougherty equation (eq. *(8)*), compared to the plastic viscosity (μ) measured in the laboratory (Appendix B). In Figure 19, only the A-, B- and D-series with varying intrinsic viscosity ([η]) are presented, since these are the series with the best correlation coefficients of all the series, while Figure 20 illustrates the plot of all the series with no silica and varying intrinsic viscosity ([η]). All of the plots can be found in Appendix H.

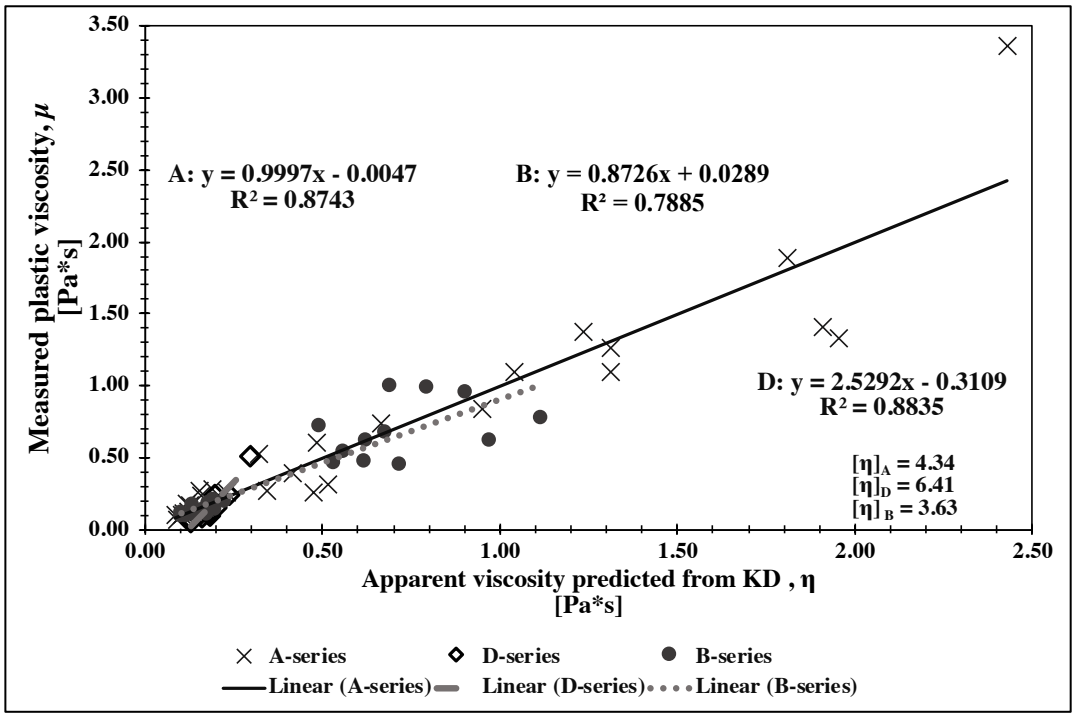

Figure 19 The plastic viscosity measured from matrices (μ) plotted against the apparent viscosity of pore fluid (η) calculated by the Krieger-Dougherty equation with varying intrinsic viscosity ([η]) for the A-, B- and D-series.

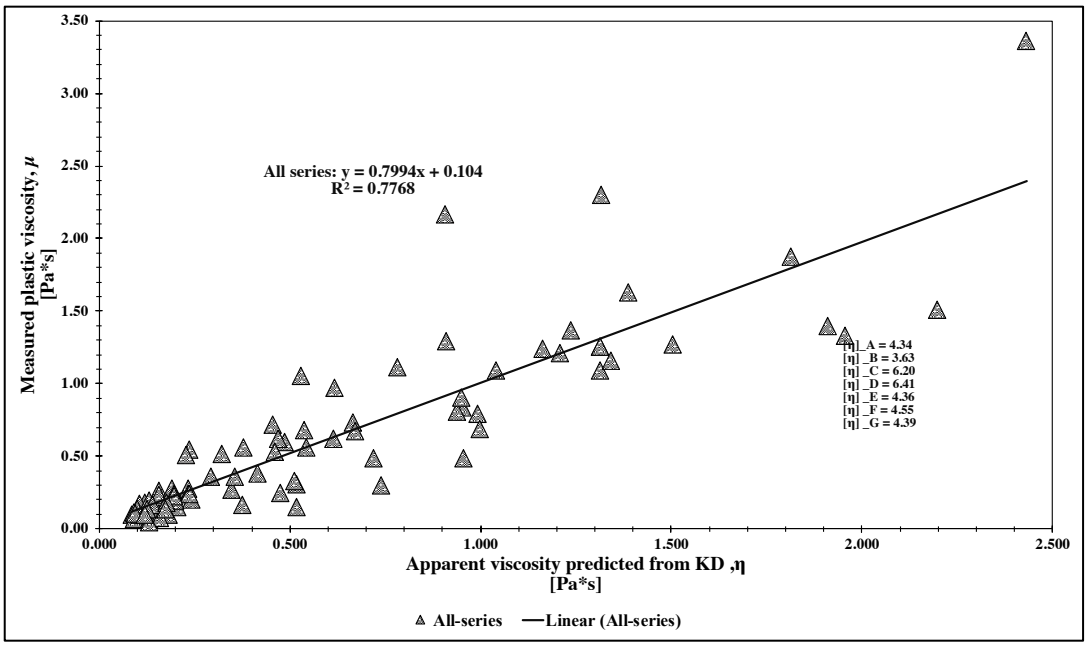

Figure 20 The plastic viscosity measured from matrices (μ) plotted against the apparent viscosity of pore fluid (η) calculated by the Krieger-Dougherty equation with no silica and varying intrinsic viscosity ([η]) all series.

As demonstrated in Figure 19 and Figure 20, the Krieger-Dougherty's equation of the apparent viscosity of pore fluid (η) has a clear relationship with the measured plastic viscosity of matrices (μ), where only the A- B- and D- series provided a reasonable prediction. This means that the Krieger-Dougherty equation (eq.*(8)*) can be applied to predict a reasonable value of plastic viscosity of a matrix (filler-modified paste) with the same conditions as the A-, B- and D-series.

As with Section 3.4.2, Figure 18, and in this section, Figure 19 and Figure 20 display a mix in the A-series with the highest value of measured plastic viscosity (μ), which is mix no. A21 (see Appendix B). This is discussed further in Section 3.9.1.

Figure 21 (a) and (b) illustrate the relationships between the measured plastic viscosity of matrices (μ) and the apparent viscosity of pore fluid (η) calculated by the Krieger-Dougherty equation (eq.(8)) with varying intrinsic viscosity ([η]) for (a) the A-, B- and D-series, and (b) all the series without silica fume, where the intercept of each regression line was forced to zero.

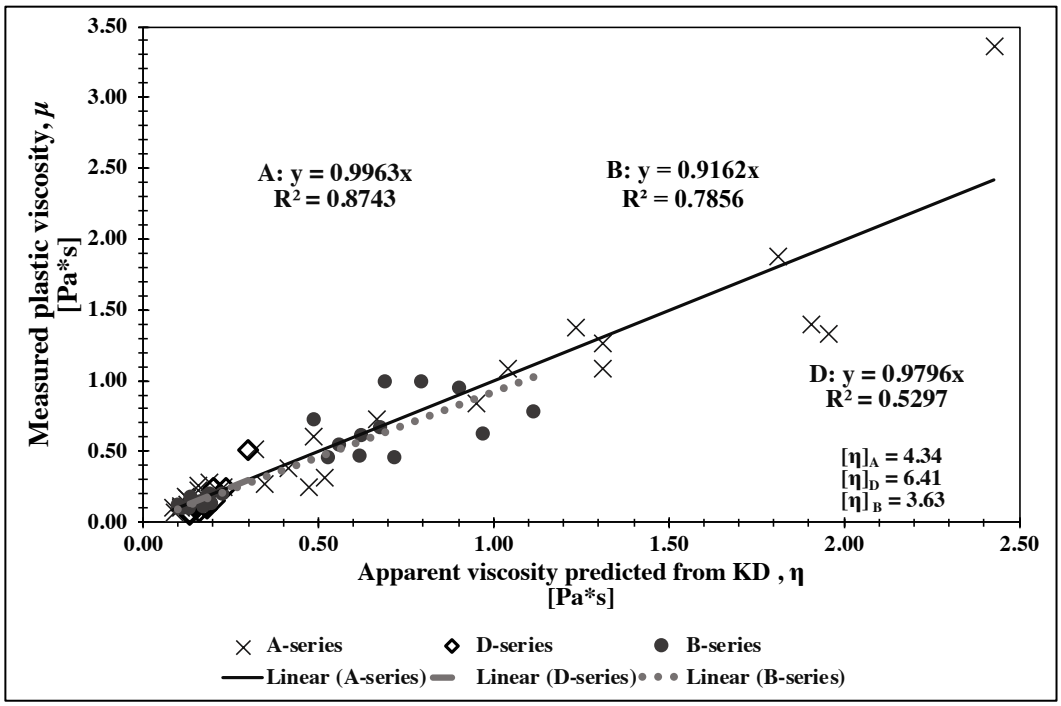

(a)

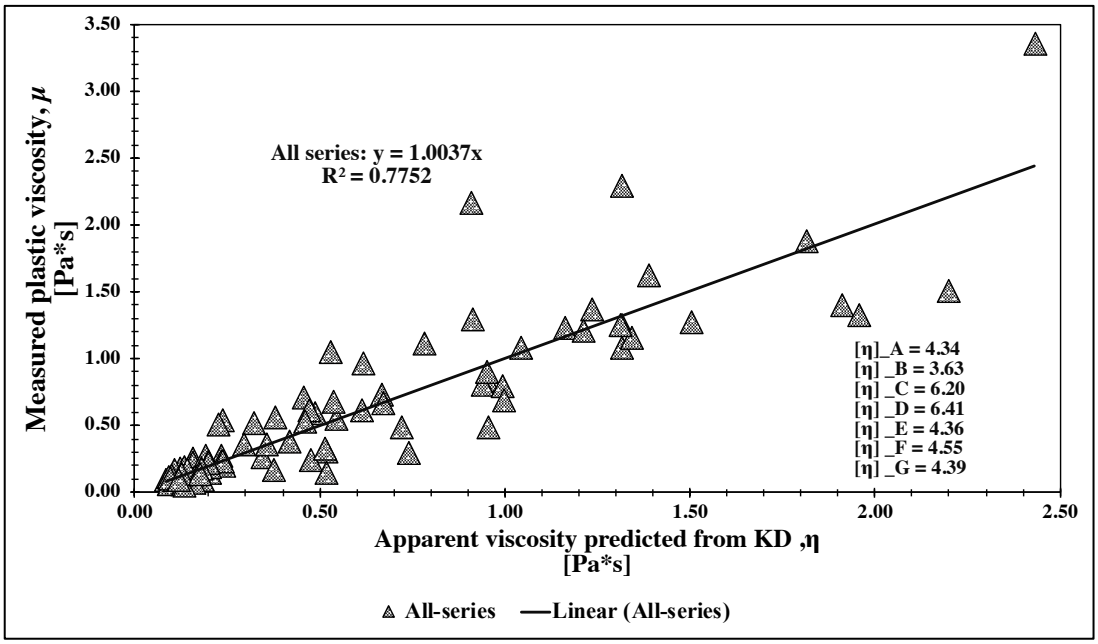

(b)

Figure 21 The plastic viscosity measured from matrices (μ) plotted against the apparent viscosity of pore fluid (η) calculated by the Krieger-Dougherty equation with varying intrinsic viscosity for (a) the A-, B- and D-series, and (b) all series without silica fume, when the regression lines are forced through the origin.

Figure 19 clearly demonstrates that in the D-series, the relationship is not a one-to-one relationship. When forcing the intercept of each series (A-, B-, D- and all series) to zero, a lower correlation was provided for each of the series, especially for the D-series, as demonstrated in Figure 21 (a). This means that only the A- and B-series came the closest to a one-to-one relationship, and they provided a reasonable prediction for the relationships between the Krieger-Dougherty apparent viscosity of pore fluid (eq.*(8)*), and the measured plastic viscosity of matrices (Appendix B).

However, Figure 21 (b) indicates that when considering all series, the Krieger-Dougherty equation (eq.*(8)*) also provides a reasonable correlation coefficient for the measured plastic viscosity (μ), despite the poor R^2 values from the C-, E-, F- and G-series displayed in Table 9 (which would be even lower when the intercept is forced to zero), and the D-series illustrated in Figure 21 (a). These poor correlation coefficients should be concerned, if the apparent viscosity of pore fluid from the Krieger-Dougherty model (eq.*(8)*) for all the series will be used for further studies.

3.6. The Chong's relative viscosity

The Chong's apparent viscosity equation (eq.*(10)*) was described in Section 2.1.5, and the full calculations and values of the Chong's apparent viscosity (η) can be found in Appendix I. This section presents the summarized correlation coefficients (R^2 values) of the relationships between the apparent viscosity of pore fluid (η) from the Chong's equation, and the plastic viscosity (μ) measured from the laboratory. In addition, the relationships are introduced as graphic plots further in this section.

The measured plastic viscosity (μ) in this section were previously measured in the laboratory on matrices with the batch size of 2.05L by Skare (see Appendix B). The trendline function described in Section 2.2.7 was used to calculate the R^2 values.

3.6.1. The correlation values of relationships between the Chong's apparent viscosity of pore fluid and the measured plastic viscosity of matrices

Table 11 presents the summarized R^2 values from all of the relationships between the Cong's apparent viscosity of pore fluid, η, (eq.*(10)*), and the plastic viscosity (μ) measured in the laboratory (Appendix B). The values of the apparent viscosity of pore fluid by Chong [2] (η) are summarized in Table I 1 in Appendix I.

Table 11 The R^2 values from the relationships between the apparent viscosity of pore fluid by the Chong's equation (eq. (10)), and the measured plastic viscosity of matrices from the laboratory.

	R^2 values from Chong's viscosity							
	Series	A	B	C	D	E	F	G
Parameter	Plastic viscosity	0.83	0.80	0.83	0.88	0.27	0.27	0.16

0.00-0.09	**0.10-0.49**	**0.50-0.59**	**0.60-0.69**	**0.70-0.79**	**0.80-0.89**	**0.90-1.00**

Table 11 demonstrates that the Chong's equation (eq.*(10)*) gives some reasonable correlation coefficients for the A-, B-, C- and D-series. The correlation coefficients for the B-, C-, and D-series from the Chong's equation (eq.*(10)*) are better than coefficients for the Krieger-Dougherty equation (eq.(*8*)), see Table 9 and Table 10. The Krieger-Dougherty apparent viscosity (eq.*(10)*) gives a better R^2 value for the A-series (see Table 9 and Table10), but the correlation coefficient is still in the same color range (0.80-0.89) as the Chong's viscosity in Table 11.
Comparing the Chong's apparent viscosity (eq.*(10)*) from Table 11 to the relative concentration of solids (ϕ/ϕ_{max}) in Table 8, ϕ/ϕ_{max} provides better R^2 values for the measured plastic viscosity (μ), except for the D-series.

The Chong's apparent viscosity (eq.*(10)*) has the advantage that there is no constant parameter such as intrinsic viscosity ([η]) required for the calculation, which makes the Chong's model (eq.*(10)*) more practical to use than the Krieger-Dougherty model (eq.*(8)*).

3.6.2. The graphic plots of relationships between the Chong's apparent viscosity of pore fluid and the measured plastic viscosity of matrices

Figure 22 illustrates graphic plots from the linear regression of the relationships between the measured plastic viscosity (μ), see Appendix B, and the apparent viscosity of pore fluid (η) predicted by applying the Chong's equation (eq.*(10)*), see Appendix I for the Chong's viscosity.

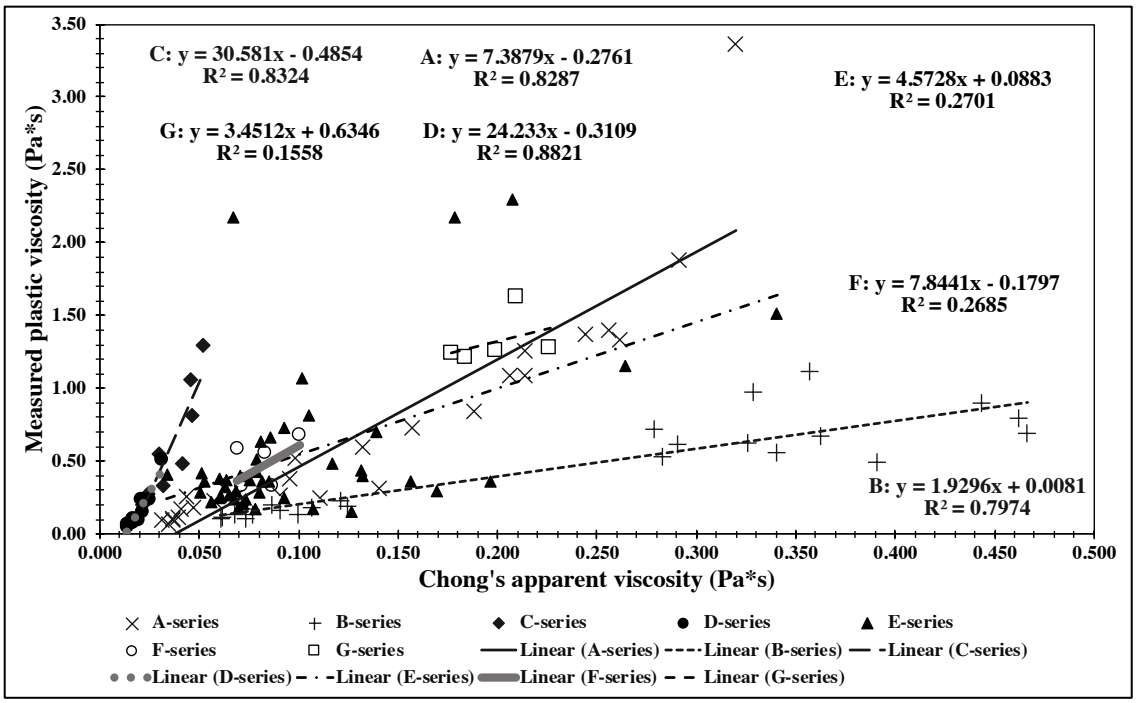

Figure 22 The plastic viscosity (μ) measured on matrices plotted against the apparent viscosity of pore fluid (η) calculated by the Chong's equation for the A-, B-, C-,D-, E-, F- and G-series.

As demonstrated in Figure 22, for the A-, B-, C- and D-series, the Chong's apparent viscosity of pore fluid (eq.*(10)*) gives a good linear relationship to the measured plastic viscosity of matrices.

The good correlations in the A-, B-, C- and D-series mean that the Chong's equation (eq.*(10)*) can be applied to predict a reasonable value for plastic viscosity (μ) of a cement paste (filler-modified paste) under the same conditions as the A-, B-, C- and D-series.
As with Figure 18, Figure 19, Figure 20 and in this section, Figure 22 demonstrates a data point in the A-series with the highest value of measured plastic viscosity (μ), which is from mix no. A21 (see Appendix B). This is discussed further in Section 3.9.1.

Figure 23 illustrates the relationships between the measured plastic viscosity of matrices (μ) and the apparent viscosity of pore fluid (η) calculated by the Chong's equation (eq.(10)), when the intercept of each regression line is forced to zero.

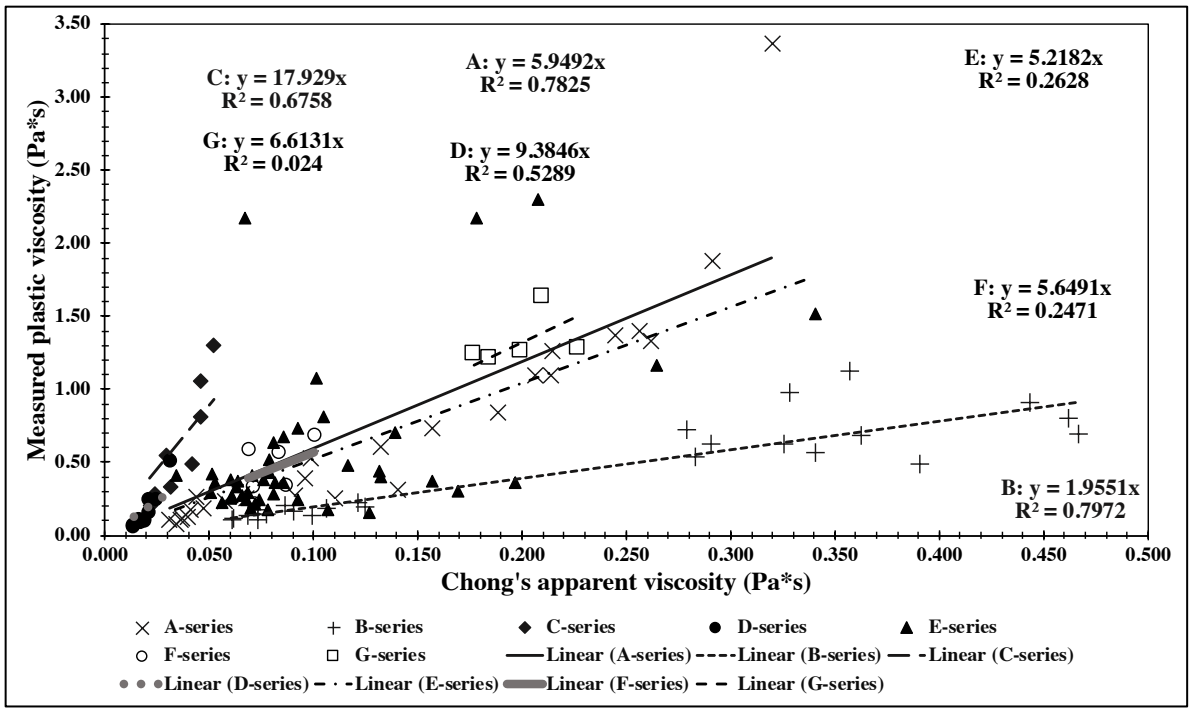

Figure 23 The plastic viscosity measured from matrices plotted against the apparent viscosity of pore fluid calculated by the Chong's equation, when the regression line for each series is forced through the origin.

As displayed in Figure 22, many of the series have either a sloping or flat regression line, which indicates that there was no one-to-one relationship. When the intercept of each series is forced through the origin, a lower correlation for each series is provided, as indicated in Figure 23. This means that the A-series is the only series where the Chong's relative viscosity (eq.(10)) can provide a reasonable prediction (R^2=0.78), with a relationship that is close to a one-to-one relationship.

3.7. The liquid thicknesses and rheology

The liquid thicknesses were described in Section 2.1.6, where equation (11) was applied for the LT1 and equation (12) for the LT2. The full calculations for LT1 had been performed by Skare (Appendix B). The full calculations for LT2 can be found in Appendix J. The values of LT1 and LT2 are summarized in Table J *1* in Appendix J.

This section presents and discusses the relationships between liquid thicknesses (LT1 and LT2) and the four rheological parameters: mini slump flow, flow resistance ratio (λ_Q), plastic viscosity (μ) and yield stress (τ_0). LT1 and LT2 are also compared and displayed as graphic plots against the latter four rheological parameters.

The four rheological parameters in this section had been measured in the laboratory on matrices with the batch size of 2.05L by Skare (see Appendix B). The trendline function described in section 2.2.7 was used to calculate the correlation coefficients (R^2 values).

3.7.1. The R^2 values of the relationships between liquid thicknesses and rheological parameters

Table 12 displays the summarized R^2 values from all of the relationships between LT1 (see Appendix J) and the four rheological parameters: average mini slump flow, the flow resistance ratio (λ_Q), the measured plastic viscosity (μ), and yield stress (τ_0) (see Appendix B for the rheology's values). The R^2 values were obtained through the trendline function (mentioned in Section 2.2.7).

Table 12 The R^2 values from the relationship between rheology and LT1.

	R^2 values from Liquid thickness 1								
	Series	A	B	C	D	E	E - no silica	F	G
Parameter	Flow resistance ratio	0.95	0.97	0.50	0.74	0.01	0.84	0.24	0.96
	Mini slump flow	0.92	0.72	0.48	0.76	0.17	0.56	0.04	0.97
	Yield stress	0.92	0.55	0.53	0.78	0.40	0.28	0.01	0.95
	Plastic viscosity	0.96	0.94	0.56	0.82	0.07	0.81	0.48	0.81

0.00-0.09	**0.10-0.49**	**0.50-0.59**	**0.60-0.69**	**0.70-0.79**	**0.80-0.89**	**0.90-1.00**

Table 13 demonstrates the summarized R^2 values from all of the relationships between LT2 (see Appendix J) and the four rheological parameters: average mini slump flow, the flow resistance ratio (λ_Q), the measured plastic viscosity (μ) and yield stress (τ_0) (see Appendix B for the values of rheology). The R^2 values were obtained through the trendline function (mentioned in section 2.2.7).

Table 13 The R^2 values from the relationships between rheology and LT2.

	R^2 values from Liquid thickness 2								
	Series	A	B	C	D	E	E - no silica	F	G
Parameter	Flow resistance ratio	0.97	0.97	0.73	0.79	0.12	0.64	0.24	0.21
	Mini slump flow	0.94	0.75	0.71	0.89	0.22	0.30	0.04	0.27
	Yield stress	0.94	0.57	0.68	0.90	0.21	0.12	0.01	0.31
	Plastic viscosity	0.97	0.94	0.68	0.95	0.08	0.58	0.48	0.36

0.00-0.09	0.10-0.49	0.50-0.59	0.60-0.69	0.70-0.79	0.80-0.89	0.90-1.00

Comparing Table 12 and Table 13, the correlation coefficients between rheology and liquid thickness were improved with the LT2 for the A-, B-, C- and D-series. The highest R^2 values from LT2 were obtained in the A-, B- and D-series, which means that adjusting the SSA, VFF, and the volume of the solid fraction can be used to predict the rheology's values in a cement paste (filler-modified paste) with the same conditions as these series.

There were almost no improvements for the correlation coefficients for the E- and F-series, since they remained in the same color range in Table 12 and Table 13. However, by excluding the mixes with silica fume from the E-series, the correlation coefficients of rheological parameters improved for LT1 and LT2, except for yield stress (τ_0). The possible errors of τ_0 are further discussed in Section 3.9.2. The F-series also contained mixes with silica fume, but since there were only two mixes (of six mixes) with no silica fume in the F-series (Appendix B), more data are required to analyze the effect of silica fume on the F-series.
The highly positive improvements in the E-series without silica fume and the G-series for LT1 seem to be questionable. This is discussed further in Section 3.7.2 with Figure 26 for the E-series, and in Section 3.9.3 for the G-series.

3.7.2. The graphic plots of relationships between liquid thickness models and rheology of matrices

Figure 24 illustrates the relationships of liquid thicknesses (LT1 and LT2) plotted against the flow resistance ratio (λ_Q), see Appendix B, and Figure 25 illustrates the relationships of liquid thicknesses (LT1 and LT2) plotted against the plastic viscosity (μ), see Appendix B.
Figure 24 and Figure 25 provide some examples of the graphic plots from the relationships between LT1, LT2, and rheology, with the best correlation coefficients from Table 12 and Table 13. All the plots of relationships between LT1 and LT2 and rheology can be found in Appendix J, Figure J 1 to Figure J 8.

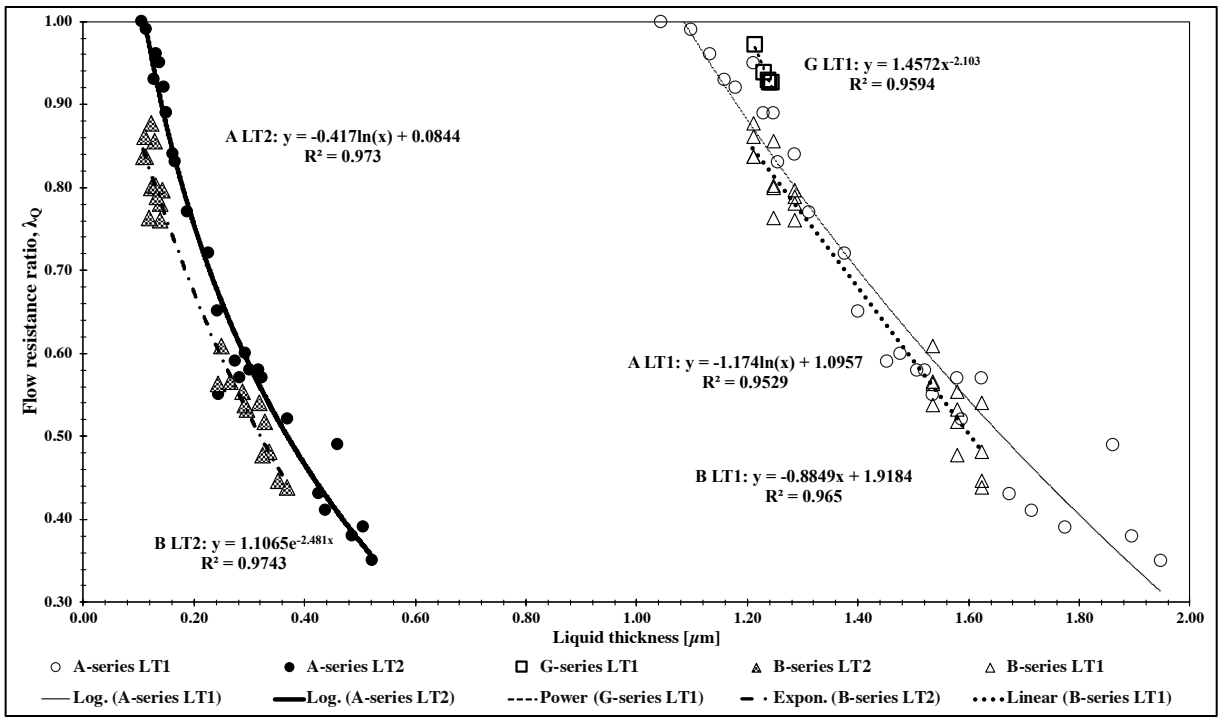

Figure 24 The relationships of liquid thicknesses (LT1 and LT2) on flow resistance ratio (λ_Q) from the series with the best R^2 values.

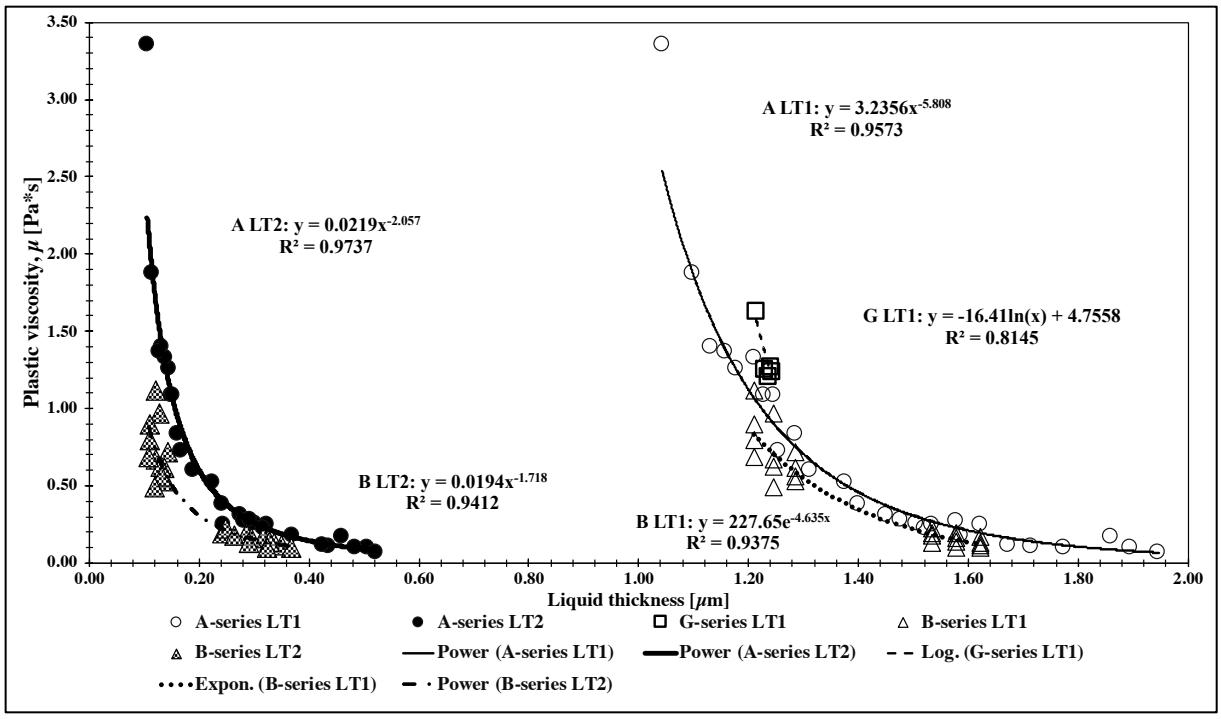

Figure 25 The relationships of liquid thicknesses (LT1 and LT2) on plastic viscosity (μ) from the series with the best R^2 values.

The relationships in Figure 24 and Figure 25 imply that the flow resistance (λ_Q) and plastic viscosity (μ) decrease with increasing LT1 and LT2. As demonstrated in Section 2.1.6, equation *(11)* and *(12)* indicate that a higher SSA would provide a lower value of liquid thickness. This means that the matrices pastes (or filler-modified pastes) are more viscous with lower liquid thickness. Jacobsen et al. [6] also states that a cement paste with a denser and thicker consistency is less flowable and has a higher flow resistance ratio. The same reasoning applies to mini slump flow, where the mini slump flow increases with increasing LT1 and LT2 (see Appendix J, Figure J 3 and Figure J 4).

Yield stress (τ_0) also decreases with increasing LT1 and LT2 (see Appendix J, Figure J 5and Figure J 6) The behavior of τ_0 can be described by the Bingham fluid model (mentioned in Section 2.1.2), where a thick and dense paste with a high yield stress will require more load or stress before the paste starts to flow.

Figure 25 also displays a data point in the A-series with the highest measured plastic viscosity (μ), mix no. A21 (see Appendix B). This is discussed further in section 3.9.1.

It should be noted that for some of the plots from the E- and F-series, the behaviors above only appeared when the mixes with or without silica fume were separated. Figure 26 (a) and (b) illustrate some examples of these type of plots, and all the plots can be found in Appendix J, Figure J 1 to Figure J 8.

Figure 26 (a) and (b) illustrate the relationships between LT1, LT2, and measured λ_Q (Appendix B) from the E- and F-series, with (a) regression analysis for all mixes for each series and (b) regression analysis separated by mixes with and without silica fume for each series.

Figure 26 (a) illustrates the plots of LT1, LT2, and measured λ_Q from all the mixes in the E- and F- series, where the LT2 for the F-series and the LT1 for the E- and F-series behaved in the opposite way from the other series, as discussed above. Figure 26 (b) demonstrates that after separating the mixes in the E- and F-series with or without silica fume, the relationships behaved in the same way as with the other series.

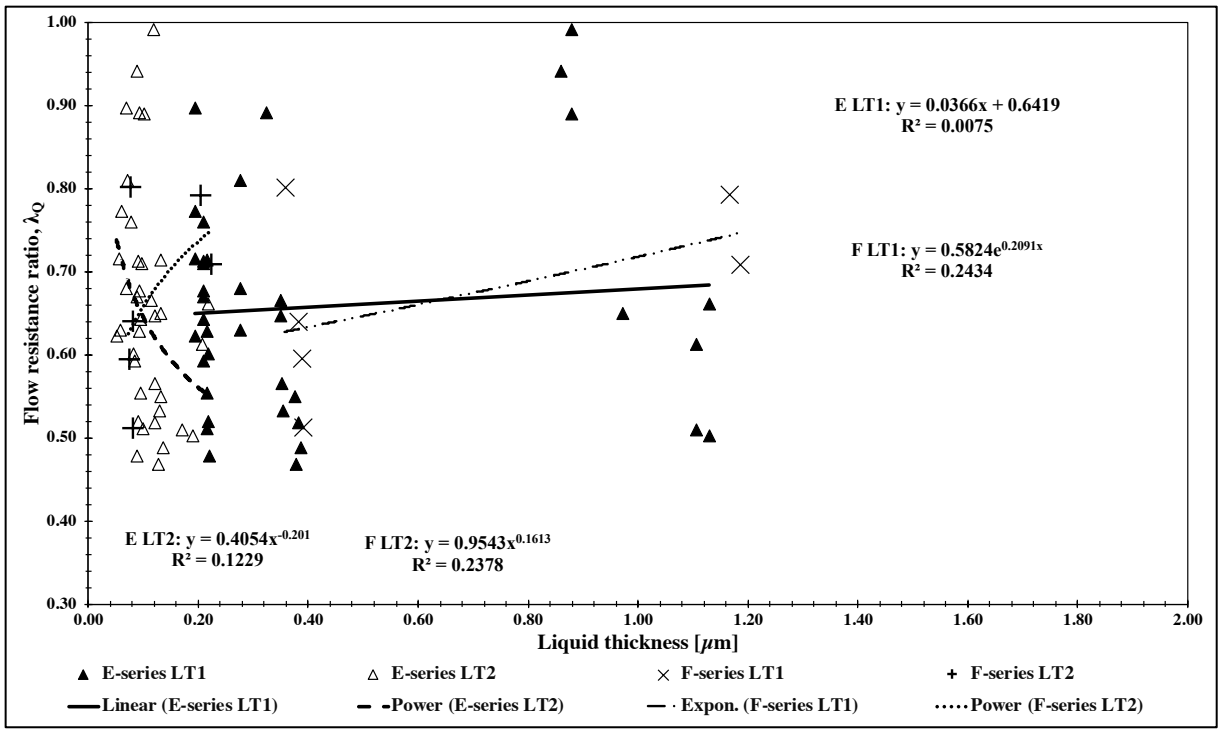

(a)

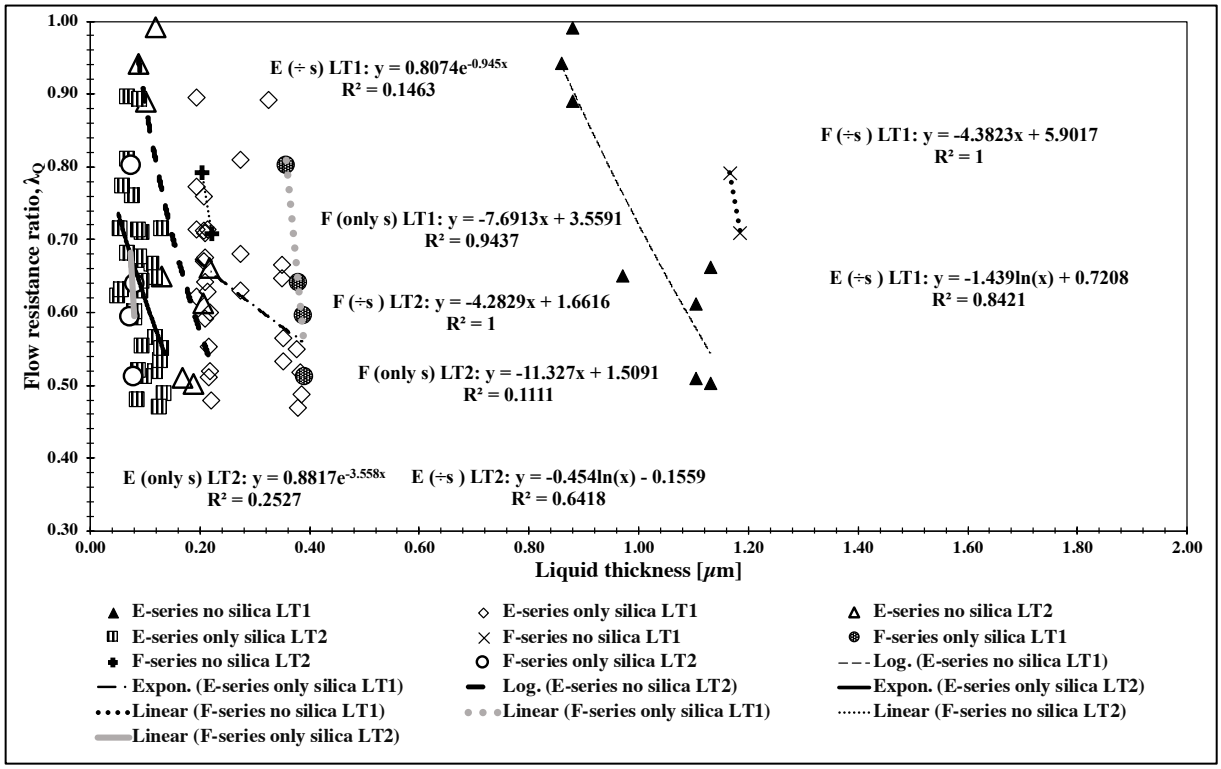

(b)

Figure 26 The relationships between liquid thicknesses (LT1, LT2) and flow resistance ratio measured on matrices (λ_Q) from the E- and F-series, with (a) regression analysis for all mixes for each series and (b) regression analysis separated by mixes with and without silica fume for each series.

In addition, Figure 26 (b) also illustrates the separation of the E- and F-series into two different groups of data sets, which clearly displays as the plots of the E-series for LT1, and the F-series for LT1 and LT2. This seems to be the explanation for the highly positive improvements in the E-series with on silica fume for LT1, mentioned in Section 3.7.1. Since the data points from the E-series with no silica are clumped in a group, the mixes without silica fume are clearly much more highly correlated than all the mixes in the E-series analyzed together.

The separations of LT1 in the E- and F-series into two different groups (see Figure 26 (b)), have indicated that LT1 seems to be the parameter that can be used to sort out the effect of silica fume on liquid thickness. Additionally, LT1 (for the E-series) indicates that the mixes with no silica fume had a much higher liquid thickness than the mixes containing silica fume.

It should be taken into account that there were 44 measurable mixes in the E-series, while there were only 6 mixes in the F-series (see Appendix B). Therefore, it is too soon to draw any conclusions for the F-series, since the results could either be related to silica fume content or could only be a coincidence. However, Figure 26 (b) has clearly demonstrated that silica fume affected the relationship between the suspension parameters, LT1 and LT2, in the E-series.
This will be further studied and investigated by Skare in her doctoral thesis.

3.8. The empirical model

The empirical model (eq.*(3)*) was described in section 2.1.3, and the full calculations and values of flow resistance ratio (λ_Q) can be found in Appendix A.

This section introduces the summarized values of constants k_c, k_s, k_{fa}, k_{sp} and k_f, and their correlation coefficients (R^2 values). The constants in this section were calculated through the Microsoft Excel add-in program "Solver" as the analysis tool, and the trendline function in Microsoft Excel was used to calculate the R^2 values (as mentioned in Sections 2.1.7 and 2.2.7). The detailed calculations of regression analysis by Solver, trendline function, and the values of calculated flow resistance ratio (λ_Q) from the empirical model (eq.*(3)*) are summarized in Table A 1 and Table A 2 in Appendix A.

This section also presents the relationships between the calculated flow resistance ratio from the empirical model (eq.*(3)*) and the measured flow resistance from the laboratory,

The measured flow resistance (λ_Q) in this section had been measured in the laboratory on matrices with the batch size of 2.05L by Skare (see Appendix B).

3.8.1. The constants k_c, k_s, k_{fa}, k_{sp}, k_f and R^2 values solved by Solver

Table 14 and Table 15 display the summarized constants k_c, k_s, k_{fa}, k_{sp}, k_f and R^2 values calculated by the Solver (see Sections 2.1.7 and 2.2.7) using the new empirical model (eq. *(3)*), compared to the measured flow resistance (λ_Q) from the laboratory (Appendix B).

The values in Table 14 were calculated to fit the regression line for each of the series individually (varying k_c, k_s, k_{fa}, k_{sp} and k_f), while the values in Table 15 were calculated to fit the regression line for all series (constant k_c, k_s, k_{fa}, k_{sp} and k_f), see Appendix A.

For the A-, B- and G- series, there were no values for k_{fa} and k_s since the series did not contain any FA or silica fume. Similarly for the C- and D-series, there were no values for k_s because they did not contain silica fume.

The values of all the calculated flow resistance ratios (λ_Q) are summarized in Table A 1 and Table A 2 in Appendix A.

Table 14: The constants (k_c, k_s, k_{fa}, k_{sp} and k_f) and R^2 values from the regression analysis of the empirical model solved with varying constants (k_c, k_s, k_{fa}, k_{sp} and k_f) for each series.

	The empirical model with varying constants								
	Series	**A**	**B**	**C**	**D**	**E**	**F**	**G**	**All**
Constant	k_c	0.507	0.385	0.769	0.101	0.414	0.972	0.950	-
	k_{fa}	-	-	1.272	-1.291	1.499	5.998	-	-
	k_s	-	-	-	-	2.725	-7.049	-	-
	k_f	0.003	-0.0001	0.005	-0.002	0.000002	0.008	-0.042	-
	k_{sp}	-0.709	-0.114	-1.266	0.818	-0.150	-2.048	0.985	-
λ_Q	R^2	0.97	0.93	0.96	0.86	0.53	0.79	-	0.88

0.00-0.09	0.10-0.49	0.50-0.59	0.60-0.69	0.70-0.79	0.80-0.89	0.90-1.00

Table 15 The constants (k_c, k_s, k_{fa}, k_{sp} and k_f) and R^2 values from the regression analysis of the empirical model solved with constant constants (k_c, k_s, k_{fa}, k_{sp} and k_f) for all series.

	The empirical model with constant constants								
	Series	**A**	**B**	**C**	**D**	**E**	**F**	**G**	**All**
Constant	k_c	-	-	-	-	-	-	-	0.403
	k_{fa}	-	-	-	-	-	-	-	0.779
	k_s	-	-	-	-	-	-	-	4.043
	k_f	-	-	-	-	-	-	-	0.0005
	k_{sp}	-	-	-	-	-	-	-	-1.165
λ_Q	R^2	0.90	0.91	0.64	0.43	0.42	0.38	-	0.72

0.00-0.09	0.10-0.49	0.50-0.59	0.60-0.69	0.70-0.79	0.80-0.89	0.90-1.00

Table 14 and Table 15 have clearly demonstrated that when using Solver to calculate the constants (k_c, k_s, k_{fa}, k_{sp} and k_f) for each series, the correlation coefficients were better than when constants k_c, k_s, k_{fa}, k_{sp} and k_f were used for all the series. This is because the calculation of λ_Q with the constants k_c, k_s, k_{fa}, k_{sp} and k_f for all series was performed to obtain an average value to fit all series. This meant that the empirical model (eq.*(3)*) would give the best results when the constants are analyzed for each series.

From Table 14 and Table 15, the A-, B- and C-series provided the best R^2 values of all the series, while the E- and F-series presented the poorest correlation coefficients of all the series. There was no R^2 value for the G-series, because the λ_Q values from the empirical model (calculated by Solver) were calculated to be the same value for all the mixes in the G-series. The plot of the G-series is a flat vertical line with the undefined R^2 value (see Section 3.8.2 for the graphic plot).

Comparing Table 8, Table 13 and Table 14 the empirical model provides a better correlation coefficient for the measured flow resistance than the relative concentration of solids (ϕ/ϕ_m) and the LT2, when only the A-, C- and D-series are compared. ϕ/ϕ_m and LT2 provided a better R^2 value for the measured flow resistance (λ_Q) in the B-series, where $R^2 = 0.97$ for ϕ/ϕ_m and LT2, and $R^2 = 0.93$ for the empirical model (see Table 8, Table 13 and Table 14). However, $R^2 = 0.93$ for the empirical model (for the B-series) is still in the green color range and can also be considered as one of the best correlation coefficients for the measured flow resistance ratio (λ_Q).
This means that the empirical model (eq.(*3*)) has been proven to be the best model for predicting the values of the flow resistance. However, the relative concentration of solids (ϕ/ϕ_m) and the LT2 still provided high R^2 values for the flow resistance, which means that the parameters would still offer an ideal prediction or (almost) one-to-one relationship for the flow resistance ratio (λ_Q) under certain conditions (as the series with best R^2 values).

In addition, some negative values of the constants k_s, k_{fa}, k_{sp} and k_f in some series can be observed from Table 14. This should be studied further in Skare's doctoral thesis.

3.8.2. The graphic plots of predicted flow resistance from the empirical model compared to flow resistance ratio measured from the laboratory

Figure 27 (a) and (b) illustrate the relationships of the predicted flow resistance ratio, λ_Q predicted (Appendix A) plotted against the measured flow resistance on matrices from the laboratory, λ_Q measured (Appendix B). Figure 27 (a) and (b) contain some examples from the graphic plots of the relationships between λ_Q predicted and λ_Q measured, with the best R^2 values from Table 14 and Table 15, except for the G-series (undefined R^2). All the plots of relationship between λ_Q predicted and λ_Q measured can be found in Appendix A, Figure A 1 to Figure A 4.

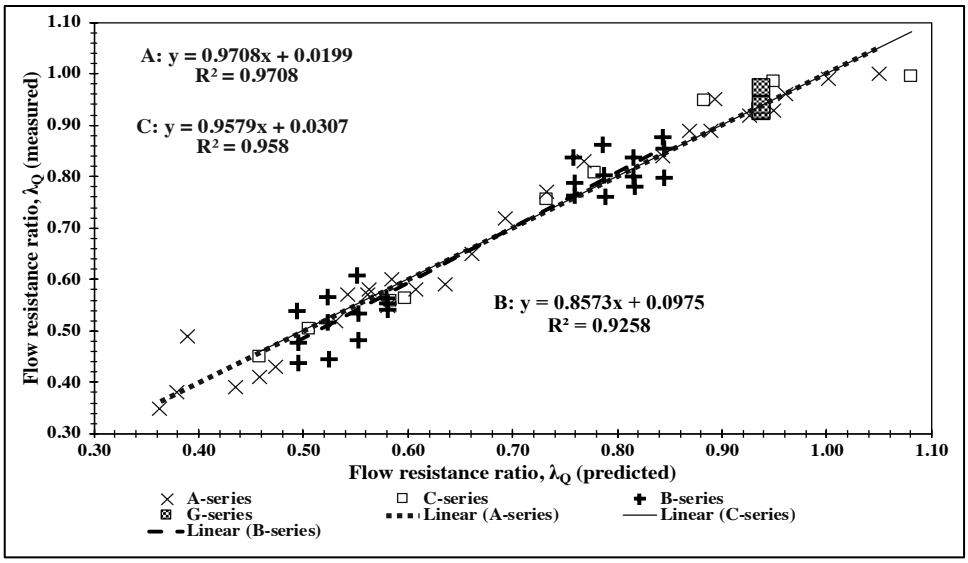

(a)

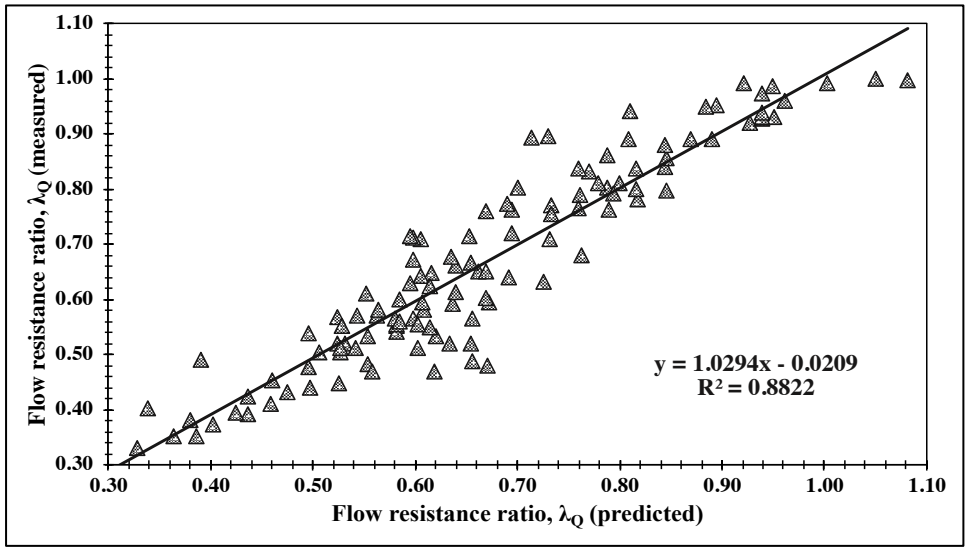

(b)

Figure 27 The relationships between the predicted flow resistance ratio (λ_Q predicted) from the empirical model and the measured flow resistance (λ_Q measured) on matrices from laboratory, from (a) the series with the best R^2 values, except for the G-series and (b) all the series.

As indicated in Figure 27 (a) and (b), λ_Q predicted from the empirical model (Appendix A) has clear relationships with λ_Q measured on matrices from the laboratory (Appendix B). The best R^2 values were from the A-, B- and C-series, with a reasonable correlation coefficient for all series (see Table 14 and Table 15), with varying constants (k_c, k_s, k_{fa}, k_{sp} and k_f). The high correlation coefficients in Table 14 and Table 15 imply that the empirical model (eq.*(3)*) can be used to predict the flow resistance for the filler-modified paste with the same type of materials and volume fractions of particles, as Mørtsell found in his first empirical model in his doctoral thesis [7].

Figure 28 (a) and (b), see the next page, illustrate the relationships between predicted flow resistance ratio (λ_Q predicted) from the empirical model (eq.(3)), and measured flow resistance (λ_Q measured) on matrices from the laboratory with varying intrinsic viscosity for (a) the A-, B- and C-series, and (b) all series, when the intercept of each regression line is forced to zero.

As demonstrated in Figure 28 (a) and (b), Mørtsell's empirical model (eq.(3)) has been proven to be the model that provides the best prediction for measured flow resistance (λ_Q measured) on matrices from laboratory, especially for the A-, B-, C-, D- and all series. A reasonable prediction was also obtained for the F-series, but since there were only six mixes in the F-series (see Appendix B) it is too soon to draw any conclusions for the F-series.
It should be noted that the E-series still provides a poor correlation coefficient, even though the R^2 value for all series is high, as indicated in Figure 28 (b). This should be considered when using the empirical model for a filler-modified paste with the same conditions as the mixes in the E-series.

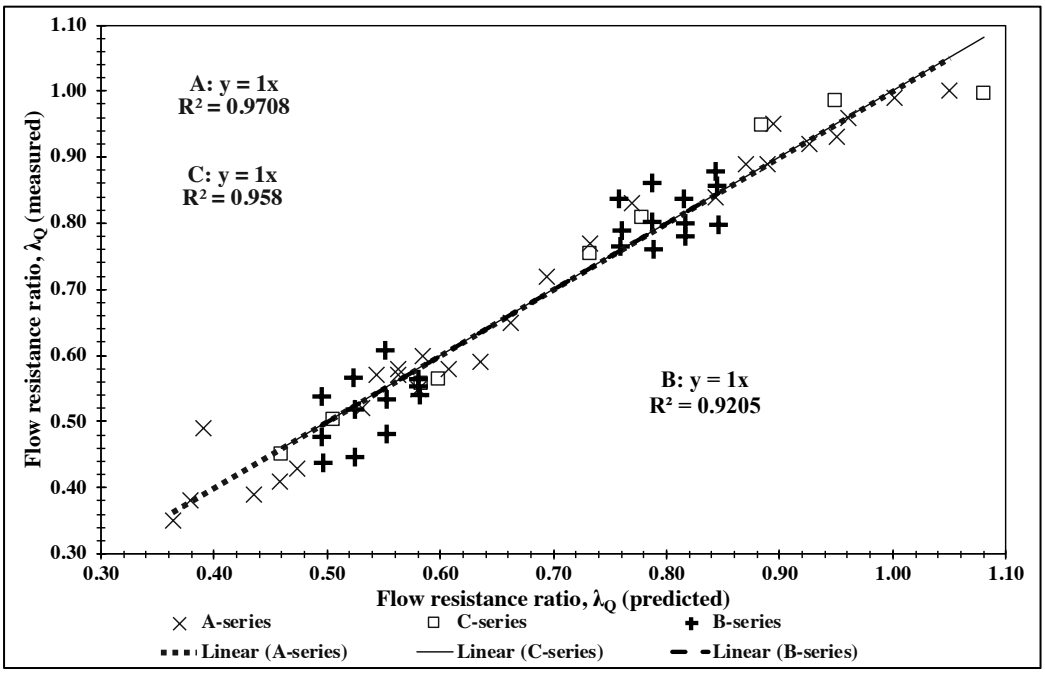

(a)

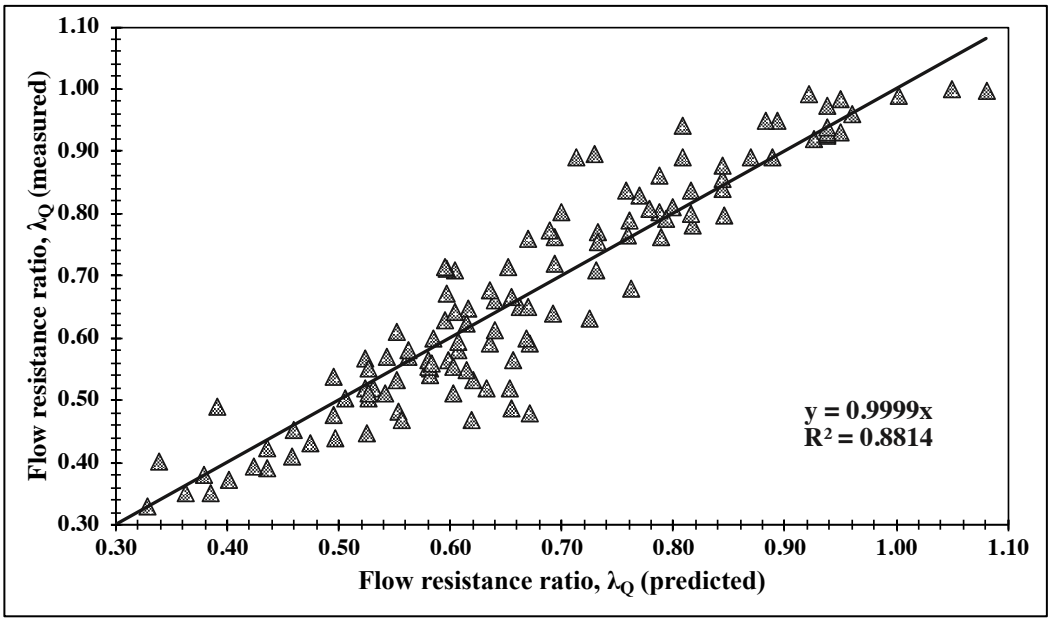

(b)

Figure 28 The relationships between the predicted flow resistance ratio (λ_Q predicted) from the empirical model and the measured flow resistance (λ_Q measured) on matrices from the laboratory for (a) the A-, B- and C-series and (b) all series, when the regression lines are forced through the origin.

3.9. Errors and sensitivity of regression analysis

From the analysis and values in Chapter 3 so far, some unusual values and plots have been observed that may be caused by the constituents of the mix, or errors in the regression analysis from Microsoft Excel. The sections below describe some of the errors that were found in this study.

3.9.1. Problematic mix with high filler content and solid fraction

As displayed in Figure 18, Figure 19, Figure 20, Figure 21, Figure 22, and Figure 25, mix no. A21 was observed to produce the highest value of plastic viscosity (μ) measured on matrices with the batch size of 2.05L by Skare (see Appendix B). As with the plots for yield stress (τ_0) for the A-series, which can be seen in Figure F 4 (a) and Figure J 5 (a).
By looking closely at the mix's constituents/parameters, it appears that the A21 had the lowest w/b with high fi/b and solid fraction. Additionally, the filler type for this mix was the "fine" filler (see Appendix B), which were the finest filler's particles.
This means that it is difficult to predict a mix with high fi/b, solid fraction, and low w/b like mix A21 with the micro-proportioning models/parameters in this study.

3.9.2. Problematic calculation of the R^2 values

As mentioned in Section 3.7.1, the relationships between LT1, LT2, and yield stress (τ_0) were not improved by excluding the mixes with silica fume, as indicated in Table 12 and Table 13. This can be explained by the graphic plot of the relationship between LT1 and τ_0 (see Figure 29 (a) and (b)).

Figure 29 (a) and (b) illustrate the graphic plots of the relationships between LT1 and τ_0 from the E-series with the line of the average yield stress of each of the plots. Figure 29 (a) illustrates the relationship between yield stress and LT1 for all of the mixes from the E-series, and Figure 29 (b) illustrates the same relationship where the mixes from E-series are separated by mixes without silica fume and mixes with only silica fume.

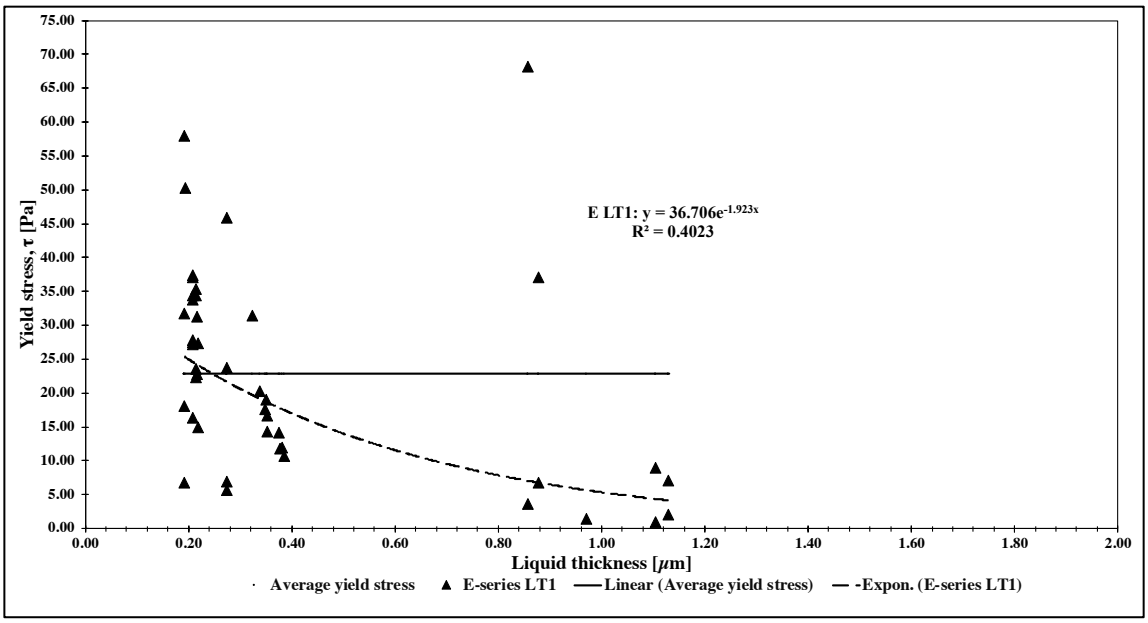

(a)

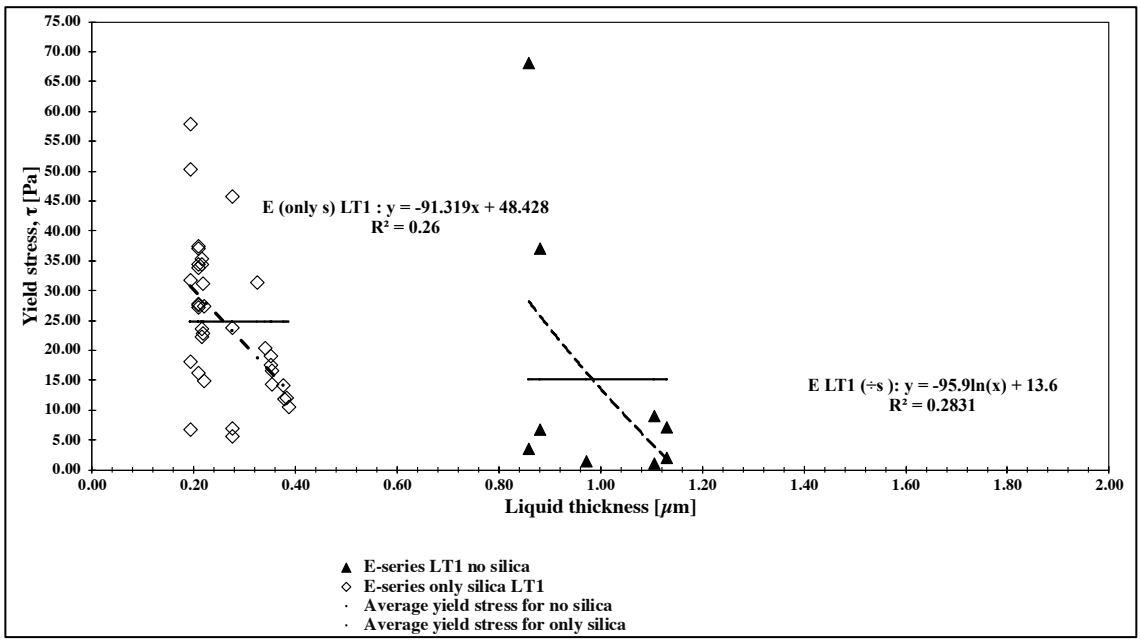

(b)

Figure 29 The relationships of LT1 and yield stress (τ_0) with the average line of yield stress values from (a) all the mixes from the E-series and (b) the mixes without silica fume and the mixes with only silica fume from the E-series

Figure 29 (a) demonstrates that the LT1 for the E-series has $R^2 = 0.40$, while Figure 29 (b) has $R^2 = 0.28$ (no silica) and $R^2 = 0.26$ (only silica). This result seems odd due to the larger/wider spread of the data in Figure 29 (a), which should have provided a lower correlation coefficient, while the data in Figure 29 (b) were clumped in two different groups and the correlations should therefore be more accurate.

This clearly demonstrates the error with the regression analysis by the trendline function in Excel. The analysis of the R^2 value is based on the mean value from the y-axis (see equation *(13)*, *(14)* and *(15)* in Section 2.1.7). This means that the regression line responds to the mean value from the y-axis, disregarding the data from x-axis. Therefore, the correlation coefficient in Figure 29 (a) is higher than the coefficients in Figure 29 (b), since many of the data points are closer to the mean value of y.

This means that the R^2 value obtained through the trendline function in Excel may not be relevant in some situations. One should interpret the values together with illustration of the data as a graphic plot or find more suitable methods to evaluate the data.
It should be noted that Figure 29 (a) and (b) are just some examples of the plots with these problems; all of the plots can be found in Appendix J.

3.9.3. Sensitivity of trendline function

Figure 30 illustrates the graphic plots of the relationships between LT1, LT2, and yield stress (τ_0) from the G-series, which indicates that the data from the G-series for both LT1 and LT2 seem very similar, but the R^2 value for LT1 is much higher than for LT2.

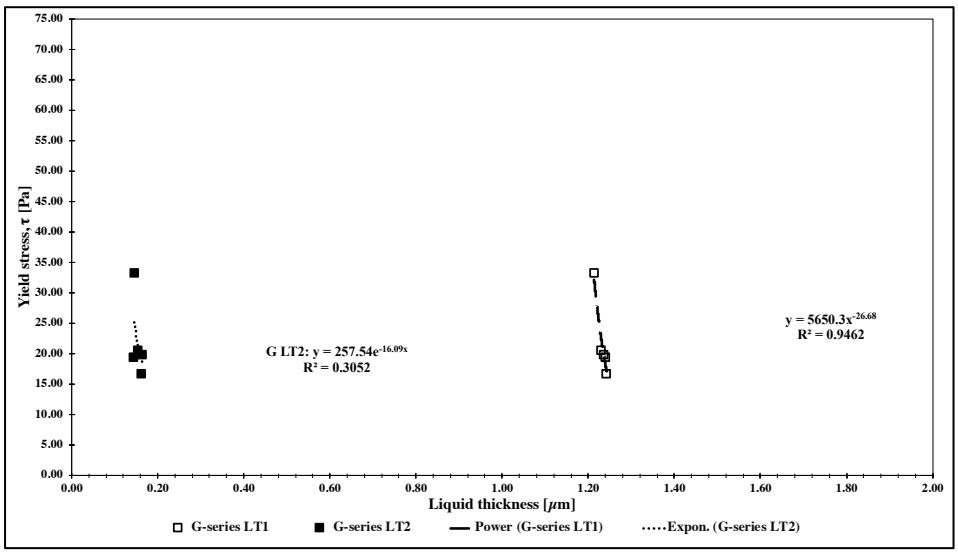

Figure 30 The relationships of liquid thickness models (LT1 and LT2) on yield stress (τ_0) from G-series.

Figure 30 indicates another problem of the trendline function in Excel, which is its sensitivity to small group of data points, where a small value could cause extreme changes to the correlation coefficient. It is therefore important to be more critical of the R^2 value of a regression line from a small number of data points/series.

4. Conclusion and further work

The following main conclusions can be drawn from this study.

The methods in the laboratory:

- The trial and error test demonstrated that in order to obtain the most EF volume with the least solids remaining, the best method for handling samples after the centrifugation is to pour EF directly into a beaker/cup, and then use a syringe and a filter of a proper size.
- The opacity and transparency of EF depends on the SP dosage, FA content, and silica content in the pastes.
- The solids content in the EF is independent of its filtration. It seems to be unpredictable, and what remains in the filter should be investigated further if possible.
- The centrifugation of maximum packing was simple and precise, and it resulted in well packed particles/pastes.
- When the SP dosage was 1.75% of the cement content, the particles could not be packed, and the pastes were not stiff after the centrifugation.
- The dynamic viscosity of pore fluid increases with increasing SP dosage, with a saturation point at SP dosage=1.50% of the cement content
- The flow time measurements were precise since it provided an accurate set of times.
- The viscometer no. 75 with no filtration gave less accurate results than the viscometer no. 50 with filtration.
- The inaccuracy of the viscometer in time measurements led to inaccuracy in the dynamic viscosity of pore fluid.
- It would be more accurate if a volumetric flask were used to measure the exact volume of the EF, in order to find the accurate density of the EF.
- Solids content in the EF has little effect on its kinematic viscosity and dynamic viscosity. Therefore, inaccuracy in the density of the EF also has little effect on its dynamic viscosity and kinematic viscosity.

The regression analysis:

Mini slump flow, flow resistance ratio (λ_Q), plastic viscosity (η), and yield stress (τ_0) have been proven to be dependent on the characteristics of the materials in the mixture, as demonstrated by the high correlation coefficients of the five micro-proportioning approaches from the regression analysis: the Krieger-Dougherty model [1], the relative viscosity by Chong et al. [2], the relative concentration of solids (ϕ /ϕ_{max}) [2-5], the liquid thickness based on Powers, 1968 [6], and the empirical model of Mørtsell [7].

The best correlation coefficients in this study were assumed to be when the R^2 values are between 0.90 and 1.00, in accordance with Skare and Professor Jacobsen. While the R^2 values between 0.70 and 0.89 are considered to be reasonable correlation coefficients, according to Bentz et al. [5]. The reasonable to best correlations demonstrate that the micro-proportioning approaches may, in certain conditions, be used to determine the rheological properties of a cement paste (filler-modified paste).

The following main conclusions from the regression analysis are as follows:

- The relative concentration of solids (ϕ/ϕ_m), the Chong's apparent viscosity of pore fluid (eq.*(10)*), and the empirical model (eq.*(3)*) provide good correlations with the rheology for the A-, B-, C- and D-series.
- The Krieger-Dougherty model (eq.*(8)*) and the liquid thicknesses (LT1, LT2) provide high correlations for the A-, B- and D-series, but not for the C-series.
- The E-, F- and G-series were problematic for the models and suspension parameters in this study, either because of the silica content or the small number of data points.
- The A-series is the only series that provided the best or reasonable correlation coefficients for all five of the micro-proportioning approaches.
- The empirical model (eq.*(3)*) is the best model for predicting the flow resistance ratio (λ_Q) of filler-modified pastes.
- The negative values of the constants k_s, k_{fa}, k_{sp} and k_f from the empirical model (eq.*(3)*) will be studied in Skare's doctoral thesis.
- LT1 seems to be the suspension parameter that can sort out the effect of silica fume on liquid thickness, since it separated the E-series into two groups: one with silica fume and one without silica fume.

- It is difficult to predict a mix with high fi/b, solid fraction and low w/b with the micro-proportioning models/parameters in this study.
- The R^2 value from the trendline function in Excel may not be relevant in some situations. The interpretation of the values should be studied together with illustration of the data, or more suitable methods should be found to evaluate the data.

The study of these models and parameters has proven that a quantitative analysis of these micro-proportioning approaches on particle characteristics, with proper methods, can be used to control or predict the rheological properties of a cement paste.
However, this master thesis is only a small part of the bigger project, the MiKS project, which is supposed to last until 2021. There are more works and investigations that need to be undertaken in Skare's doctoral thesis.

The further work from this master thesis is to study the E-, F- and G-series further, in order to find suitable models for these types of mixes/pastes, or to develop a larger series with more data. There is also a possibility of developing the empirical model by adding more parameters such as the apparent viscosity of pore fluid from the Krieger-Dougherty equation, the relative concentration of solids, and the liquid thicknesses. Certainly, with the good correlation coefficients from the A-, B-, C- and D-series, these series should be investigated further to ascertain their usefulness and determine the possibility of creating a cement paste made of crushed aggregates.

References

[1] I.M. Krieger, T.J. Dougherty, A mechanism for non-Newtonian flow in suspensions of rigid spheres, Transactions of the Society of Rheology, 3 (1959) 137-152.

[2] J.S. Chong, E.B. Christiansen, A.D. Baer, Rheology of concentrated suspensions, 15 (1971) 2007-2021.

[3] H. Justnes, H.J.A.T.N.R.S. Vikan, Viscosity of cement slurries as a function of solids content, 13 (2005) 75-82.

[4] L. Struble, G.-K. Sun, Viscosity of Portland cement paste as a function of concentration, Advanced Cement Based Materials, 2 (1995) 62-69.

[5] D.P. Bentz, C.F. Ferraris, M.A. Galler, A.S. Hansen, J.M. Guynn, Influence of particle size distributions on yield stress and viscosity of cement–fly ash pastes, Cement and Concrete Research, 42 (2012) 404-409.

[6] S. Jacobsen, M. Maage, S. Smeplass, K.O. Kjellsen, E.J. Sellevold, J. Lindgård, R. Cepuritis, R. Myrdal, Ø. Bjørntegaard, M. Geiker, Concrete Technology, NTNU, Trondheim, 2016.

[7] E. Mørtsell, Modellering av delmaterialenes betydning for betongens konsistens, Department of Structural Engineering, Group for Concrete, NTNU, Trondheim, 1996.

[8] R. Cepuritis, Development of Crushed Sand for Concrete Production with Microproportioning, Department of Structural Engineering, NTNU, Trondheim, 2016.

[9] R. Cepuritis, S. Jacobsen, S. Smeplass, E. Mørtsell, B.J. Wigum, S. Ng, Influence of crushed aggregate fines with micro-proportioned particle size distributions on rheology of cement paste, Cement and Concrete Composites, 80 (2017) 64-79.

[10] R. Cepuritis, S. Jacobsen, T. Onnela, Sand production with VSI crushing and air classification: Optimising fines grading for concrete production with micro-proportioning, Minerals Engineering, 78 (2015) 1-14.

[11] R. Cepuritis, E.J. Garboczi, C.F. Ferraris, S. Jacobsen, B.E. Sørensen, Measurement of particle size distribution and specific surface area for crushed concrete aggregate fines, Advanced Powder Technology, 28 (2017) 706-720.

[12] B.J. Wigum, S.W. Danielsen, O. Hotvedt, B. Pedersen, Production and Utilisation of Manufatured Sand. COIN Project report 12-2009, SINTEF, Trondheim, 2009.

[13] E.L. Skara, R. Cepuritis, S. Jacobsen, Microproportioning with Crushed Sand, 2018.

[14] PennState, 1.5 - The Coefficient of Determination, r-squared, Regression Methods, The Pennsylvania Statet University, 2018.
[15] Micromeritics, SediGraph III PLUS Particle Size Analyzer, U.S.A.
[16] StandardNorge, NS-EN 196-6:2010, Methods of testing cement, Part 6: Determination of fineness, Standard.no, 2010.
[17] D.A. Williams, A.W. Saak, H.M. Jennings, The influence of mixing on the rheology of fresh cement paste, Cement and Concrete Research, 29 (1999) 1491-1496.
[18] S. Ng, H. Mujica, S. Smeplass, Design of a simple and cost-efficient mixer for matrix rheology testing, Nordic Concrete Research, 51 (2014) 15-28.
[19] R. Cepuritis, S. Jacobsen, B. Pedersen, H.V. Vikan, K. De Weerdt, Rheology of matrix and SCC with different mineral fillers and admixtures. COIN Project report 41-2012, SINTEF, Trondheim, 2012.
[20] Hettich, UNIVERSAL 320/R BENCHTOP CENTRIFUGE.
[21] S. Ng, Kinematic viscosity of filler pore solution with and without superplasticizers, Memo, SINTEF, Norway, 2016.
[22] CannonInstrument, Cannon-Fenske Routine Viscometers.
[23] ASTM Designation D 2515, Specification for kinematic glass viscometers, ASTM International, 1966.
[24] FrontlineSolvers, Excel Solver Tutorial - Step by Step Easy to use guide for Excel's solver, 2018.
[25] J. Kestin, M. Sokolov, W.A.J.J.o.P. Wakeham, C.R. Data, Viscosity of liquid water in the range− 8 C to 150 C, 7 (1978) 941-948.
[26] E.L. Skare, The influence of paste constituents on viscosity of filler modified paste, 2018.

Appendix A Flow resistance ratio from the empirical model and Solver's analysis

The full calculation and Solver's analysis of flow resistance ratio from the empirical model (eq. *(3)*) can be found as an online appendix uploaded as an excel file "The empirical model-Lambda Q analysis.xlsx" on:

https://www.dropbox.com/s/t42yalf3fb29we2/The%20empirical%20model-Lambda%20Q%20analysis.xlsx?dl=0

Note that the measured flow resistance (λ_Q) in this Appendix had been taken from Appendix B.

All the online Appendixes are uploaded in the folder "TKT4925 Concrete Technology Master's thesis Appendices – Metathip Sihaklang" on:
https://www.dropbox.com/sh/2b6ybeshelxa0km/AAB0KqYhQlAyVkCcG64TCbCva?dl=0

Table A 1 The measured flow resistance ration from laboratory and the flow resistance ratio from empirical model calculated by Solver analysis for all series (constant k_c, k_s, k_{fa} k_{sp} and k_f)

A-series									C-series			D-series		
Mix no.	$\lambda_{Q,P}$	$\lambda_{Q,M}$	**Mix no.**	$\lambda_{Q,P}$	$\lambda_{Q,M}$	**Mix no.**	$\lambda_{Q,P}$	$\lambda_{Q,M}$	**Mix no.**	$\lambda_{Q,P}$	$\lambda_{Q,M}$	**Mix no.**	$\lambda_{Q,P}$	$\lambda_{Q,M}$
1	0.91	0.89	**10**	0.90	0.84	**19**	0.93	0.93	**1**	0.69	0.81	**1**	0.69	0.76
2	0.92	0.92	**11**	0.90	0.87	**20**	0.94	0.99	**2**	0.78	0.99	**2**	0.60	0.55
3	0.93	0.96	**12**	0.91	0.89	**21**	0.96	1.00	**3**	0.63	0.56	**3**	0.54	0.39
4	0.66	0.58	**13**	0.64	0.54	**22**	0.69	0.72	**4**	0.60	0.50	**4**	0.49	0.33
5	0.67	0.59	**14**	0.65	0.56	**23**	0.70	0.77	**5**	0.59	0.45	**5**	0.60	0.47
6	0.68	0.65	**15**	0.66	0.58	**24**	0.71	0.83	**6**	0.65	0.56	**6**	0.52	0.42
7	0.52	0.39	**16**	0.50	0.36	**25**	0.55	0.52	**7**	0.74	1.00	**7**	0.51	0.37
8	0.53	0.41	**17**	0.50	0.38	**26**	0.56	0.58	**8**	0.67	0.95	**8**	0.46	0.40
9	0.53	0.43	**18**	0.51	0.39	**27**	0.57	0.60	**9**	0.62	0.75	**9**	0.67	0.35
												10	0.60	0.33

B-series														
Mix no.	$\lambda_{Q,P}$	$\lambda_{Q,M}$	**Mix no.**	$\lambda_{Q,P}$	$\lambda_{Q,M}$	**Mix no.**	$\lambda_{Q,P}$	$\lambda_{Q,M}$	**Mix no.**	$\lambda_{Q,P}$	$\lambda_{Q,M}$	**Mix no.**	$\lambda_{Q,P}$	$\lambda_{Q,M}$
1	0.86	0.80	**6**	0.84	0.84	**11**	0.76	0.76	**16**	0.57	0.48	**21**	0.55	0.57
2	0.87	0.86	**7**	0.79	0.76	**12**	0.77	0.84	**17**	0.58	0.53	**22**	0.50	0.44
3	0.88	0.88	**8**	0.80	0.80	**13**	0.61	0.54	**18**	0.58	0.61	**23**	0.51	0.48
4	0.82	0.78	**9**	0.80	0.86	**14**	0.61	0.55	**19**	0.54	0.45	**24**	0.51	0.54
5	0.83	0.80	**10**	0.75	0.79	**15**	0.62	0.56	**20**	0.54	0.52			

E-series														
Mix no.	$\lambda_{Q,P}$	$\lambda_{Q,M}$	**Mix no.**	$\lambda_{Q,P}$	$\lambda_{Q,M}$	**Mix no.**	$\lambda_{Q,P}$	$\lambda_{Q,M}$	**Mix no.**	$\lambda_{Q,P}$	$\lambda_{Q,M}$	**Mix no.**	$\lambda_{Q,P}$	$\lambda_{Q,M}$
1	0.90	0.99	**9**	0.65	0.67	**18**	0.50	0.51	**26**	0.56	0.52	**38**	0.62	0.71
2	0.79	0.89	**10**	0.64	0.52	**19**	0.51	0.67	**29**	0.51	0.64	**39**	0.58	0.62
3	0.65	0.66	**11**	0.57	0.53	**20**	0.51	0.63	**30**	0.50	0.55	**45**	0.71	0.81
4	0.66	0.61	**12**	0.57	0.47	**21**	0.63	0.59	**31**	0.51	0.71	**46**	0.67	0.68
5	0.54	0.50	**13**	0.58	0.65	**22**	0.63	0.48	**32**	0.51	0.71	**47**	0.64	0.63
6	0.55	0.51	**14**	0.57	0.55	**23**	0.63	0.76	**34**	0.68	0.90	**48**	0.62	0.65
7	0.64	0.56	**16**	0.80	0.94	**24**	0.63	0.60	**35**	0.70	0.89	The mixes that are not included in the table were not able to measure λ_Q		
8	0.64	0.49	**17**	0.51	0.71	**25**	0.56	0.68	**37**	0.65	0.77			

F-series									G-series					
Mix no.	$\lambda_{Q,P}$	$\lambda_{Q,M}$	**Mix no.**	$\lambda_{Q,P}$	$\lambda_{Q,M}$	**Mix no.**	$\lambda_{Q,P}$	$\lambda_{Q,M}$	**Mix no.**	$\lambda_{Q,P}$	$\lambda_{Q,M}$	**Mix no.**	$\lambda_{Q,P}$	$\lambda_{Q,M}$
1	0.64	0.71	**3**	0.60	0.80	**5**	0.69	0.59	**1**	0.91	0.93	**4**	0.91	0.94
2	0.65	0.79	**4**	0.68	0.51	**6**	0.60	0.64	**2**	0.91	0.93	**5**	0.91	0.97
									3	0.91	0.93			

$\lambda_{Q,P}$ **= Predicted** λ_Q $\lambda_{Q,M}$ **= Measured** λ_Q

Table A 2 The measured flow resistance ration from laboratory and the flow resistance ratio from empirical model calculated by Solver analysis for each series (varying k_c, k_s, k_{fa} k_{sp} and k_f)

A-series									C-series			D-series		
Mix no.	$\lambda_{Q,P}$	$\lambda_{Q,M}$	**Mix no.**	$\lambda_{Q,P}$	$\lambda_{Q,M}$	**Mix no.**	$\lambda_{Q,P}$	$\lambda_{Q,M}$	**Mix no.**	$\lambda_{Q,P}$	$\lambda_{Q,M}$	**Mix no.**	$\lambda_{Q,P}$	$\lambda_{Q,M}$
1	0.89	0.89	**10**	0.84	0.84	**19**	0.95	0.93	**1**	0.78	0.81	**1**	0.69	0.76
2	0.93	0.92	**11**	0.87	0.89	**20**	1.00	0.99	**2**	0.95	0.99	**2**	0.53	0.55
3	0.96	0.96	**12**	0.89	0.95	**21**	1.05	1.00	**3**	0.60	0.56	**3**	0.42	0.39
4	0.61	0.58	**13**	0.54	0.57	**22**	0.69	0.72	**4**	0.51	0.50	**4**	0.33	0.33
5	0.64	0.59	**14**	0.56	0.55	**23**	0.73	0.77	**5**	0.46	0.45	**5**	0.56	0.47
6	0.66	0.65	**15**	0.58	0.35	**24**	0.77	0.83	**6**	0.58	0.56	**6**	0.44	0.42
7	0.44	0.39	**16**	0.36	0.38	**25**	0.53	0.52	**7**	1.08	1.00	**7**	0.40	0.37
8	0.46	0.41	**17**	0.38	0.39	**26**	0.56	0.58	**8**	0.88	0.95	**8**	0.34	0.40
9	0.47	0.43	**18**	0.39	0.49	**27**	0.58	0.60	**9**	0.73	0.75	**9**	0.39	0.35
												10	0.29	0.33

B-series														
Mix no.	$\lambda_{Q,P}$	$\lambda_{Q,M}$	**Mix no.**	$\lambda_{Q,P}$	$\lambda_{Q,M}$	**Mix no.**	$\lambda_{Q,P}$	$\lambda_{Q,M}$	**Mix no.**	$\lambda_{Q,P}$	$\lambda_{Q,M}$	**Mix no.**	$\lambda_{Q,P}$	$\lambda_{Q,M}$
1	0.85	0.80	**6**	0.82	0.84	**11**	0.76	0.76	**16**	0.55	0.48	**21**	0.52	0.57
2	0.84	0.86	**7**	0.79	0.76	**12**	0.76	0.84	**17**	0.55	0.53	**22**	0.50	0.44
3	0.84	0.88	**8**	0.79	0.80	**13**	0.58	0.54	**18**	0.55	0.61	**23**	0.50	0.48
4	0.82	0.78	**9**	0.79	0.86	**14**	0.58	0.55	**19**	0.52	0.45	**24**	0.49	0.54
5	0.82	0.80	**10**	0.76	0.79	**15**	0.58	0.56	**20**	0.52	0.52			

E-series														
Mix no.	$\lambda_{Q,P}$	$\lambda_{Q,M}$	**Mix no.**	$\lambda_{Q,P}$	$\lambda_{Q,M}$	**Mix no.**	$\lambda_{Q,P}$	$\lambda_{Q,M}$	**Mix no.**	$\lambda_{Q,P}$	$\lambda_{Q,M}$	**Mix no.**	$\lambda_{Q,P}$	$\lambda_{Q,M}$
1	0.92	0.99	**9**	0.65	0.67	**18**	0.60	0.51	**26**	0.63	0.52	**38**	0.65	0.71
2	0.81	0.89	**10**	0.65	0.52	**19**	0.60	0.67	**29**	0.60	0.64	**39**	0.61	0.62
3	0.64	0.66	**11**	0.62	0.53	**20**	0.59	0.63	**30**	0.60	0.55	**45**	0.80	0.81
4	0.64	0.61	**12**	0.62	0.47	**21**	0.67	0.59	**31**	0.60	0.71	**46**	0.76	0.68
5	0.53	0.50	**13**	0.62	0.65	**22**	0.67	0.48	**32**	0.59	0.71	**47**	0.72	0.63
6	0.53	0.51	**14**	0.61	0.55	**23**	0.67	0.76	**34**	0.73	0.90	**48**	0.67	0.65
7	0.66	0.56	**16**	0.81	0.94	**24**	0.67	0.60	**35**	0.71	0.89	The mixes that are not included in the table are not able to measure λ_Q		
8	0.66	0.49	**17**	0.60	0.71	**25**	0.63	0.68	**37**	0.69	0.77			

F-series									G-series					
Mix no.	$\lambda_{Q,P}$	$\lambda_{Q,M}$	**Mix no.**	$\lambda_{Q,P}$	$\lambda_{Q,M}$	**Mix no.**	$\lambda_{Q,P}$	$\lambda_{Q,M}$	**Mix no.**	$\lambda_{Q,P}$	$\lambda_{Q,M}$	**Mix no.**	$\lambda_{Q,P}$	$\lambda_{Q,M}$
1	0.73	0.71	**3**	0.70	0.80	**5**	0.61	0.59	**1**	0.94	0.93	**4**	0.94	0.94
2	0.79	0.79	**4**	0.54	0.51	**6**	0.69	0.64	**2**	0.94	0.93	**5**	0.94	0.97
									3	0.94	0.93			

$\lambda_{Q,P}$ **= Predicted** λ_Q $\lambda_{Q,M}$ **= Measured** λ_Q

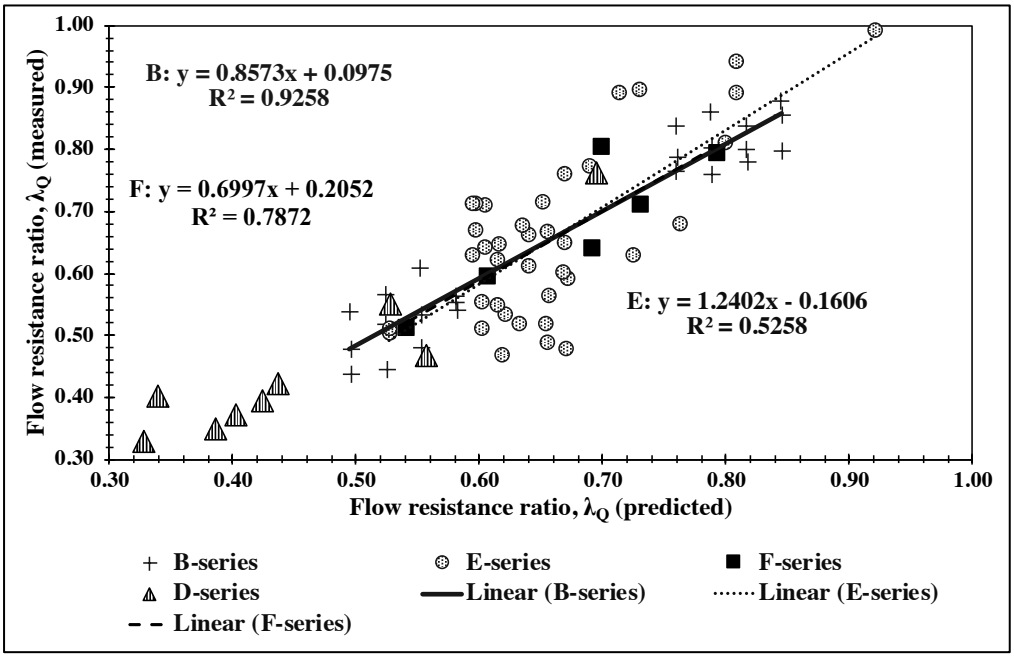

Figure A 1 The relationships between the predicted flow resistance ratio (λ_Q predicted) from the empirical model and the measured flow resistance (λ_Q measured) on matrices from laboratory, from the B-, E- and F-series with varying k_c, k_s, k_{fa}, k_{sp} and k_f

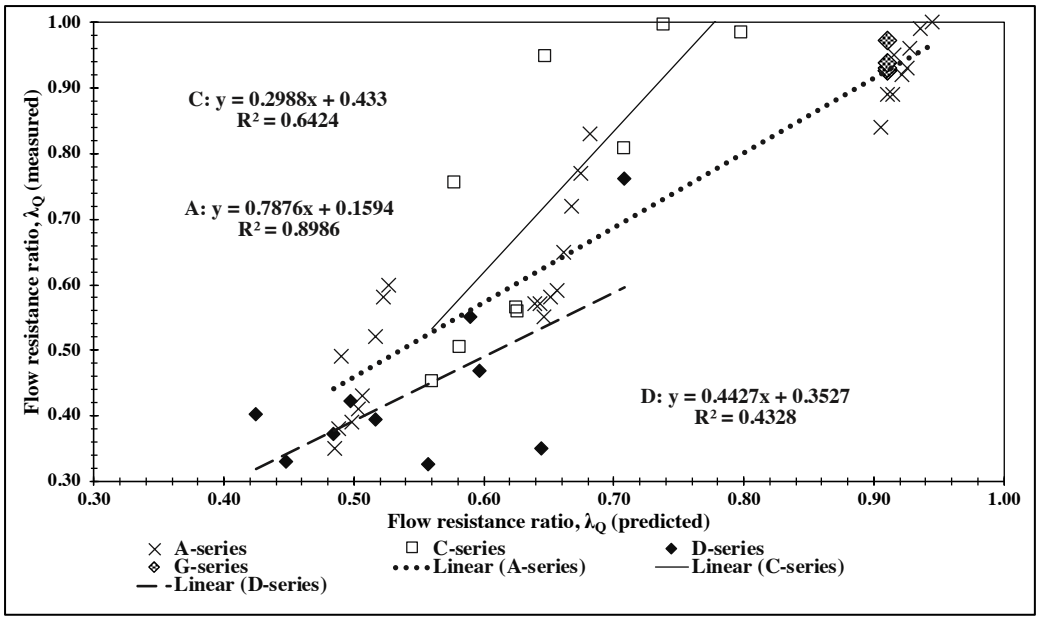

Figure A 2 The relationships between the predicted flow resistance ratio (λ_Q predicted) from the empirical model and the measured flow resistance (λ_Q measured) on matrices from laboratory, from the A-, C-, D- and G-series with constant k_c, k_s, k_{fa}, k_{sp} and k_f

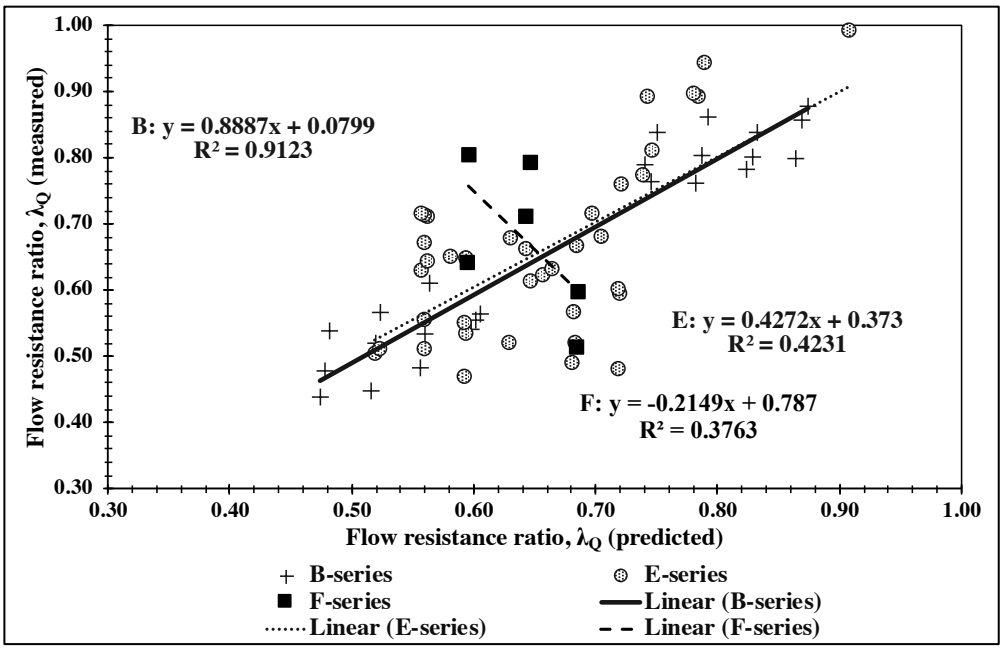

Figure A 3 The relationships between the predicted flow resistance ratio (λ_Q predicted) from the empirical model and the measured flow resistance (λ_Q measured) on matrices from laboratory, from the B-, E- and F-series with constant k_c, k_s, k_{fa}, k_{sp} and k_f

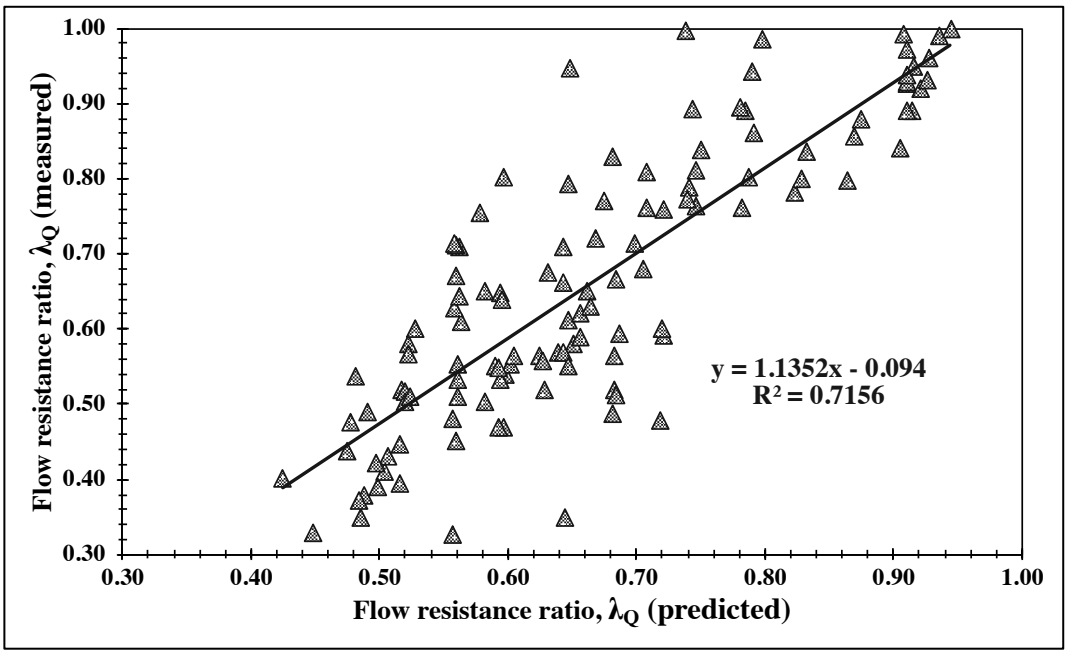

Figure A 4 The relationships between the predicted flow resistance ratio (λ_Q predicted) from the empirical model and the measured flow resistance (λ_Q measured) on matrices from laboratory, from all the series with constant k_c, k_s, k_{fa}, k_{sp} and k_f

Appendix B: The material parameters and the rheological parameters

The information in this Appendix is the laboratory work for the unpublished paper of Ph.D. candidate Elisabeth Leite Skare [26].

Due to the large amount of information and calculation details, the complete information and detail of all the parameters are uploaded as an excel file "129 mixes from Skare E.L.xlsx". The file is attached on:
https://www.dropbox.com/s/6cghy8l63l3og8q/129%20mixes%20from%20Skare%20E.L.xlsx?dl=0

The most important information that were used in this thesis can be found in the sheet "Parameterplan", "Glimmerresepter", "Feiringresepter" and the sheet "Lab.results" in the excel file attached above.

All the online Appendixes are uploaded in the folder "TKT4925 Concrete Technology Master's thesis Appendices – Metathip Sihaklang" on:
https://www.dropbox.com/sh/2b6ybeshelxa0km/AAB0KqYhQlAyVkCcG64TCbCva?dl=0

Appendix C: Matrix proportioning

Figure C 1: The calculation sheet used for proportioning of the mixes from the excel file "Matrice Weight Calculation.xlsx"

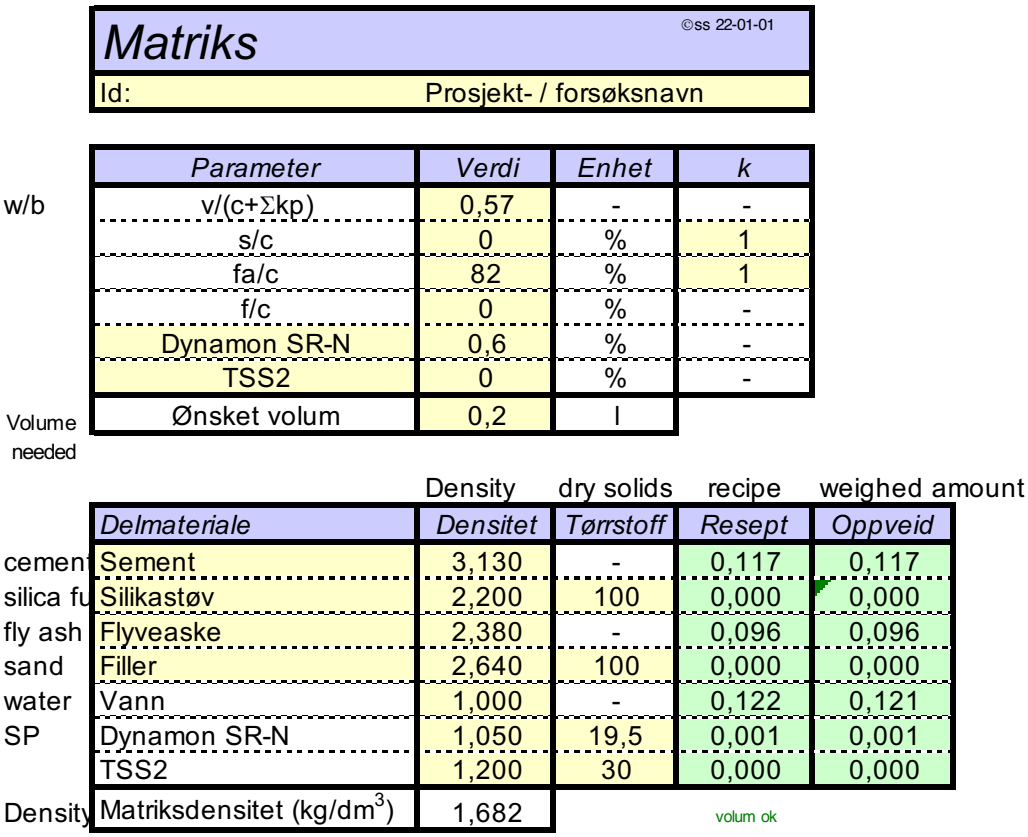

Matriks ©ss 22-01-01

Id: Prosjekt- / forsøksnavn

	Parameter	*Verdi*	*Enhet*	*k*
w/b	v/(c+Σkp)	0,57	-	-
	s/c	0	%	1
	fa/c	82	%	1
	f/c	0	%	-
	Dynamon SR-N	0,6	%	-
	TSS2	0	%	-
Volume needed	Ønsket volum	0,2	l	

	Delmateriale	*Densitet*	*Tørrstoff*	*Resept*	*Oppveid*
		Density	dry solids	recipe	weighed amount
cement	Sement	3,130	-	0,117	0,117
silica fu	Silikastøv	2,200	100	0,000	0,000
fly ash	Flyveaske	2,380	-	0,096	0,096
sand	Filler	2,640	100	0,000	0,000
water	Vann	1,000	-	0,122	0,121
SP	Dynamon SR-N	1,050	19,5	0,001	0,001
	TSS2	1,200	30	0,000	0,000
Density	Matriksdensitet (kg/dm^3)	1,682		volum ok	

The full calculation sheet is attached as an excel file "Matrice Weight Calculation.xlsx", which was given by Rolands Cepuritis and it is uploaded on:

https://www.dropbox.com/s/xdjk60islxf7sbi/Matrice_Weight_Calculation.xlsm?dl=0

All the online Appendixes are uploaded in the folder "TKT4925 Concrete Technology Master's thesis Appendices – Metathip Sihaklang" on:

https://www.dropbox.com/sh/2b6ybeshelxa0km/AAB0KqYhQlAyVkCcG64TCbCva?dl=0

Appendix D: Accuracy of excess fluid measurement method

The full detail and calculation of the accuracy of excess fluid (EF) can be found in an excel file "The trial and error test.xlsx" and it is uploaded on: **https://www.dropbox.com/s/x41h80ml3z60117/The%20trial%20and%20error%20test.xlsx?dl=0**

Table D 1 shows the results from the trial and error test taken from the Excel file "The trial and error test.xlsx", where the differences of EF (in g), VFF (in %), maximum packing, ϕ_{max} (in %) and EF fraction (in %) between the two methods were calculated.

Table D 1: The results from the trial and error test taken from the Excel file "The trial and error test.xlsx"

Method 1 With syringe and filter	
Total weight of the samples (g)	291.22
density (Theoritical)	1.68
Solid fraction (Theoritical)	0.39
EF Fraction	0.236
phi max	0.510
Vff	0.374
Fresh density	1.648

EF from M1 (g) for 291,22 g of paste	**40.87**
EF from M2 (g) for 289,75 g of paste	**41.53**
€	41.74

The difference of EF between M1 and M2 (g)	**0.87**

Method 2 Pouring directly	
Total weight of the samples (g)	289.75
density (Theoritical)	1.68
Solid fraction (Theoritical)	0.39
EF Fraction	0.241
phi max	0.514
Vff	0.369
Fresh density	1.650

Difference between the 2 methods		
Vff	**phi max**	**EF fraction**
1.34%	**0.66%**	**2.09%**
*1,34% more in M1	*0,66% more in M2	*2,09% more in M2

Difference between the fresh density and theoritical density	
1.79%	*1,79% more in theoritical

All the online Appendixes are uploaded in the folder "TKT4925 Concrete Technology Master's thesis Appendices – Metathip Sihaklang" on: **https://www.dropbox.com/sh/2b6ybeshelxa0km/AAB0KqYhQlAyVkCcG64TCbCva?dl=0**

Appendix E: Description and procedure of Ostwald viscometer

Manufacture's certificate for capillary viscometer, Cannon-Fenske-Routine viscometer from [21].

See the next pages (3).

Translation of the legally binding german version.

Traduction de la version allemande légale.

MANUFACTURER'S CERTIFICATE FOR CAPILLARY VISCOMETER

(Manufacturer's certificate M according to DIN 55 350, Part 18)

Subject: Cannon-Fenske-Routine viscometer for the determination of the kinematic viscosity according to ISO/DIS 3105 and ASTM D 2515/D 446 and BS 188.

Manufacturer: SCHOTT-GERÄTE,Mainz

Viscometer: Type and capillary no.: 513 03 / 50
Apparatus no.: 1023324

This viscometer is suitable to determine the kinematic viscosity of newtonian liquids according to ISO/DIS 3105, Annex A. The instrument constant **K** refers to the timing marks during the visual survey of the meniscus passage. It comes to

It was determined by using comparative measurements with reference viscometers, of which the constants were determined at the Physikalisch-Technischen Bundesanstalt, D-38116 Braunschweig.

The instrument constant **K** is valid for liquids with a surface tension of 20 to 30 mN/m and an acceleration of the fall of 9.8105 m/s^2. For temperatures up to 100 °C it is not required to pay attention to the heat expansion of the viscometer. The kinematic viscosity ν within mm^2/s of liquids can be calculated using the instrument constant in the equation:

whereby **t** is the flow time in seconds which was corrected -if necessary- according to ISO/DIS 3105, Part 6.2.

The relative uncertainty of the mentioned numerical value of **K** comes to 1.2 % at a confidence level of 95 %.

It is required to check the instrument constant in regular intervals. In particular any change to the viscometer, for example when using liquids that corrode glass or a glass blowing repair took place, makes a new determination of the instrument constant necessary.

CERTIFICAT DU FABRICANT DE TUBE VISCOSIMETRIQUE CAPILLAIRE

(Certificat du fabricant M selon DIN 55 350, Partie 18)

Objet: Viscosimètre de routine Cannon-Fenske pour la détermination de la viscosité cinématique selon ISO/DIS 3105 et ASTM D 2515/D 446 et BS 188.

Fabricant: SCHOTT-GERÄTE, Mainz

Viscosimètre: No. de type et de capillaire: 513 03 / 50
No. d'appareil: 1023324

Ce viscosimètre est approprié pour la détermination de la viscosité cinématique de liquides newtoniens selon ISO/DIS 3105, Annex A. La constante de l'instrument **K** est valable pour des index rotatifs avec une saisie visuelle du passage du ménisque. Elle est de

$K = 0{,}003818\ mm^2/s^2$.

Elle a été déterminée par des mesures de comparaison avec des viscosimètres étalons dont les constantes ont été déterminées auprès de la Physikalisch-Technischen Bundesanstalt, D-38116 Braunschweig.

La constante **K** de l'instrument est valable pour des liquides avec une tension de surface de 20 à 30 mN/m et avec une accélération de la pesanteur de 9,8105 m/s^2. Dans le cas de températures jusqu'à 100 °C, il n'est pas nécessaire de tenir compte de la dilatation thermique du viscosimètre. La viscosité cinématique ν en mm^2/s de liquides peut être calculée à l'aide de la constante de l'instrument selon l'équation:

$$\nu = K \cdot t,$$

t est le temps d'écoulement en secondes qui a été corrigé -si nécessaire- selon ISO/DIS 3105, Partie 6.2.

L'insécurité relative de la valeur numérique de **K** indiquée est de 1,2 % dans le cas d'un niveau de confiance de 95 %.

Il est nécessaire de contrôler la constante de l'instrument en intervalles réguliers. Une nouvelle détermination de la constante de l'instrument devient absolument nécessaire lors de toute modification du viscosimètre, par exemple, en raison de l'utilisation de liquides qui attaquent le verre, ou dans le cas de réparations par un souffleur de verre.

SCHOTT-GERÄTE GmbH, Hattenbergstraße 10, D-55122 Mainz

AGQSF0027-810M-00/950524

Viscometers within quality assurance systems

mmendations for companies that have introduced a quality assurance system in dance with the DIN EN ISO 9001 standards. In this quality assurance system, an ction of the measuring equipment is planned. The intervals and required accuracy can be ed by each company according to its own requirements. The standard DIN/ISO 10 012, 1 serves as a guideline in this matter. We recommend regular inspection of the meters in defined intervals.

ection of the viscometer constants:

Calibration using comparative measurements with reference measuring standards

parative measurements must be performed with a viscometer (reference measuring dard) which was tested at the PTB (Federal German Physical-Technical Institute) and ded with a constant. During this comparative measurement, the viscometer to be cted and the PTB - tested viscometer were placed simultaneously in the same thermostat The test liquid tested, the viscosity of which must not be known exactly, is filled into both meters, tempered and the flow-through time then measured. The constants of the meters to be inspected are then calculated according to the following equation:

$$= \frac{K_{Uref} \cdot t_{Uref}}{t}$$

= constant of the tested viscometer
= constant of the standard reference viscometer
= low time (HC) of the tested viscometer (corrected by Hagenbach-Couette)
= flow time (HC) of the standard reference viscometer (corrected by Hagenbach-Couette)

n the quality assurance system in accordance with DIN EN ISO 9001, traceability of the suring equipment to national measuring standards is demanded. This traceability can be ved by inspecting the comparative viscometers (reference measuring standards) at lar intervals at the PTB. The time intervals are defined according to the specifications made e quality assurance system of the user.

Calibration of the capillary viscometer with normal oils of the PTB

ng this calibration, a normal oil from the PTB with known viscosity is used as a reference suring standard. The measurement is performed by means of flow-through measurement e PTB normal oil in the viscometer to be inspected in a temperature bath, the temperature hich must correspond precisely to the test temperature of the PTB. In this case, it is mely important to make sure that the temperature is absolutely correct. In case of perature variation, this will always result in a constant for the viscometer that deviates from constant applied. A temperature variation of 0.01 K, for instance, will result in a measuring of up to 0.01 %. The calibration of the deviating temperature into the viscometer constant it permitted.

Inspection by SCHOTT Instruments with quality certificates in accordance with 55 350-18-4.2.2

inspection at **SCHOTT Instruments** is carried out by means of comparative meas- nents using viscometers as reference measuring standards that were tested at the PTB esponds to Item 1).

rmation on the stability of viscometer constants

h inspection (even with a certificate) can guarantee the technical measuring direction only for iited period of time. The constants of viscometers made of the borosilicate glass DURAN®, ever, can remain unchanged for long periods of time if the viscometers are kept away from ed influences. Especially extreme changes can be expected, for instance, during the use of ds that attack glass, in particular hot caustic soda hydrated (NaOH) or during glass-blowing irs (even for apparently insignificant repairs).
ids whose components adhere to the glass wall also cause errors. In such cases, regular ning is required whereby the corrosive action cleaning agent on the glass must be inated.
this reason, we recommend that the user should write up a special processing instructions all important measurements and include them in his quality assurance manual in ordance with DIN EN ISO 9001. In all cases the user is responsible for the correctness of measuring and testing equipment and is not released from his responsibility for quality (cp. 55 350, Part 18).

egistered trademark for SCHOTT GLAS, Mainz

1 Description

The Cannon-Fenske Routine Viscometer consists essentially of 2 tubes, the tube with capillary (1) and the venting tube (2), the reservoir (3), the upper timing mark M1 (4), the lower timing mark M2 (5), the pre-run sphere (6), the capillary (7) and the measuring sphere (8) The Cannon-Fenske Routine Viscometer is in accordance of technical measurements to standard like ISO 3105, ASTM 446 and D 2515. With the tube expanding (9), the viscometer is also convenient for automatic measuring system.

2 Preparation of sample

Low viscosity samples must be filtered through a SCHOTT glass filter porosity 2 to 4 (10 ... 100 µm) before the measurement; high viscosity samples, through a sieve with 0.3 mm mesh width (test sieve cloth 0.2, DIN 4 188). Samples, whose stock value in accordance with DIN 51 583 or pour point in accordance with DIN 51 597 is not at least 30 °C lower than the test temperature must be heated up to 80 °C before the measurement.

3 Selection of capillary

The size of the capillary is to be selected in such a way that the uncertainty inherent in the kinetic energy correction (HC) does not exceed the allowable error for the time measurement (see table). For precision measurements, the correction seconds in brackets should not be used. If necessary, a viscometer with a narrower capillary is to be used.

4 Cleaning the viscometer

Before the first use, a cleaning with 15 % H_2O_2 and 15 % HCl is recommended. The viscometer should then be rinsed with a suitable solvent. It must be completely dry and dust-free and can thereby be used for automatic measurements.

5 Filling the viscometer

For filling, the Cannon-Fenske Routine Viscometer is placed on its „head". The tube with capillary (1) is submerged in the liquid to be measured while suction using a hose is applied to the venting tube (2) until the liquid reaches the lower timing mark M2. During automatic measurement after being turned back into the normal measuring position, the viscometer connected with its particular hose accessories (look at Operating Instructions for the corresponding AVS device) and fixed in the measurement stand with the fitting type no. 065 99 is placed in a **Transparent Thermostat from SCHOTT Instruments GmbH**. During manual measurement the viscometer will be fitted after inverting to normal measuring position with its stand type no. 064 99 vertically into a **Transparent Thermostat from SCHOTT Instruments GmbH.**

6 Adaptation of the sample to the bath temperature

If the accuracy of the viscometer measurement is to be fully utilised, the thermostat should keep the measuring temperature constant within ± 0.01 °C (**Transparent Thermostat from SCHOTT Instruments GmbH**). The measurement should only be carried out after a waiting time of approx. 10 minutes.

7 Manual measuring

(Viscometer type no. 513 ..)

For manual viscosity measuring operation use constant marked „K".

For measuring, draw the liquid drained into the reservoir (3) back into the pre-run sphere (6) passing the upper timing mark M1 (4) and the lower timing mark M2. Then measure the flow time between the upper timing mark (M1) and the lower timing mark (M2). The measurement can be repeated any time.

8 Automatic measuring

Automatic viscosity measurement systems (AVS) from **SCHOTT Instruments** GmbH replace the manual measurement of viscosity. Subjective measurement errors are eliminated, the measured times are available in the data memory and are printed out depending upon the device. To carry out the measurement, please see the operating instructions for the particular measurement device.

The viscometer is inserted into the fitting out of PTFE of the measuring stand type no. AVS/S-CF. The time measurement is made in the measurement levels from M1 to M2. Light barriers replace the ring markers hereby. For automatic viscosity measurement, the constant identified with "AK = ..." is to be used.

9 Viscosity calculation

The seconds contribution given in the table for the kinetic energy correction (HC) is to be subtracted from the measured flow time for the various capillaries. Intermediate values can be interpolated.

With absolute measurements, the corrected flow time multiplied by the viscometer constant K, produces the kinematic viscosity [mm^2/s] *) directly.

$$\nu = K (t - \vartheta)$$

The viscometer constant K is mentioned in the enclosed production certificate.

10 Example of evaluation

CANNON FENSKE VISCOMETER

Type no. 513 10
Capillary no. 100
Constant = 0.01500
Flow time (averaged) = 100.00 [s]
Kinetic energy correction (HC) for 180,00 s = 0.27 [s]
Kinematic viscosity ν = K (t - 9)
= 0.015·(100,00 - 0,27)
= 1.495 [mm^2/s]*

*) previously centistokes [cSt]; 1 [cSt] = 1 [mm^2/s]

11 Table of the kinetic energy correction (HC)

(Hagenbach Couette Correction)

Cannon-Fenske Routine Viscometer type no. 513 .., 520 ..

Correction seconds[1]:

Flow time	Capillary No.				
[s]	25	50	75	100	150
50	–	–	–	1,09	0,28
60	–	–	(2,10) [2]	0,76	0,19
70	–	–	(1,55) [2]	0,56	0,14
80	(4,71) [2]	(3,70) [2]	1,18	0,43	0,11
90	(3,72) [2]	(2,93) [2]	0,93	0,34	0,09
100	(3,01) [2]	(2,37) [2]	0,76	0,27	0,07
110	2,49	1,96	0,63	0,23	0,06
120	2,09	1,65	0,53	0,19	0,05
130	1,78	1,40	0,45	0,16	0,04
140	1,54	1,21	0,39	0,14	0,03
150	1,34	1,05	0,34	0,12	0,03
160	1,18	0,93	0,30	0,11	0,03
170	1,04	0,82	0,26	0,09	0,02
180	0,93	0,73	0,23	0,08	0,02
190	0,83	0,66	0,21	0,08	0,02
200	0,75	0,59	0,19	0,07	0,02
220	0,62	0,49	0,16	0,06	0,01
240	0,52	0,41	0,13	0,05	0,01
260	0,45	0,35	0,11	0,04	0,01
280	0,38	0,30	0,10	0,03	0,01
300	0,33	0,26	0,08	0,03	0,01
350	0,25	0,19	0,06	0,02	0,01
400	0,19	0,15	0,05	0,02	< 0,01
450	0,15	0,12	0,04	0,01	< 0,01
500	0,12	0,10	0,03	0,01	< 0,01

[1] The correction seconds given are based on the particular theoretical constant.

[2] For precision measurements, the correction seconds in the brackets should not be used. If necessary, a viscometer with a narrower capillary is to be used.

Type No.	Capillary no.	Capillary $\varnothing_i$ (mm)	Constant K (Approx. value)	Measurement range mm^2/s (cSt) (Approx. value)		
... 00	25	0,30	0,002	0,4	to	1,6
... 03	50	0,44	0,004	0,8	to	3,2
... 01	75	0,54	0,008	1,6	to	6,4
... 10	100	0,63	0,015	3	to	15
... 13	150	0,77	0,035	7	to	35
... 20	200	1,01	0,1	20	to	100
... 23	300	1,26	0,25	50	to	200
... 21	350	1,52	0,5	100	to	500
... 30	400	1,92	1,1	240	to	1200
... 33	450	2,30	2,5	500	to	2500
... 40	500	3,20	8	1600	to	8000
... 43	600	4,10	20	4000	to	20000

www Schott Instruments GmbH

Hinweis:
Ausführliche Viskosimeter-Gebrauchsanleitungen und weitere Produktinformationen in den Sprachen Deutsch, Englisch, Französisch und Spanisch stehen auf unseren Internetseiten als Download zur Verfügung. Das von Schott-Geräte hergestellte Viskosimeter-Programm erfüllt z.B. folgende Normen: ISO/DIS 3105, DIN 51 562, Teil 1 und Teil 2, BS 188, NFT 60-100, ASTM D 2515, ASTM D 446.

Comment:
Detailed operating instructions for our viscometers and further product information are available for downlaod in German, English, French and Spanish at our homepage. Schott-Geräte's range of viscometers are in accordance with the following standards: ISO/DIS 3105, DIN 51 562, part 1 and part 2, BS 188, NFT 60-100, ASTM D 2515, ASTM D 446.

Commentaire :
Les modes d'emploi des viscosimètres et des informations complémentaires sur nos produits sont téléchargeables en allemand, anglais, français, espagnol à partir de notre site Internet. Le programme de viscosimètres fabriqués par Schott Geräte répond, par exemple, aux normes : ISO/DIS 3105, DIN 51 562, Partie 1 et Partie 2, BS 188, NFT 60-100, ASTM D 2515, ASTM D 446.

Observaciónes :
Está a su disposición en nuestra página de internet, que podrá decagar, amplia información de las istrucciones de manejo de los viscosímetros y otras informaciones de producto en español, francés, inglés y alemán. El completo programa de viscosimetría de fabricados de Schott-Geräte cumplen por ejemplo las siguientes normas: ISO/DIS 3105, DIN 51 562, parte 1 et parte 2, BS 188, NFT 60-100, ASTM D 2515, ASTM D 446.

SCHOTT instruments GmbH
Hattenbergstraße 10
55122 Mainz
Germany

Tel: +49 (0) 6131 / 66 - 5111
Fax: +49 (0) 6131 / 66 - 5001
avs@schott-instruments.com
www.schott.instruments.com

00848021 1

SCHOTT Instruments

Gebrauchsanleitung **Cannon-Fenske-Routineviskosimeter**

Operating Instructions **Cannon-Fenske Routine Viscometer**

Bescheinigung des Herstellers

Wir bestätigen, dass das oben genannte Gerät gemäß DIN EN ISO 9001, Absatz 8.2.4 (Endprüfung) geprüft wurde und dass die festgelegte Qualitätsanforderung an das Produkt erfüllt werden.

Supplier's Certificate

We certify that the equipment DIN EN ISO 9001, part 8.2.4 (Final inspection and testing) and that the specified requirements for the product are met

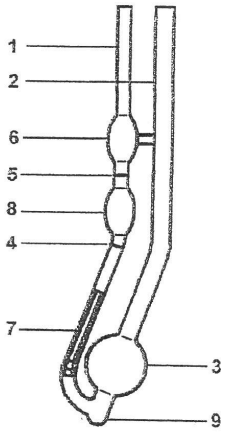

1 Kapillarrohr
Tube with capillary
Tube avec capillaire
Tubo con capilar

2 Belüftungsrohr
Venting tube
Tube de ventilation
Tubo de ventilación

3 Vorratsgefäß
Reservoir
Réservoir
Reservorio

4 Untere Ringmessmarke M2
Lower timing mark M2
Marque annulaire M2 en bas
Marca anular inferior de medida M2

5 Obere Ringmessmarke M1
Upper timing mark M1
Marque annulaire M1 en haut
Marca anular superior de medida M1

6 Vorlaufkugel
Pre-run sphere
Boule d'entrée
Bola de entrada

7 Kapillare
Capillary
Tube capillaire
Capilar

8 Messgefäß
Measuring sphere
Boule de mesure
Bola de medición

9 Roherweiterung
Tube expanding
Elargissement du tube
Extensión del tubo

SCHOTT Instruments

Appendix F: Raw data from laboratory, EF fraction, maximum packing, voids filling fluid, solid content in EF, density of EF and viscosity measurements

All the raw data from the laboratory and the full calculations of EF fraction, maximum packing (ϕ_{max}), voids filling fluid (VFF), solid content, density of EF, kinematic viscosity and dynamic viscosity can be found in an online appendix uploaded as an excel file "Raw data, EF fraction, maximum packing, VFF, solid content in EF, density of EF and viscosity measurements.xlsx" on (note that this file must be downloaded due to the large size of the file):

https://www.dropbox.com/s/hu82bgwktx98c7b/Raw%20data%2C%20EF%20fraction%2C%20maximum%20packing%2C%20VFF%2C%20Solid%20content%20in%20EF%2C%20Density%20of%20EF%20and%20viscosity%20measurements.xlsx?dl=0

Note that the pictures of the F- and G-series are marked with E-series and A-series respectively. This is because the F- and G-series were developed from the E- and A-series but used different types of filler.

All the online Appendixes are uploaded in the folder "TKT4925 Concrete Technology Master's thesis Appendices – Metathip Sihaklang" on:
https://www.dropbox.com/sh/2b6ybeshelxa0km/AAB0KqYhQlAyVkCcG64TCbCva?dl=0

Table F 1 EF fraction, maximum packing (ϕ_{max}), voids filling fluid (VFF), solid content in EF and density of EF from the A-series

A-series					
Mix no.	**EF fraction (V=1)**	**ϕ_{max}**	**VFF**	**Solid content**	**Density of EF (g/cm³)**
1	0.060	0.550	0.423	1.92%	1.007
2	0.059	0.565	0.409	4.01%	1.016
3	0.054	0.577	0.400	4.06%	1.017
4	0.106	0.549	0.403	3.15%	1.013
5	0.097	0.530	0.425	2.52%	1.010
6	0.087	0.551	0.410	2.44%	1.009
7	0.160	0.528	0.396	2.30%	1.009
8	0.140	0.530	0.404	2.12%	1.008
9	0.138	0.538	0.398	2.25%	1.008
10	0.062	0.551	0.421	4.06%	1.017
11	0.058	0.564	0.411	3.94%	1.016
12	0.053	0.576	0.402	3.80%	1.015
13	0.105	0.534	0.417	2.99%	1.012
14	0.092	0.540	0.417	2.85%	1.011
15	0.080	0.547	0.417	2.92%	1.011
16	0.150	0.523	0.405	2.34%	1.009
17	0.140	0.530	0.404	2.22%	1.008
18	0.134	0.535	0.403	2.25%	1.008
19	0.055	0.547	0.429	4.04%	1.017
20	0.049	0.559	0.419	4.60%	1.019
21	0.047	0.572	0.408	4.01%	1.016
22	0.087	0.523	0.435	3.31%	1.013
23	0.074	0.530	0.435	2.65%	1.010
24	0.067	0.539	0.430	2.82%	1.011
25	0.130	0.511	0.425	2.38%	1.009
26	0.114	0.515	0.430	2.27%	1.008
27	0.107	0.519	0.429	2.38%	1.009

Table F 2 EF fraction, maximum packing (ϕ_{max}), voids filling fluid (VFF), solid content in EF and density of EF from the B-series

B-series					
Mix no.	**EF fraction (V=1)**	**ϕ_{max}**	**VFF**	**Solid content (%)**	**Density of EF (g/ cm³)**
1	0.054	0.546	0.429	4.22%	1.017
2	0.049	0.559	0.419	4.51%	1.019
3	0.047	0.572	0.408	4.40%	1.018
4	0.053	0.545	0.431	5.23%	1.022
5	0.046	0.558	0.422	4.75%	1.020
6	0.043	0.570	0.412	4.83%	1.020
7	0.053	0.546	0.430	5.26%	1.022
8	0.049	0.559	0.419	4.91%	1.021
9	0.042	0.570	0.412	4.81%	1.020
10	0.051	0.544	0.433	5.62%	1.024
11	0.046	0.557	0.423	5.64%	1.024
12	0.041	0.569	0.413	5.21%	1.022
13	0.103	0.533	0.419	3.29%	1.013
14	0.094	0.541	0.416	3.28%	1.013
15	0.080	0.546	0.417	3.27%	1.013
16	0.110	0.537	0.413	3.59%	1.015
17	0.096	0.543	0.413	3.38%	1.014
18	0.082	0.547	0.416	3.32%	1.013
19	0.115	0.540	0.408	3.64%	1.015
20	0.108	0.550	0.402	3.83%	1.016
21	0.087	0.551	0.410	3.78%	1.015
22	0.120	0.543	0.402	3.75%	1.015
23	0.106	0.549	0.403	3.91%	1.016
24	0.096	0.556	0.401	4.75%	1.020

Table F 3 EF fraction, maximum packing (ϕ_{max}), voids filling fluid (VFF), solid content in EF and density of EF from the C-series

C-series					
Mix no.	**EF fraction (V=1)**	**ϕ_{max}**	**VFF**	**Solid content (%)**	**Density of EF (g/ cm³)**
1	0.157	0.462	0.453	4.60%	1.019
2	0.126	0.475	0.458	5.08%	1.021
3	0.169	0.487	0.426	3.82%	1.016
4	0.181	0.502	0.408	3.22%	1.013
5	0.182	0.507	0.403	3.05%	1.012
6	0.149	0.518	0.411	3.43%	1.014
7	0.115	0.499	0.444	4.52%	1.019
8	0.127	0.519	0.420	3.65%	1.015
9	0.130	0.532	0.407	3.07%	1.012

Table F 4 EF fraction, maximum packing (ϕ_{max}), voids filling fluid (VFF), solid content in EF and density of EF from the D-series

D-series					
Mix no.	**EF fraction (V=1)**	**ϕ_{max}**	**VFF**	**Solid content (%)**	**Density of EF (g/ cm³)**
1	0.180	0.475	0.430	4.56%	1.019
2	0.190	0.481	0.420	3.65%	1.015
3	0.214	0.497	0.395	2.85%	1.011
4	0.239	0.512	0.371	2.40%	1.009
5	0.173	0.472	0.437	3.41%	1.014
6	0.186	0.479	0.424	2.96%	1.012
7	0.205	0.490	0.406	3.00%	1.012
8	0.202	0.489	0.408	2.54%	1.010
9	0.213	0.496	0.397	2.46%	1.009
10	0.237	0.511	0.373	3.08%	1.012

Table F 5 EF fraction, maximum packing (ϕ_{max}), voids filling fluid (VFF), solid content in EF and density of EF from the E-series

E-series					
Mix no.	**EF fraction (V=1)**	ϕ_{max}	**VFF**	**Solid content**	**Density of EF (g/cm³)**
1	0.067	0.552	0.418	5.07%	1.021
2	0.057	0.546	0.428	5.46%	1.023
3	0.102	0.537	0.416	4.26%	1.018
4	0.096	0.549	0.408	4.23%	1.017
5	0.088	0.529	0.430	4.48%	1.019
6	0.079	0.539	0.425	4.77%	1.020
7	0.111	0.545	0.405	4.01%	1.016
8	0.105	0.549	0.403	2.94%	1.012
9	0.102	0.555	0.399	4.03%	1.017
10	0.092	0.556	0.403	2.98%	1.012
11	0.117	0.560	0.389	4.31%	1.018
12	0.100	0.555	0.401	4.94%	1.021
13	0.107	0.569	0.385	4.20%	1.017
14	0.102	0.571	0.386	3.36%	1.013
15	0.062	0.568	0.406	5.02%	1.021
16	0.049	0.560	0.419	5.31%	1.022
17	0.126	0.576	0.370	3.22%	1.013
18	0.122	0.577	0.371	2.54%	1.010
19	0.113	0.582	0.371	3.53%	1.014
20	0.112	0.585	0.368	2.64%	1.010
21	0.113	0.549	0.400	3.84%	1.016
22	0.106	0.552	0.400	2.55%	1.010
23	0.102	0.559	0.396	3.87%	1.016
24	0.097	0.562	0.396	2.79%	1.011
25	0.122	0.566	0.381	3.77%	1.015
26	0.110	0.563	0.389	3.36%	1.013
27	0.109	0.573	0.380	3.91%	1.016
28	0.103	0.573	0.383	2.82%	1.011
29	0.124	0.575	0.372	3.46%	1.014
30	0.117	0.574	0.376	3.16%	1.013
31	0.116	0.584	0.367	3.42%	1.014
32	0.159	0.618	0.321	2.63%	1.010
33	0.101	0.549	0.405	4.22%	1.017
34	0.098	0.561	0.396	4.26%	1.018
35	0.086	0.566	0.396	4.41%	1.018
36	0.092	0.573	0.388	4.26%	1.018
37	0.082	0.567	0.397	4.19%	1.017
38	0.077	0.564	0.403	4.19%	1.017
39	0.071	0.560	0.409	4.25%	1.018
44	0.087	0.567	0.395	4.84%	1.020
45	0.076	0.560	0.407	5.59%	1.024
46	0.076	0.560	0.407	5.75%	1.024
47	0.063	0.553	0.419	6.89%	1.030
48	0.069	0.540	0.428	7.24%	1.031

Table F 6 EF fraction, maximum packing (ϕ_{max}), voids filling fluid (VFF), solid content in EF and density of EF from the F-series

F-series					
Mix no.	**EF fraction (V=1)**	**ϕ_{max}**	**VFF**	**Solid content (%)**	**Density of EF (g/ cm³)**
1	0.100	0.535	0.418	4.21%	1.017
2	0.090	0.545	0.414	3.96%	1.016
3	0.106	0.568	0.387	3.92%	1.016
4	0.105	0.549	0.404	2.92%	1.011
5	0.095	0.558	0.400	2.92%	1.011
6	0.105	0.573	0.382	3.00%	1.012

Table F 7 EF fraction, maximum packing (ϕ_{max}), voids filling fluid (VFF), solid content in EF and density of EF from the G-series

G-series					
Mix no.	**EF fraction (V=1)**	**ϕ_{max}**	**VFF**	**Solid content (%)**	**Density of EF (g/ cm³)**
1	0.063	0.567	0.406	4.16%	1.017
2	0.056	0.563	0.413	3.89%	1.016
3	0.063	0.568	0.405	3.72%	1.015
4	0.060	0.566	0.408	3.89%	1.016
5	0.058	0.564	0.411	3.86%	1.016

Table F 8 Average flow time from viscosity measurements, kinematic viscosity and dynamic viscosity from the A-series

A-series			
Mix no.	**Average flow time (sec.)**	**Kinematic viscosity (m^2/s)**	**Dynamic viscosity (mPa*s)**
1	315	1.259E-06	1.268E+00
2	320	1.279E-06	1.300E+00
3	315	1.267E-06	1.288E+00
4	297	1.187E-06	1.202E+00
5	319	1.275E-06	1.287E+00
6	305	1.219E-06	1.230E+00
7	312	1.247E-06	1.258E+00
8	292	1.167E-06	1.176E+00
9	304	1.215E-06	1.225E+00
10	307	1.227E-06	1.247E+00
11	299	1.195E-06	1.214E+00
12	306	1.223E-06	1.242E+00
13	308	1.231E-06	1.245E+00
14	320	1.279E-06	1.293E+00
15	296	1.183E-06	1.197E+00
16	310	1.239E-06	1.250E+00
17	290	1.159E-06	1.168E+00
18	297	1.187E-06	1.197E+00
19	307	1.227E-06	1.247E+00
20	301	1.203E-06	1.226E+00
21	297	1.187E-06	1.206E+00
22	308	1.231E-06	1.247E+00
23	303	1.211E-06	1.223E+00
24	295	1.179E-06	1.192E+00
25	326	1.303E-06	1.315E+00
26	307	1.227E-06	1.237E+00
27	309	1.235E-06	1.246E+00

Table F 9 Average flow time from viscosity measurements, kinematic viscosity and dynamic viscosity from the B-series

B-series			
Mix no.	**Average flow time (sec.)**	**Kinematic viscosity (m^2/s)**	**Dynamic viscosity (mPa*s)**
1	174	1.390E-06	1.414E+00
2	168	1.342E-06	1.367E+00
3	164	1.310E-06	1.334E+00
4	170	1.358E-06	1.388E+00
5	165	1.318E-06	1.344E+00
6	177	1.414E-06	1.443E+00
7	169	1.350E-06	1.380E+00
8	168	1.342E-06	1.369E+00
9	167	1.334E-06	1.361E+00
10	184	1.470E-06	1.505E+00
11	171	1.366E-06	1.399E+00
12	170	1.358E-06	1.388E+00
13	160	1.278E-06	1.294E+00
14	157	1.254E-06	1.270E+00
15	165	1.318E-06	1.335E+00
16	167	1.334E-06	1.353E+00
17	173	1.382E-06	1.401E+00
18	168	1.342E-06	1.360E+00
19	164	1.310E-06	1.329E+00
20	182	1.454E-06	1.477E+00
21	167	1.334E-06	1.354E+00
22	176	1.406E-06	1.428E+00
23	170	1.350E-06	1.372E+00
24	188	1.502E-06	1.532E+00

Table F 10 Average flow time from viscosity measurements, kinematic viscosity and dynamic viscosity from the C-series

C-series			
Mix no.	**Average flow time (sec.)**	**Kinematic viscosity (m^2/s)**	**Dynamic viscosity (mPa*s)**
1	285	1.139E-06	1.161E+00
2	287	1.167E-06	1.192E+00
3	270	1.079E-06	1.096E+00
4	280	1.119E-06	1.133E+00
5	279	1.115E-06	1.128E+00
6	279	1.115E-06	1.130E+00
7	290	1.119E-06	1.140E+00
8	298	1.191E-06	1.209E+00
9	295	1.139E-06	1.153E+00

Table F 11 Average flow time from viscosity measurements, kinematic viscosity and dynamic viscosity from the D-series

D-series			
Mix no.	**Average flow time (sec.)**	**Kinematic viscosity (m^2/s)**	**Dynamic viscosity (mPa*s)**
1	299	1.195E-06	1.218E+00
2	290	1.159E-06	1.176E+00
3	287	1.147E-06	1.160E+00
4	292	1.167E-06	1.177E+00
5	291	1.163E-06	1.179E+00
6	288	1.151E-06	1.164E+00
7	302	1.207E-06	1.221E+00
8	302	1.207E-06	1.219E+00
9	293	1.171E-06	1.182E+00
10	293	1.171E-06	1.185E+00

Table F 12 Average flow time from viscosity measurements, kinematic viscosity and dynamic viscosity from the E-series

E-series			
Mix no.	**Average flow time (sec.)**	**Kinematic viscosity (m^2/s)**	**Dynamic viscosity (mPa*s)**
1	166	1.326E-06	1.354E+00
2	179	1.430E-06	1.463E+00
3	172	1.374E-06	1.398E+00
4	160	1.278E-06	1.300E+00
5	171	1.366E-06	1.391E+00
6	162	1.294E-06	1.320E+00
7	171	1.366E-06	1.388E+00
8	164	1.310E-06	1.325E+00
9	167	1.334E-06	1.356E+00
10	162	1.294E-06	1.317E+00
11	166	1.326E-06	1.349E+00
12	160	1.278E-06	1.304E+00
13	164	1.310E-06	1.332E+00
14	157	1.254E-06	1.270E+00
15	167	1.334E-06	1.362E+00
16	170	1.358E-06	1.388E+00
17	164	1.310E-06	1.327E+00
18	168	1.342E-06	1.355E+00
19	164	1.310E-06	1.328E+00
20	161	1.286E-06	1.299E+00
21	170	1.358E-06	1.379E+00
22	162	1.294E-06	1.306E+00
23	169	1.350E-06	1.371E+00
24	157	1.254E-06	1.267E+00
25	158	1.262E-06	1.281E+00
26	168	1.342E-06	1.360E+00
27	163	1.302E-06	1.323E+00
28	164	1.310E-06	1.324E+00
29	157	1.254E-06	1.271E+00
30	169	1.350E-06	1.367E+00
31	164	1.310E-06	1.328E+00
32	169	1.350E-06	1.364E+00
33	169	1.350E-06	1.373E+00
34	167	1.334E-06	1.357E+00
35	160	1.278E-06	1.301E+00
36	161	1.286E-06	1.308E+00
37	164	1.310E-06	1.332E+00
38	163	1.302E-06	1.324E+00
39	164	1.310E-06	1.333E+00
44	160	1.278E-06	1.304E+00
45	165	1.318E-06	1.349E+00
46	157	1.254E-06	1.284E+00
47	163	1.302E-06	1.340E+00
48	167	1.334E-06	1.376E+00

Table F 13 Average flow time from viscosity measurements, kinematic viscosity and dynamic viscosity from the F-series

F-series			
Mix no.	**Average flow time (sec.)**	**Kinematic viscosity (m^2/s)**	**Dynamic viscosity (mPa*s)**
1	169	1.350E-06	1.373E+00
2	167	1.334E-06	1.355E+00
3	157	1.254E-06	1.274E+00
4	162	1.294E-06	1.308E+00
5	161	1.286E-06	1.300E+00
6	162	1.294E-06	1.309E+00

Table F 14 Average flow time from viscosity measurements, kinematic viscosity and dynamic viscosity from the G-series

G-series			
Mix no.	**Average flow time (sec.)**	**Kinematic viscosity (m^2/s)**	**Dynamic viscosity (mPa*s)**
1	290	1.159E-06	1.179E+00
2	295	1.179E-06	1.198E+00
3	310	1.239E-06	1.258E+00
4	302	1.207E-06	1.226E+00
5	295	1.179E-06	1.198E+00

Table F 15 The relative concentration of solids from all the series calculated by using equation (7)

A-series						C-series		D-series	
Mix no.	ϕ/ϕ_{max}	**Mix no.**	ϕ/ϕ_{max}	**Mix no.**	ϕ/ϕ_{max}	**Mix no.**	ϕ/ϕ_{max}	**Mix no.**	ϕ/ϕ_{max}
1	0.940	**10**	0.938	**19**	0.945	**1**	0.843	**1**	0.844
2	0.940	**11**	0.942	**20**	0.951	**2**	0.874	**2**	0.810
3	0.946	**12**	0.947	**21**	0.953	**3**	0.831	**3**	0.786
4	0.870	**13**	0.895	**22**	0.913	**4**	0.819	**4**	0.761
5	0.926	**14**	0.908	**23**	0.926	**5**	0.818	**5**	0.827
6	0.912	**15**	0.920	**24**	0.933	**6**	0.851	**6**	0.814
7	0.841	**16**	0.850	**25**	0.870	**7**	0.885	**7**	0.795
8	0.860	**17**	0.860	**26**	0.886	**8**	0.873	**8**	0.798
9	0.862	**18**	0.866	**27**	0.893	**9**	0.870	**9**	0.787
								10	0.763

B-series									
Mix no.	ϕ/ϕ_{max}	**Mix no.**	ϕ/ϕ_{max}	**Mix no.**	ϕ/ϕ_{max}	**Mix no.**	ϕ/ϕ_{max}	**Mix no.**	ϕ/ϕ_{max}
1	0.946	**6**	0.957	**11**	0.954	**16**	0.890	**21**	0.913
2	0.951	**7**	0.947	**12**	0.959	**17**	0.904	**22**	0.880
3	0.953	**8**	0.951	**13**	0.897	**18**	0.918	**23**	0.894
4	0.947	**9**	0.958	**14**	0.906	**19**	0.885	**24**	0.904
5	0.954	**10**	0.949	**15**	0.920	**20**	0.892		

E-series									
Mix no.	ϕ/ϕ_{max}	**Mix no.**	ϕ/ϕ_{max}	**Mix no.**	ϕ/ϕ_{max}	**Mix no.**	ϕ/ϕ_{max}	**Mix no.**	ϕ/ϕ_{max}
1	0.933	**10**	0.908	**19**	0.887	**28**	0.897	**37**	0.918
2	0.943	**11**	0.883	**20**	0.888	**29**	0.876	**38**	0.923
3	0.898	**12**	0.900	**21**	0.887	**30**	0.883	**39**	0.929
4	0.904	**13**	0.893	**22**	0.894	**31**	0.884	**44**	0.913
5	0.912	**14**	0.898	**23**	0.898	**32**	0.841	**45**	0.924
6	0.921	**15**	0.938	**24**	0.903	**33**	0.899	**46**	0.924
7	0.889	**16**	0.951	**25**	0.878	**34**	0.902	**47**	0.937
8	0.895	**17**	0.874	**26**	0.890	**35**	0.914	**48**	0.931
9	0.898	**18**	0.878	**27**	0.891	**36**	0.908		

F-series						G-series			
Mix no.	ϕ/ϕ_{max}	**Mix no.**	ϕ/ϕ_{max}	**Mix no.**	ϕ/ϕ_{max}	**Mix no.**	ϕ/ϕ_{max}	**Mix no.**	ϕ/ϕ_{max}
1	0.900	**3**	0.894	**5**	0.905	**1**	0.937	**4**	0.940
2	0.910	**4**	0.895	**6**	0.895	**2**	0.944	**5**	0.942
						3	0.937		

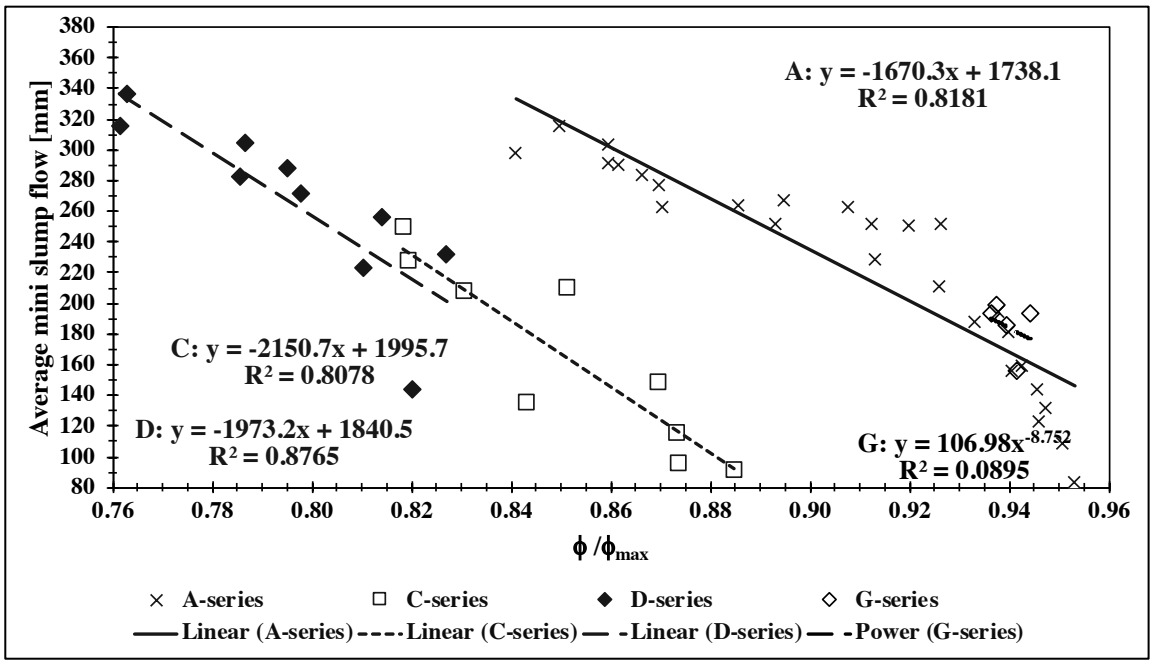
Average mini slump flow [mm]
380
360
340
320
300
280
260
240
220
200
180
160
140
120
100
80
0.76
0.78
0.80
0.82
0.84
0.86
0.88
0.90
0.92
0.94
0.96
ϕ /ϕmax
A: y = -1670.3x + 1738.1
R² = 0.8181
C: y = -2150.7x + 1995.7
R² = 0.8078
D: y = -1973.2x + 1840.5
R² = 0.8765
G: y = 106.98x-8.752
R² = 0.0895
A-series
C-series
D-series
G-series
Linear (A-series)
Linear (C-series)
Linear (D-series)
Power (G-series)

(a)

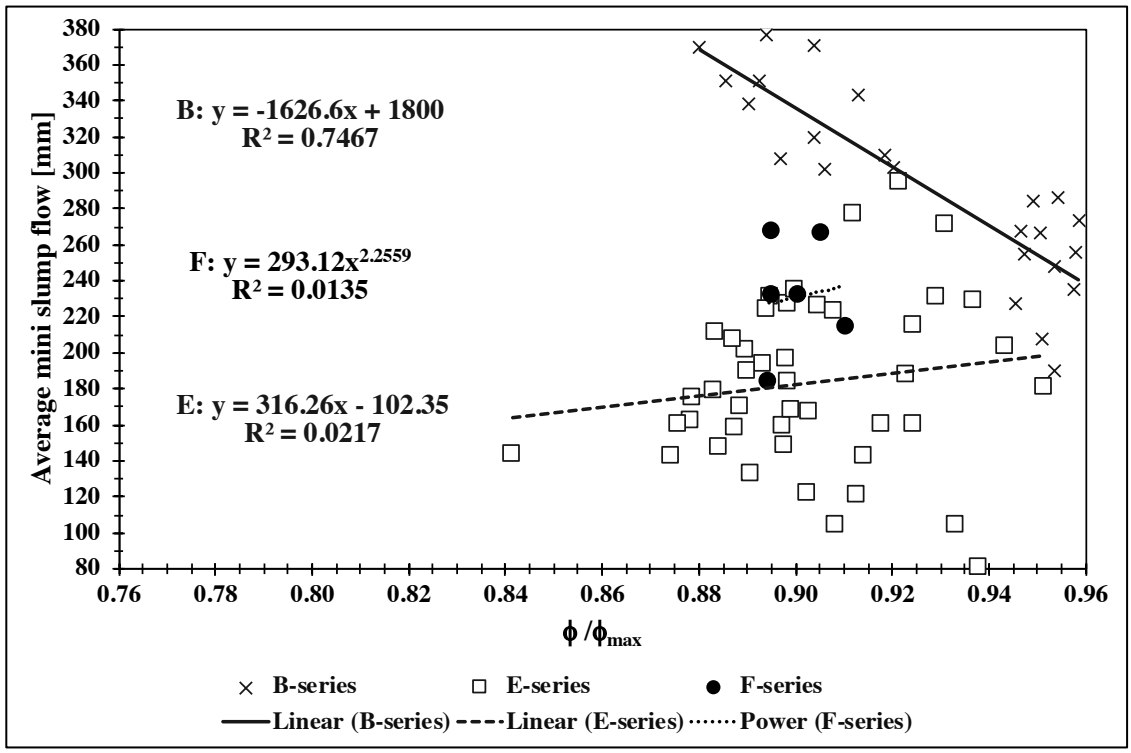
Average mini slump flow [mm]
380
360
340
320
300
280
260
240
220
200
180
160
140
120
100
80
0.76
0.78
0.80
0.82
0.84
0.86
0.88
0.90
0.92
0.94
0.96
ϕ /ϕmax
B: y = -1626.6x + 1800
R² = 0.7467
F: y = 293.12x2.2559
R² = 0.0135
E: y = 316.26x - 102.35
R² = 0.0217
B-series
E-series
F-series
Linear (B-series)
Linear (E-series)
Power (F-series)

(b)

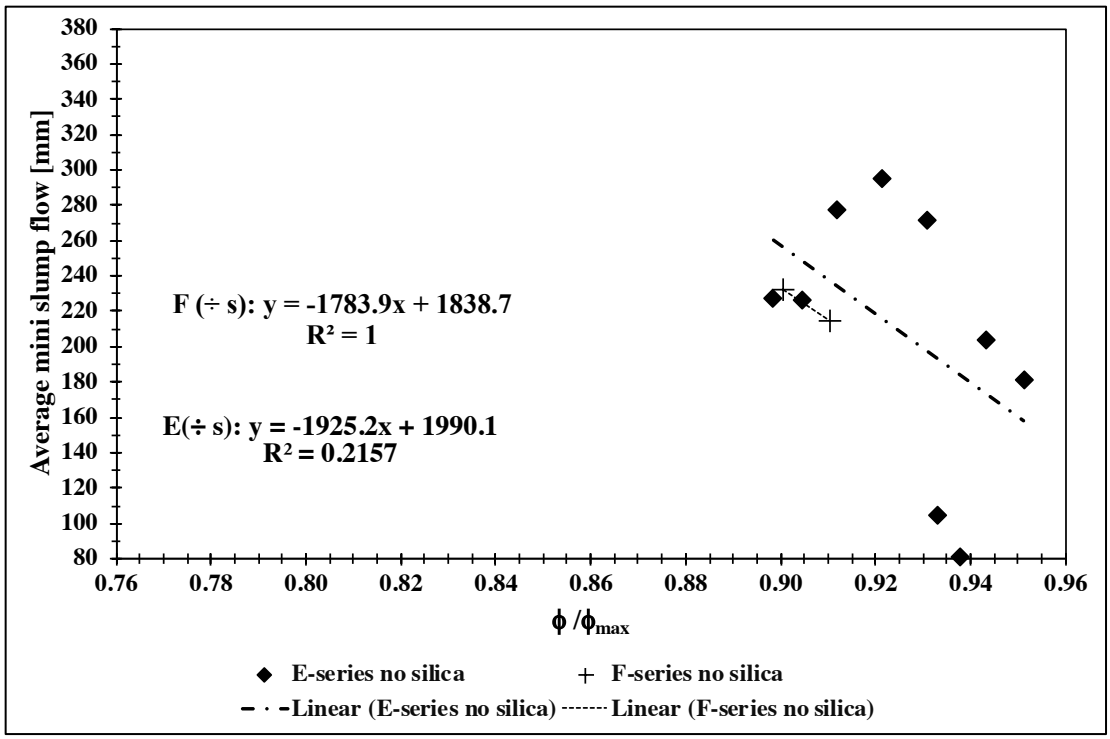

(c)

Figure F 1 The relations of relative concentration of solids on average mini slump flow (mm) from (a) the A-, C-, D- and G-series, (b) the B-, E- and F-series and (c) the E- and F-series with no silica

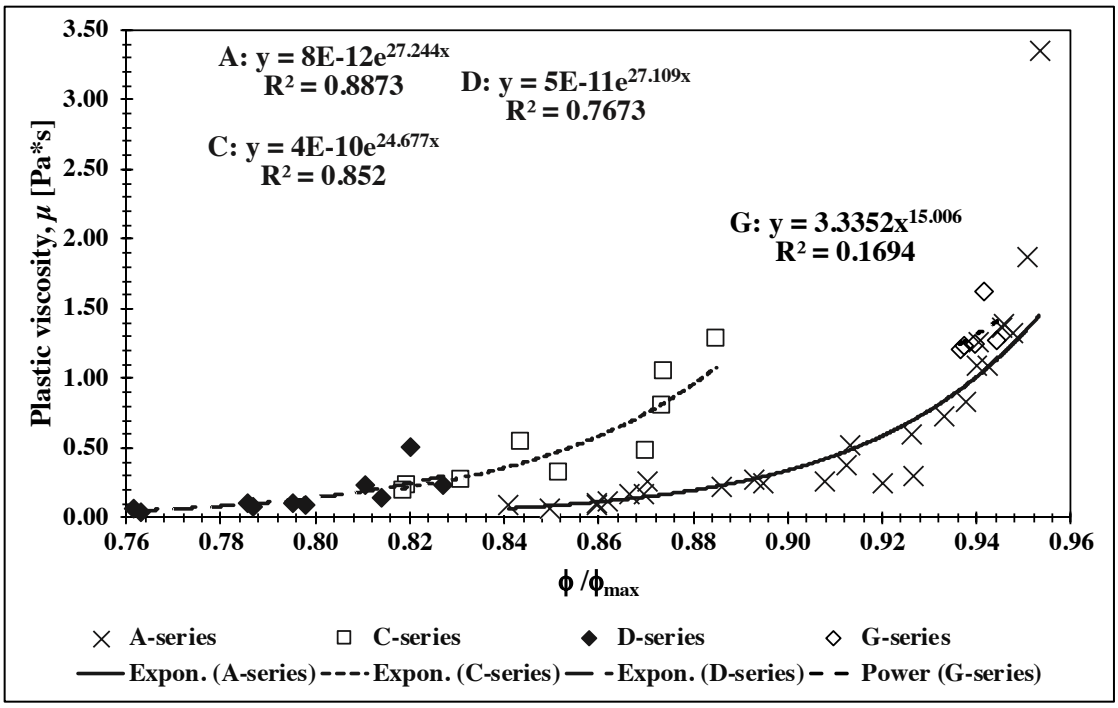

(a)

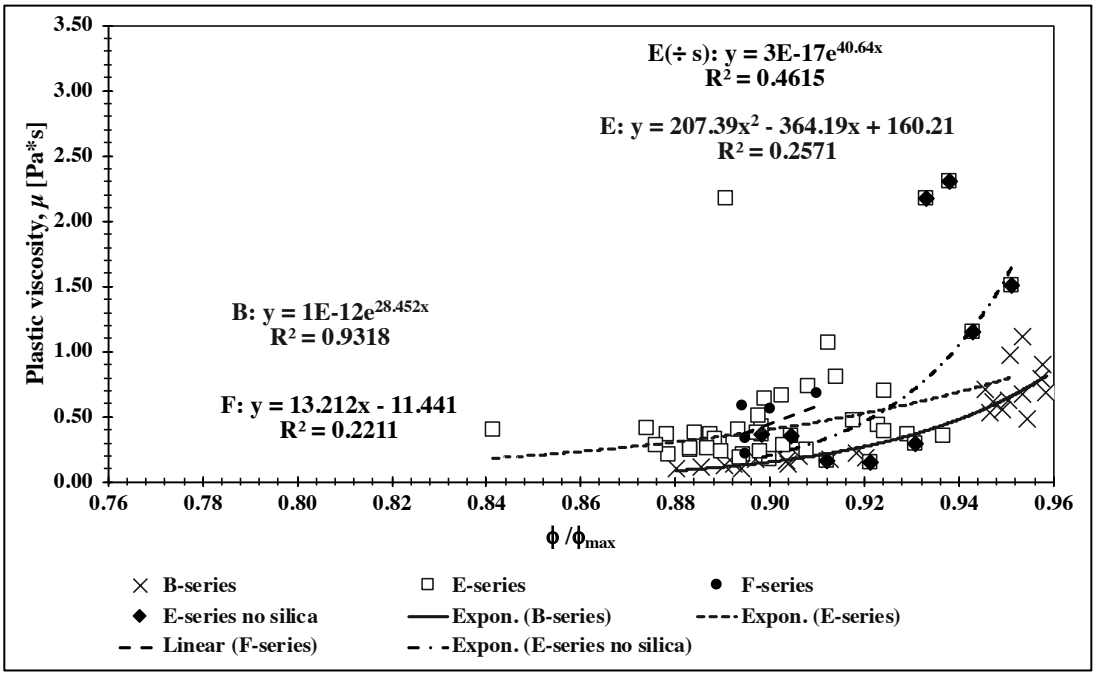

(b)

Figure F 2 The relations of relative concentration of solids on plastic viscosity (Pa*s), μ, from (a) the A-, C-, D- and G-series and (b) the B-, E- and F-series.

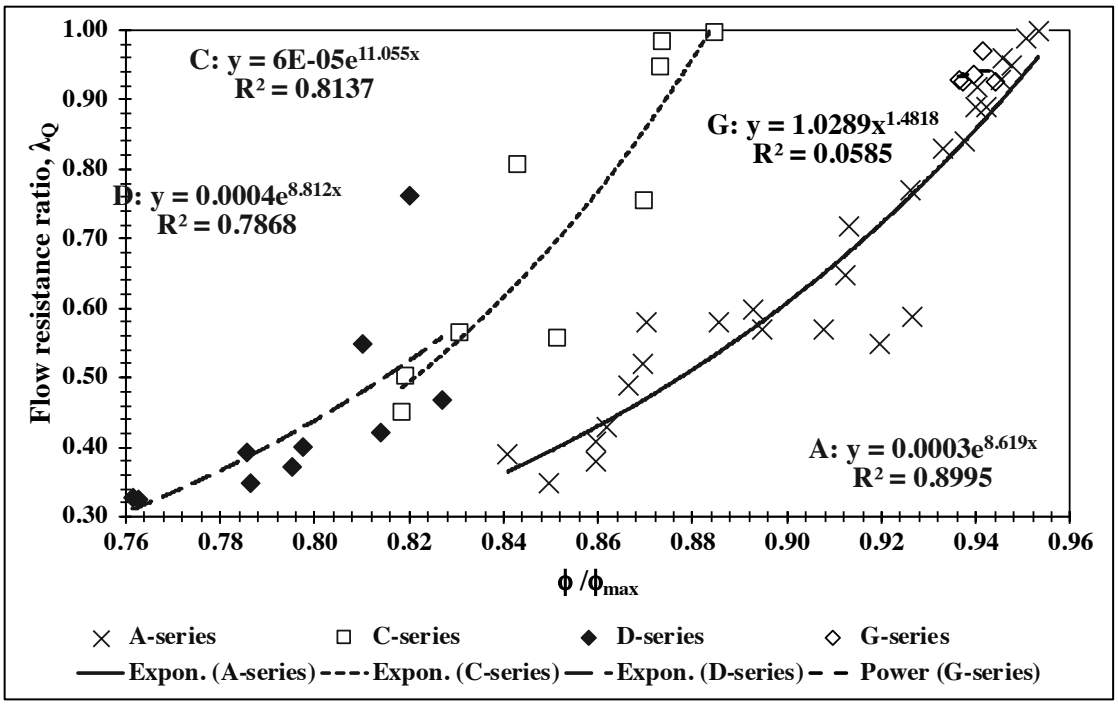

(a)

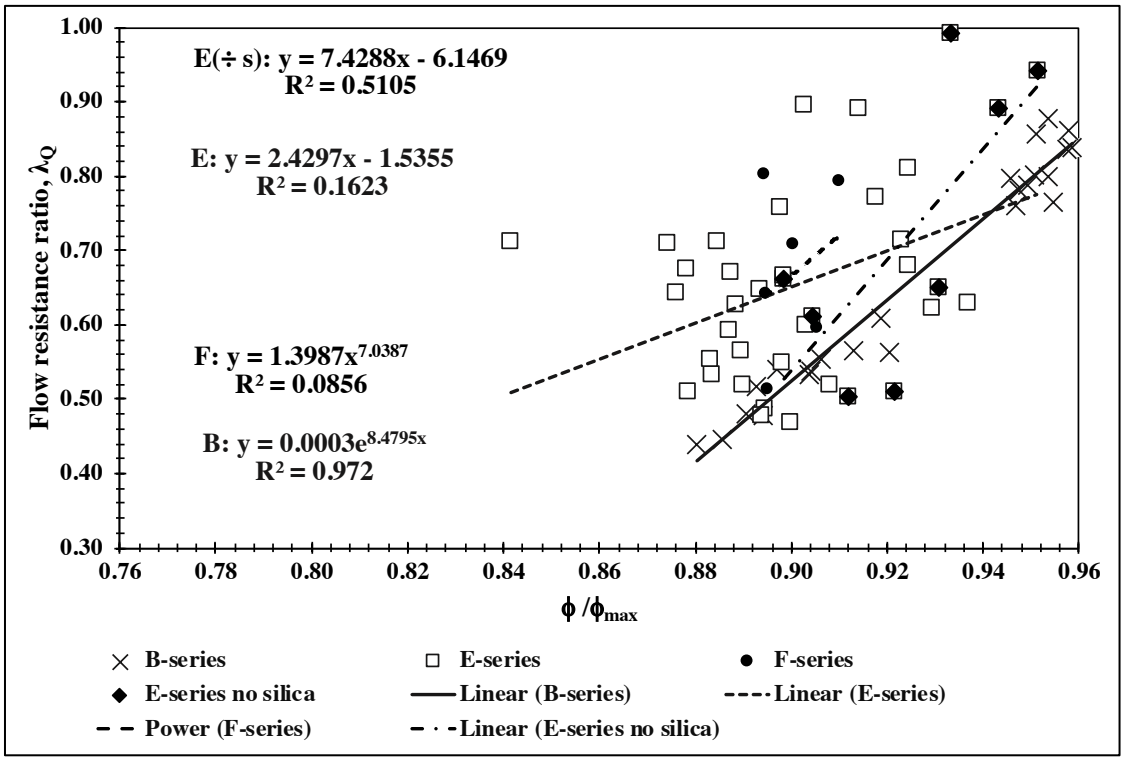

(b)

Figure F 3 The relations of relative concentration of solids on flow resistance ratio, λ_Q, from (a) the A-, C-, D- and G-series and (b) the B-, E- and F-series.

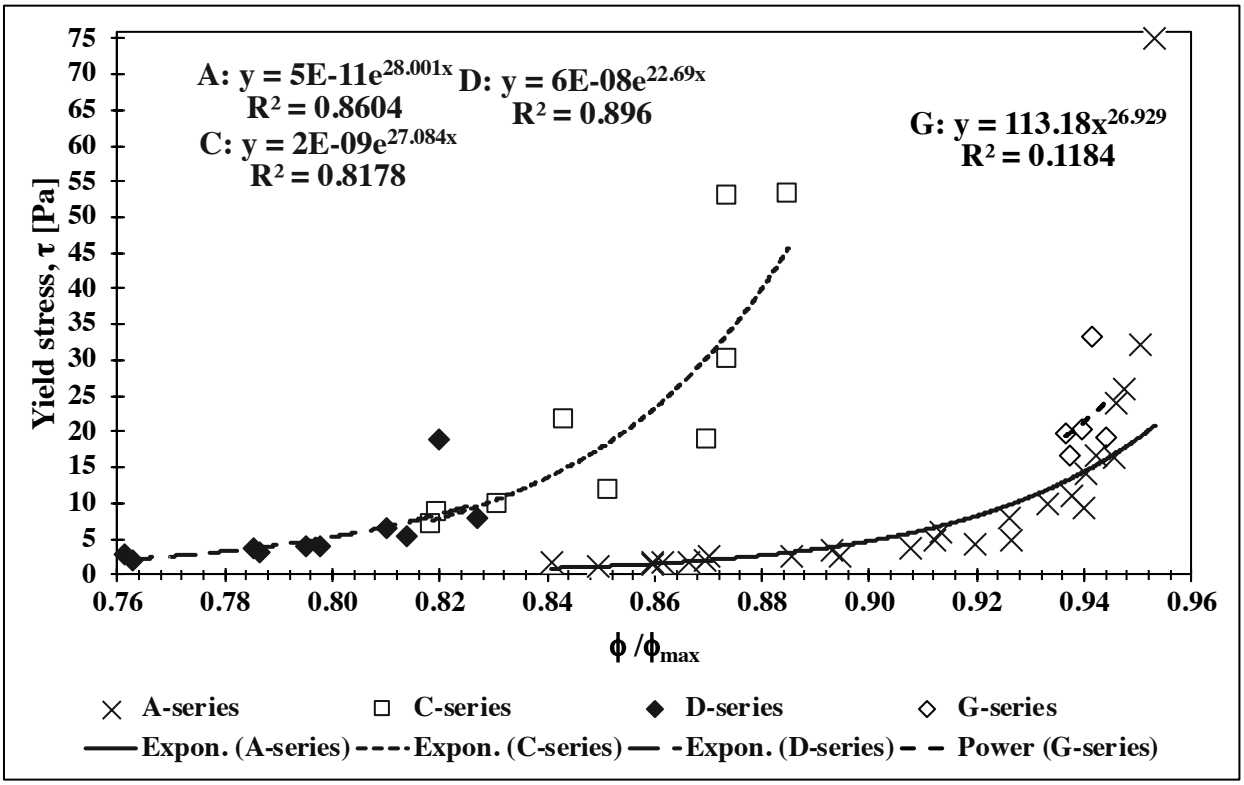
A: y = 5E-11e^28.001x
R² = 0.8604
C: y = 2E-09e^27.084x
R² = 0.8178
D: y = 6E-08e^22.69x
R² = 0.896
G: y = 113.18x^26.929
R² = 0.1184
Yield stress, τ [Pa]
ϕ /ϕmax
A-series
C-series
D-series
G-series
Expon. (A-series)
Expon. (C-series)
Expon. (D-series)
Power (G-series)

(a)

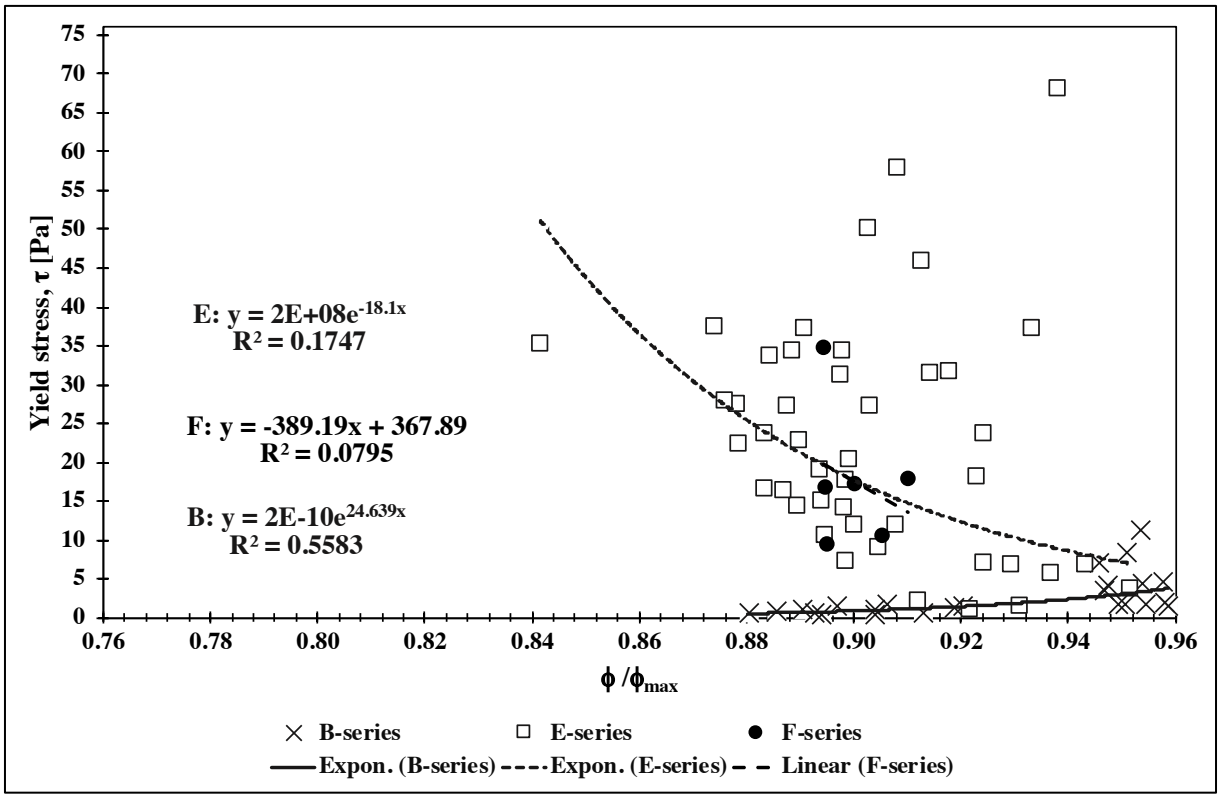
E: y = 2E+08e^-18.1x
R² = 0.1747
F: y = -389.19x + 367.89
R² = 0.0795
B: y = 2E-10e^24.639x
R² = 0.5583
Yield stress, τ [Pa]
ϕ /ϕmax
B-series
E-series
F-series
Expon. (B-series)
Expon. (E-series)
Linear (F-series)

(b)

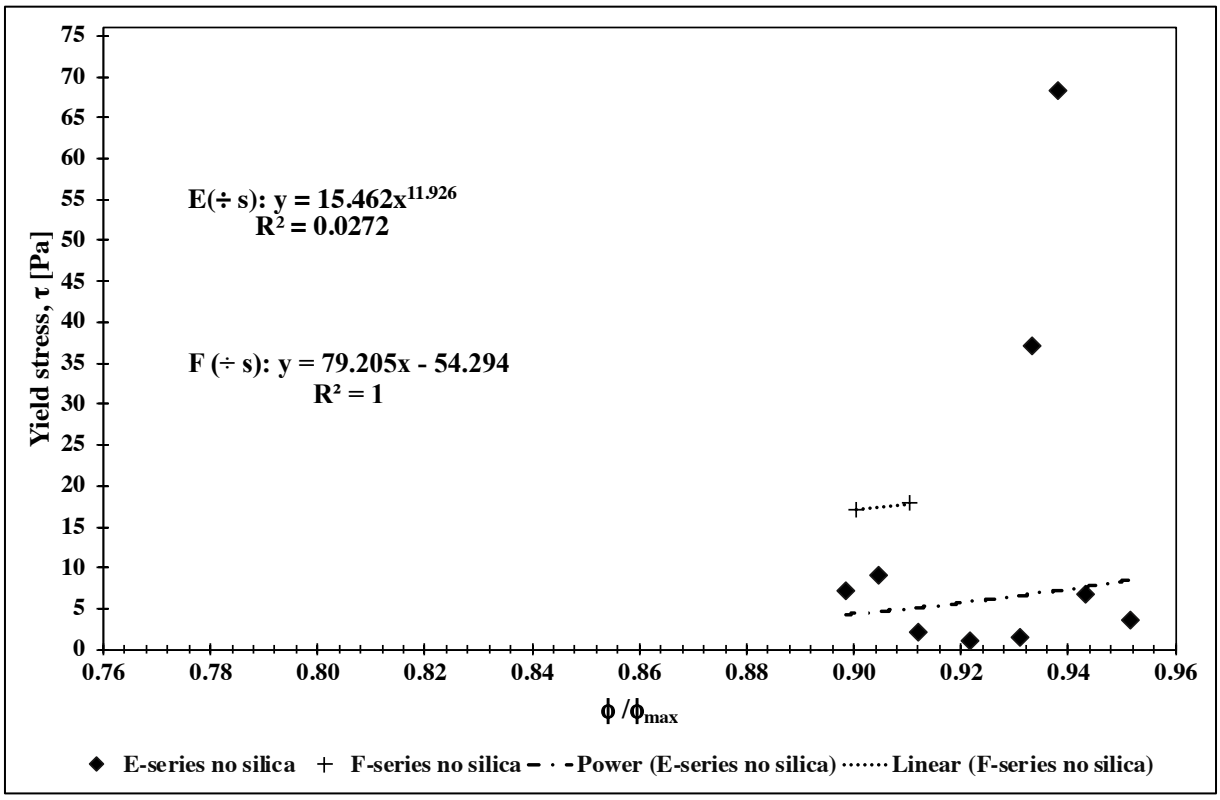

(c)

Figure F 4 The relations of relative concentration of solids on yield stress (Pa), τ, from (a) the A-, C-D- and G-series, (b) the B-, E- and F-series and (c) the E- and F-series with no silica

Appendix G: Viscosity of water

Table G 1 The average flow time, the kinematic viscosity, the dynamic viscosity measured from water from the laboratory compared to the standard dynamic viscosity from Kestin et al. [25] at 10, 20, and 30 degrees Celsius

Cannon-Fenske Routine no. 50					
Temperature (Celsius)	**Average flow time (s)**	**Kinematic viscosity (m2/s)**	**Dynamic viscosity (mPa*s)**	**Standard dynamic viscosity (mPa*s)**	**Difference in % (of the standard)**
10	372	1.487E-06	1.487E+00	1.306E+00	14
20	278	1.111E-06	1.111E+00	1.002E+00	11
30	232	9.262E-07	9.262E-01	7.97E-01	16
Cannon-Fenske Routine no. 75					
Temperature (Celsius)	**Average flow time (s)**	**Kinematic viscosity (m2/s)**	**Dynamic viscosity (mPa*s)**	**Standard dynamic viscosity (mPa*s)**	**Difference in % (of the standard)**
10	206	1.647E-06	1.647E+00	1.306E+00	26
20	159	1.270E-06	1.267E+00	1.002E+00	26
30	134	1.069E-06	1.064E+00	7.97E-01	34

The full detail and calculation of the viscosity of water from the laboratory measured at different temperatures can be found in an excel file “Viscosity of water.xlsx” and it is uploaded on: **https://www.dropbox.com/s/6s75r61cfm3nqyi/Viscosity%20of%20water.xlsx?dl=0**

All the online Appendixes are uploaded in the folder “TKT4925 Concrete Technology Master’s thesis Appendices – Metathip Sihaklang” on: **https://www.dropbox.com/sh/2b6ybeshelxa0km/AAB0KqYhQlAyVkCcG64TCbCva?dl=0**

Appendix H The Krieger-Dougherty apparent viscosity and Solver's analysis

All of the calculations and Solver's analysis (with silica, no silica, varying intrinsic viscosity and constant intrinsic viscosity) of apparent viscosity from the Krieger-Dougherty equation (eq. *(8)*) can be found as an online appendix uploaded as an Excel file "The Krieger-Dougherty equation and Intrinsic viscosity analysis.xlsx" on:
https://www.dropbox.com/s/g8mhcr6vu8ox7k9/The%20Krieger-Dougherty%20equation%20and%20Intrinsic_viscosity%20analysis.xlsx?dl=0

Note that the measured plastic viscosity in this Appendix had been taken from Appendix B.

All online Appendixes are uploaded in the folder "TKT4925 Concrete Technology Master's thesis Appendices – Metathip Sihaklang" on:
https://www.dropbox.com/sh/2b6ybeshelxa0km/AAB0KqYhQlAyVkCcG64TCbCva?dl=0

Table H 1 The apparent viscosity calculated by using the Krieger-Dougherty equation (eq. (8)) with silica and varying intrinsic viscosity for each of the series

Viscosity of excess fluid - Krieger-Dougherty equation (varying [η])															
A-series									C-series			D-series			
Mix no.	η	μ	Mix no.	η	μ	Mix no.	η	μ	Mix no.	η	μ	Mix no.	η	μ
1	1.041	1.090	**10**	0.953	0.840	**19**	1.236	1.370	**1**	0.235	0.546	**1**	0.227	0.509
2	1.315	1.260	**11**	1.315	1.090	**20**	1.813	1.880	**2**	0.529	1.057	**2**	0.198	0.240
3	1.910	1.400	**12**	1.957	1.330	**21**	2.431	3.360	**3**	0.234	0.275	**3**	0.156	0.108
4	0.156	0.260	**13**	0.230	0.250	**22**	0.320	0.520	**4**	0.234	0.237	**4**	0.131	0.068
5	0.517	0.310	**14**	0.346	0.270	**23**	0.487	0.600	**5**	0.241	0.200	**5**	0.237	0.238
6	0.416	0.384	**15**	0.476	0.250	**24**	0.666	0.730	**6**	0.514	0.333	**6**	0.204	0.153
7	0.085	0.100	**16**	0.092	0.070	**25**	0.120	0.180	**7**	0.911	1.296	**7**	0.178	0.106
8	0.108	0.110	**17**	0.107	0.100	**26**	0.157	0.230	**8**	0.939	0.810	**8**	0.183	0.096
9	0.124	0.120	**18**	0.128	0.170	**27**	0.191	0.280	**9**	0.956	0.487	**9**	0.160	0.080
												10	0.132	0.050

B-series															
Mix no.	η	μ	Mix no.	η	μ	Mix no.	η	μ	Mix no.	η	μ	Mix no.	η	μ
1	0.456	0.717	**6**	0.992	0.795	**11**	0.721	0.490	**16**	0.100	0.134	**21**	0.178	0.182
2	0.618	0.972	**7**	0.460	0.532	**12**	0.997	0.690	**17**	0.141	0.167	**22**	0.093	0.104
3	0.781	1.118	**8**	0.614	0.624	**13**	0.105	0.174	**18**	0.198	0.225	**23**	0.120	0.101
4	0.471	0.619	**9**	0.951	0.902	**14**	0.133	0.197	**19**	0.093	0.115	**24**	0.174	0.136
5	0.672	0.676	**10**	0.545	0.559	**15**	0.201	0.193	**20**	0.126	0.138			

E-series															
Mix no.	η	μ	Mix no.	η	μ	Mix no.	η	μ	Mix no.	η	μ	Mix no.	η	μ
1	0.886	2.171	**10**	0.415	0.245	**19**	0.332	0.372	**28**	0.383	0.373	**37**	0.620	0.480
2	1.310	1.157	**11**	0.249	0.246	**20**	0.342	0.325	**29**	0.232	0.286	**38**	0.698	0.439
3	0.287	0.362	**12**	0.332	0.173	**21**	0.249	0.266	**30**	0.288	0.255	**39**	0.829	0.363
4	0.349	0.361	**13**	0.334	0.403	**22**	0.281	0.184	**31**	0.315	0.376	**44**	0.525	1.073
5	0.367	0.169	**14**	0.363	0.237	**23**	0.344	0.510	**32**	0.191	0.406	**45**	0.713	0.698
6	0.506	0.149	**15**	1.283	2.300	**24**	0.372	0.284	**33**	0.326	0.635	**46**	0.679	0.396
7	0.254	0.293	**16**	2.140	1.511	**25**	0.225	0.363	**34**	0.392	0.668	**47**	1.006	0.359
8	0.281	0.209	**17**	0.236	0.419	**26**	0.299	0.239	**35**	0.543	0.811	**48**	0.723	0.297
9	0.335	0.427	**18**	0.266	0.216	**27**	0.325	2.171	**36**	0.495	0.733			

F-series									G-series					
Mix no.	η	μ	Mix no.	η	μ	Mix no.	η	μ	Mix no.	η	μ	Mix no.	η	μ
1	0.380	0.562	**3**	0.426	0.587	**5**	0.516	0.336	**1**	1.164	1.239	**4**	1.313	1.258
2	0.538	0.679	**4**	0.365	0.211	**6**	0.465	0.330	**2**	1.503	1.274	**5**	1.387	1.629
									3	1.210	1.210			

η = Predicted apparent viscosity by KD equation **μ = Measured plastic viscosity from the laboratory**

Table H 2 The apparent viscosity calculated by using the Krieger-Dougherty equation (eq. (8), no silica and varying intrinsic viscosity for each of the series

Viscosity of excess fluid - Krieger-Dougherty equation (varying [η], no silica)															
A-series									**C-series**			**D-series**			
Mix no.	η	μ	**Mix no.**	η	μ	**Mix no.**	η	μ	**Mix no.**	η	μ	**Mix no.**	η	μ	
1	1.041	1.090	**10**	0.953	0.840	**19**	1.236	1.370	**1**	0.235	0.546	**1**	0.227	0.509	
2	1.315	1.260	**11**	1.315	1.090	**20**	1.813	1.880	**2**	0.529	1.057	**2**	0.198	0.240	
3	1.910	1.400	**12**	1.957	1.330	**21**	2.431	3.360	**3**	0.234	0.275	**3**	0.156	0.108	
4	0.156	0.260	**13**	0.230	0.250	**22**	0.320	0.520	**4**	0.234	0.237	**4**	0.131	0.068	
5	0.517	0.310	**14**	0.346	0.270	**23**	0.487	0.600	**5**	0.241	0.200	**5**	0.237	0.238	
6	0.416	0.384	**15**	0.476	0.250	**24**	0.666	0.730	**6**	0.514	0.333	**6**	0.204	0.153	
7	0.085	0.100	**16**	0.092	0.070	**25**	0.120	0.180	**7**	0.911	1.296	**7**	0.178	0.106	
8	0.108	0.110	**17**	0.107	0.100	**26**	0.157	0.230	**8**	0.939	0.810	**8**	0.183	0.096	
9	0.124	0.120	**18**	0.128	0.170	**27**	0.191	0.280	**9**	0.956	0.487	**9**	0.160	0.080	
												10	0.132	0.050	

B-series															
Mix no.	η	μ	**Mix no.**	η	μ	**Mix no.**	η	μ	**Mix no.**	η	μ	**Mix no.**	η	μ	
1	0.456	0.717	**6**	0.992	0.795	**11**	0.721	0.490	**16**	0.100	0.134	**21**	0.178	0.182	
2	0.618	0.972	**7**	0.460	0.532	**12**	0.997	0.690	**17**	0.141	0.167	**22**	0.093	0.104	
3	0.781	1.118	**8**	0.614	0.624	**13**	0.105	0.174	**18**	0.198	0.225	**23**	0.120	0.101	
4	0.471	0.619	**9**	0.951	0.902	**14**	0.133	0.197	**19**	0.093	0.115	**24**	0.174	0.136	
5	0.672	0.676	**10**	0.545	0.559	**15**	0.201	0.193	**20**	0.126	0.138				

E-series															
Mix no.	η	μ	**Mix no.**	η	μ	**Mix no.**	η	μ	**Mix no.**	η	μ	**Mix no.**	η	μ	
1	0.907	2.171	**10**	-	0.245	**19**	-	0.372	**28**	-	0.373	**37**	-	0.480	
2	1.343	1.157	**11**	-	0.246	**20**	-	0.325	**29**	-	0.286	**38**	-	0.439	
3	0.293	0.362	**12**	-	0.173	**21**	-	0.266	**30**	-	0.255	**39**	-	0.363	
4	0.357	0.361	**13**	-	0.403	**22**	-	0.184	**31**	-	0.376	**44**	-	1.073	
5	0.375	0.169	**14**	-	0.237	**23**	-	0.510	**32**	-	0.406	**45**	-	0.698	
6	0.517	0.149	**15**	1.316	2.300	**24**	-	0.284	**33**	-	0.635	**46**	-	0.396	
7	-	0.293	**16**	2.199	1.511	**25**	-	0.363	**34**	-	0.668	**47**	-	0.359	
8	-	0.209	**17**	-	0.419	**26**	-	0.239	**35**	-	0.811	**48**	0.740	0.297	
9	-	0.427	**18**	-	0.216	**27**	-	2.171	**36**	-	0.733				

F-series									**G-series**					
Mix no.	η	μ	**Mix no.**	η	μ	**Mix no.**	η	μ	**Mix no.**	η	μ	**Mix no.**	η	μ
1	0.379	0.562	**3**	-	0.587	**5**	-	0.336	**1**	1.164	1.239	**4**	1.313	1.258
2	0.537	0.679	**4**	-	0.211	**6**	-	0.330	**2**	1.503	1.274	**5**	1.387	1.629
									3	1.210	1.210			

η = Predicted apparent viscosity by KD equation **μ = Measured plastic viscosity from the laboratory** **- = contained silica**

Table H 3 The apparent viscosity calculated by using the Krieger-Dougherty equation (eq. (8)) with silica and constant intrinsic viscosity for all the series

Viscosity of excess fluid - Krieger-Dougherty equation (constant [η])														
A-series									C-series			D-series		
Mix no.	η	μ	Mix no.	η	μ	Mix no.	η	μ	Mix no.	η	μ	Mix no.	η	μ
1	0.628	1.090	**10**	0.577	0.840	**19**	0.734	1.370	**1**	0.036	0.546	**1**	0.038	0.509
2	0.780	1.260	**11**	0.776	1.090	**20**	1.045	1.880	**2**	0.062	1.057	**2**	0.029	0.240
3	1.101	1.400	**12**	1.123	1.330	**21**	1.369	3.360	**3**	0.035	0.275	**3**	0.025	0.108
4	0.108	0.260	**13**	0.155	0.250	**22**	0.211	0.520	**4**	0.036	0.237	**4**	0.022	0.068
5	0.329	0.310	**14**	0.227	0.270	**23**	0.310	0.600	**5**	0.036	0.200	**5**	0.033	0.238
6	0.268	0.384	**15**	0.303	0.250	**24**	0.413	0.730	**6**	0.059	0.333	**6**	0.030	0.153
7	0.062	0.100	**16**	0.067	0.070	**25**	0.086	0.180	**7**	0.086	1.296	**7**	0.028	0.106
8	0.077	0.110	**17**	0.076	0.100	**26**	0.109	0.230	**8**	0.090	0.810	**8**	0.028	0.096
9	0.088	0.120	**18**	0.090	0.170	**27**	0.131	0.280	**9**	0.089	0.487	**9**	0.026	0.080
												10	0.023	0.050

B-series														
Mix no.	η	μ	Mix no.	η	μ	Mix no.	η	μ	Mix no.	η	μ	Mix no.	η	μ
1	0.838	0.717	**6**	1.975	0.795	**11**	1.392	0.490	**16**	0.158	0.134	**21**	0.298	0.182
2	1.177	0.972	**7**	0.848	0.532	**12**	1.994	0.690	**17**	0.229	0.167	**22**	0.145	0.104
3	1.529	1.118	**8**	1.167	0.624	**13**	0.166	0.174	**18**	0.334	0.225	**23**	0.192	0.101
4	0.869	0.619	**9**	1.897	0.902	**14**	0.216	0.197	**19**	0.145	0.115	**24**	0.286	0.136
5	1.294	0.676	**10**	1.013	0.559	**15**	0.341	0.193	**20**	0.202	0.138			

E-series														
Mix no.	η	μ	Mix no.	η	μ	Mix no.	η	μ	Mix no.	η	μ	Mix no.	η	μ
1	0.883	2.171	**10**	0.414	0.245	**19**	0.331	0.372	**28**	0.382	0.373	**37**	0.618	0.480
2	1.306	1.157	**11**	0.248	0.246	**20**	0.341	0.325	**29**	0.231	0.286	**38**	0.696	0.439
3	0.286	0.362	**12**	0.331	0.173	**21**	0.249	0.266	**30**	0.287	0.255	**39**	0.826	0.363
4	0.349	0.361	**13**	0.333	0.403	**22**	0.280	0.184	**31**	0.314	0.376	**44**	0.524	1.073
5	0.366	0.169	**14**	0.362	0.237	**23**	0.343	0.510	**32**	0.190	0.406	**45**	0.711	0.698
6	0.504	0.149	**15**	1.280	2.300	**24**	0.371	0.284	**33**	0.325	0.635	**46**	0.677	0.396
7	0.253	0.293	**16**	2.133	1.511	**25**	0.224	0.363	**34**	0.391	0.668	**47**	1.003	0.359
8	0.281	0.209	**17**	0.235	0.419	**26**	0.298	0.239	**35**	0.542	0.811	**48**	0.721	0.297
9	0.334	0.427	**18**	0.265	0.216	**27**	0.324	2.171	**36**	0.493	0.733			

F-series									G-series					
Mix no.	η	μ	Mix no.	η	μ	Mix no.	η	μ	Mix no.	η	μ	Mix no.	η	μ
1	0.195	0.562	**3**	0.214	0.587	**5**	0.254	0.336	**1**	0.647	1.239	**4**	0.726	1.258
2	0.265	0.679	**4**	0.187	0.211	**6**	0.232	0.330	**2**	0.820	1.274	**5**	0.761	1.629
									3	0.675	1.210			

η = Predicted apparent viscosity by KD equation **μ = Measured plastic viscosity from the laboratory**

Table H 4 The apparent viscosity calculated by using the Krieger-Dougherty equation (eq. (8)) no silica and constant intrinsic viscosity for all the series

Viscosity of excess fluid - Krieger-Dougherty equation (constant [η], no silica)														
A-series									C-series			D-series		
Mix no.	η	μ	**Mix no.**	η	μ	**Mix no.**	η	μ	**Mix no.**	η	μ	**Mix no.**	η	μ
1	0.609	1.090	**10**	0.561	0.840	**19**	0.713	1.370	**1**	0.036	0.546	**1**	0.038	0.509
2	0.757	1.260	**11**	0.753	1.090	**20**	1.012	1.880	**2**	0.060	1.057	**2**	0.029	0.240
3	1.066	1.400	**12**	1.087	1.330	**21**	1.325	3.360	**3**	0.035	0.275	**3**	0.025	0.108
4	0.106	0.260	**13**	0.151	0.250	**22**	0.206	0.520	**4**	0.035	0.237	**4**	0.022	0.068
5	0.321	0.310	**14**	0.222	0.270	**23**	0.302	0.600	**5**	0.036	0.200	**5**	0.032	0.238
6	0.261	0.384	**15**	0.295	0.250	**24**	0.402	0.730	**6**	0.058	0.333	**6**	0.029	0.153
7	0.061	0.100	**16**	0.065	0.070	**25**	0.084	0.180	**7**	0.084	1.296	**7**	0.027	0.106
8	0.075	0.110	**17**	0.075	0.100	**26**	0.107	0.230	**8**	0.088	0.810	**8**	0.028	0.096
9	0.086	0.120	**18**	0.088	0.170	**27**	0.128	0.280	**9**	0.087	0.487	**9**	0.025	0.080
												10	0.022	0.050

B-series														
Mix no.	η	μ	**Mix no.**	η	μ	**Mix no.**	η	μ	**Mix no.**	η	μ	**Mix no.**	η	μ
1	0.813	0.717	**6**	1.909	0.795	**11**	1.348	0.490	**16**	0.154	0.134	**21**	0.290	0.182
2	1.140	0.972	**7**	0.823	0.532	**12**	1.927	0.690	**17**	0.224	0.167	**22**	0.142	0.104
3	1.479	1.118	**8**	1.131	0.624	**13**	0.163	0.174	**18**	0.326	0.225	**23**	0.187	0.101
4	0.843	0.619	**9**	1.833	0.902	**14**	0.211	0.197	**19**	0.141	0.115	**24**	0.279	0.136
5	1.253	0.676	**10**	0.983	0.559	**15**	0.332	0.193	**20**	0.197	0.138			

E-series														
Mix no.	η	μ	**Mix no.**	η	μ	**Mix no.**	η	μ	**Mix no.**	η	μ	**Mix no.**	η	μ
1	0.528	2.171	**10**	-	0.245	**19**	-	0.372	**28**	-	0.373	**37**	-	0.480
2	0.761	1.157	**11**	-	0.246	**20**	-	0.325	**29**	-	0.286	**38**	-	0.439
3	0.188	0.362	**12**	-	0.173	**21**	-	0.266	**30**	-	0.255	**39**	-	0.363
4	0.224	0.361	**13**	-	0.403	**22**	-	0.184	**31**	-	0.376	**44**	-	1.073
5	0.235	0.169	**14**	-	0.237	**23**	-	0.510	**32**	-	0.406	**45**	-	0.698
6	0.314	0.149	**15**	0.743	2.300	**24**	-	0.284	**33**	-	0.635	**46**	-	0.396
7	-	0.293	**16**	1.191	1.511	**25**	-	0.363	**34**	-	0.668	**47**	-	0.359
8	-	0.209	**17**	-	0.419	**26**	-	0.239	**35**	-	0.811	**48**	0.438	0.297
9	-	0.427	**18**	-	0.216	**27**	-	2.171	**36**	-	0.733			

F-series									G-series					
Mix no.	η	μ	**Mix no.**	η	μ	**Mix no.**	η	μ	**Mix no.**	η	μ	**Mix no.**	η	μ
1	0.190	0.562	**3**	-	0.587	**5**	-	0.336	**1**	0.628	1.239	**4**	0.704	1.258
2	0.258	0.679	**4**	-	0.211	**6**	-	0.330	**2**	0.795	1.274	**5**	0.738	1.629
									3	0.655	1.210			

η = Predicted apparent viscosity by KD equation **μ = Measured plastic viscosity from the laboratory** **- = contained silica**

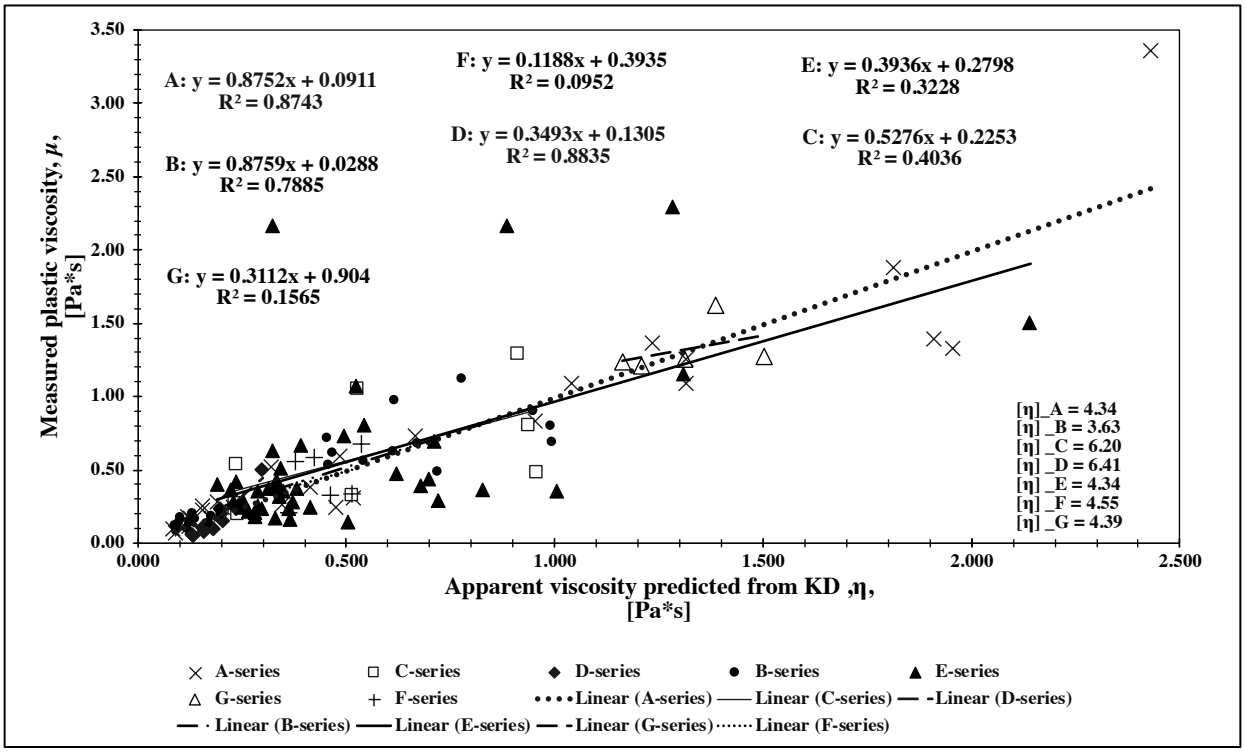

(a)

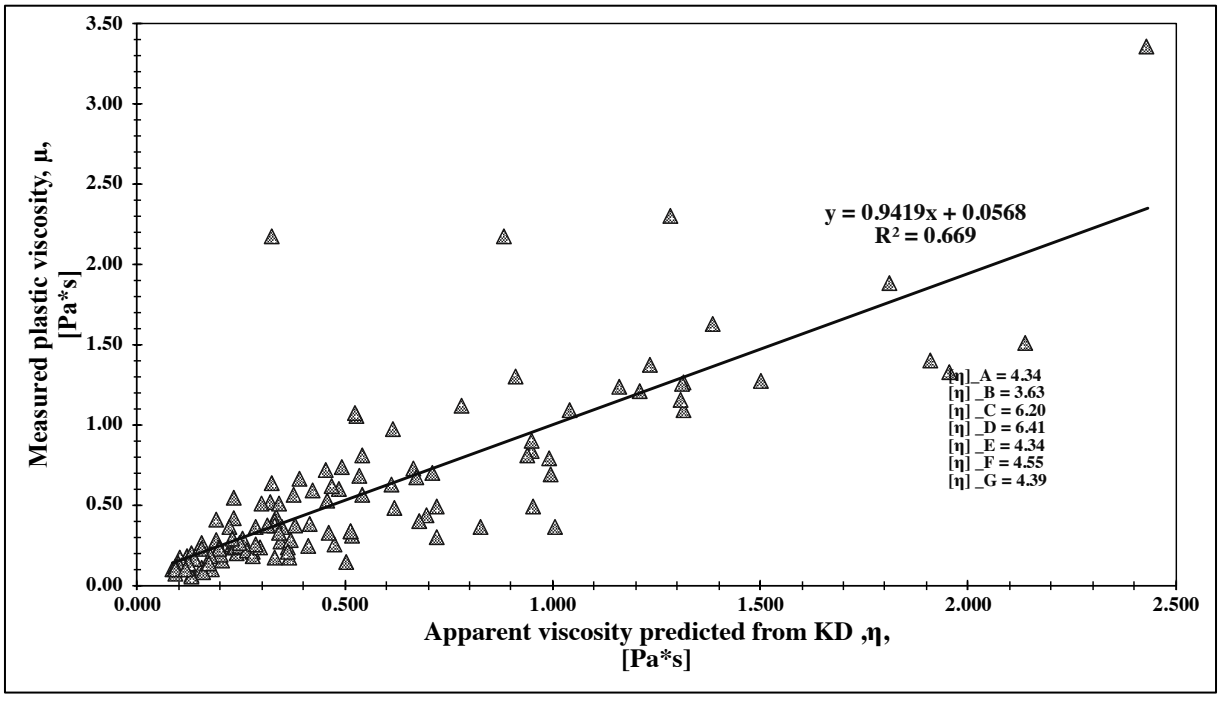

(b)

Figure H 1 The plastic viscosity measured from matrices plotted against the apparent viscosity of pore fluid calculated by the Krieger-Dougherty equation with varying intrinsic viscosity for (a) each of the series and (b) all the series

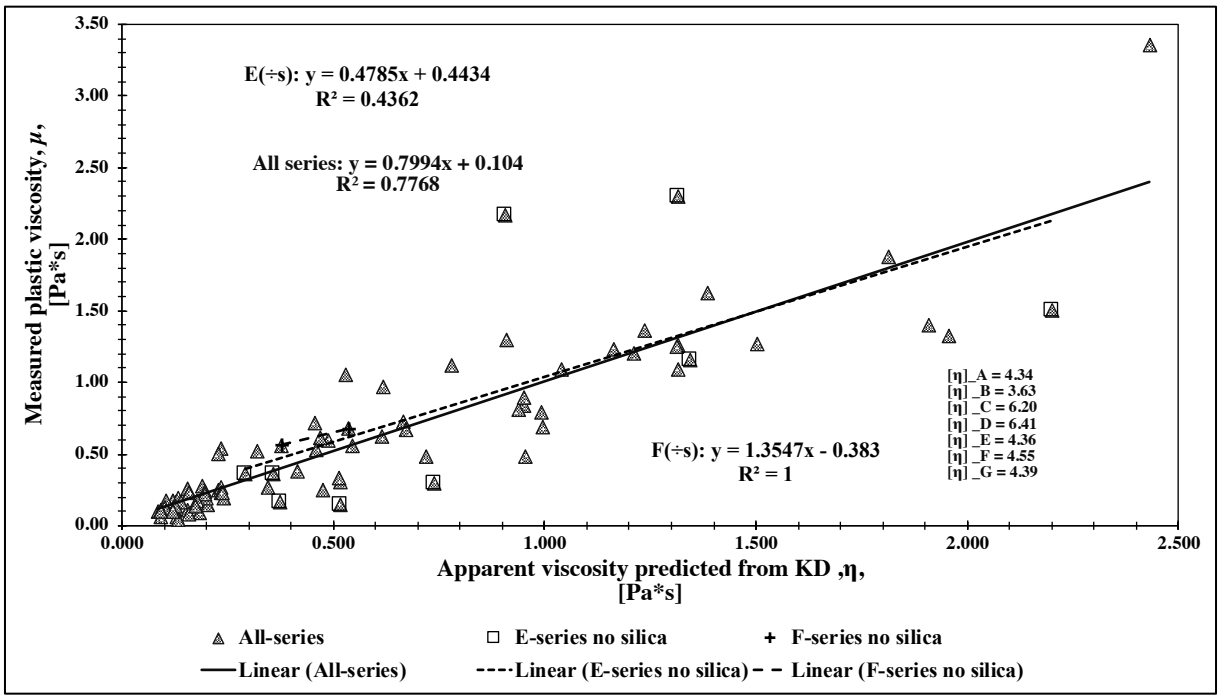

Figure H 2 The plastic viscosity measured from matrices plotted against the apparent viscosity of pore fluid calculated by the Krieger-Dougherty equation with varying intrinsic viscosity and no silica for all the series, the E- and F-series

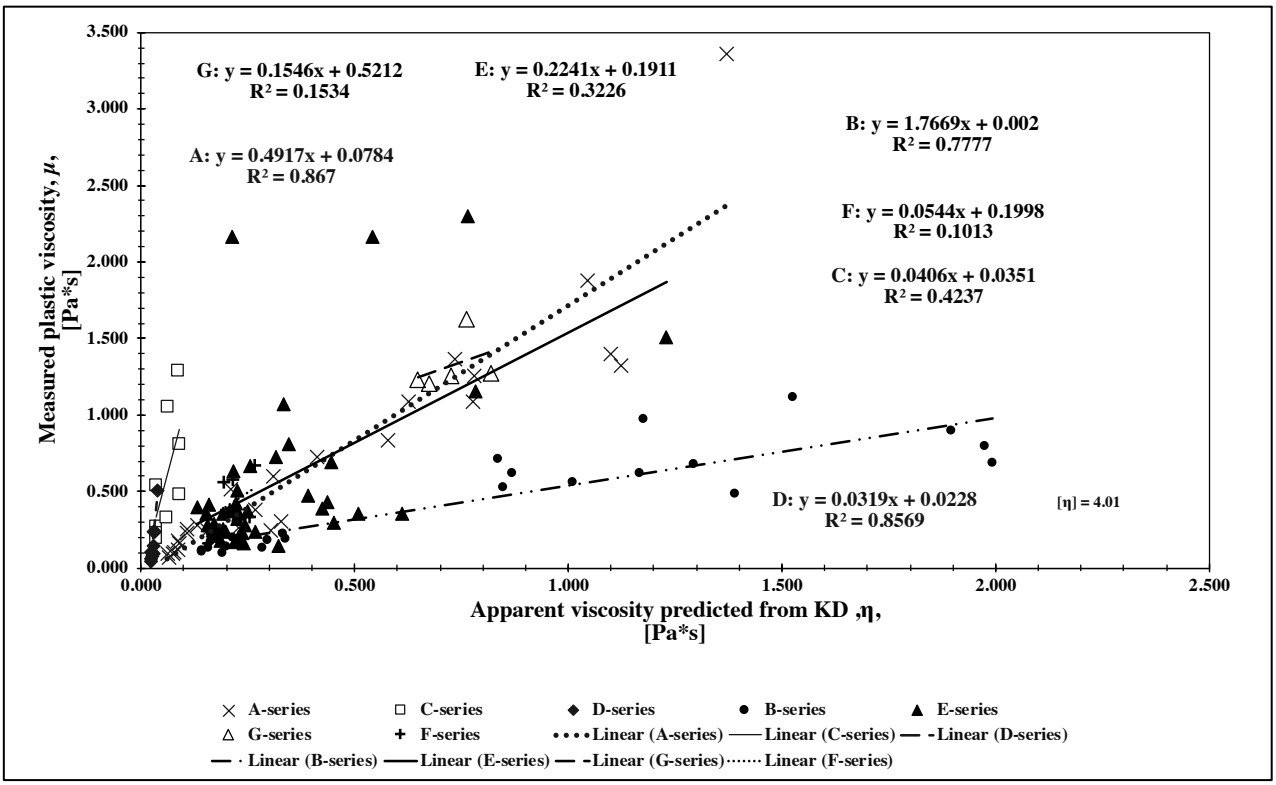

(a)

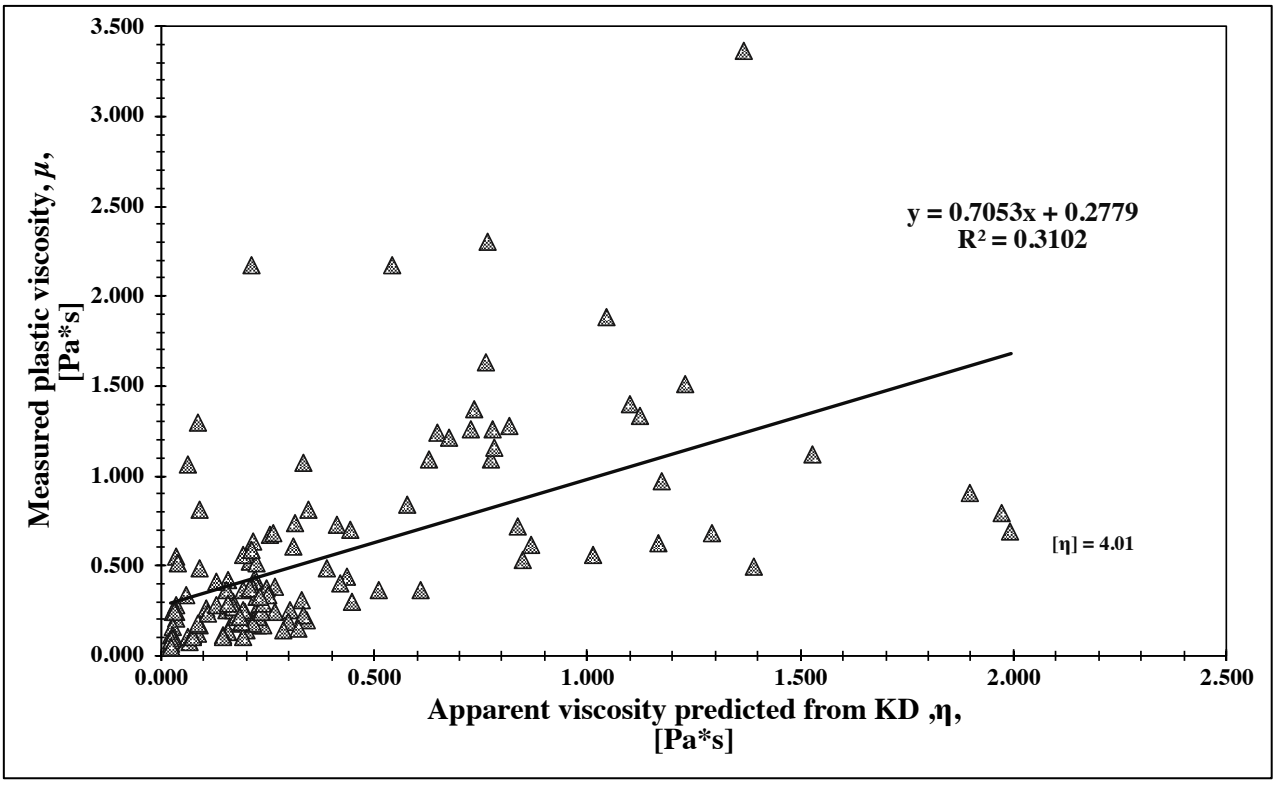

(b)

Figure H 3 The plastic viscosity measured from matrices plotted against the apparent viscosity of pore fluid calculated by the Krieger-Dougherty equation with constant intrinsic viscosity for (a) each of the series and (b) all the series.

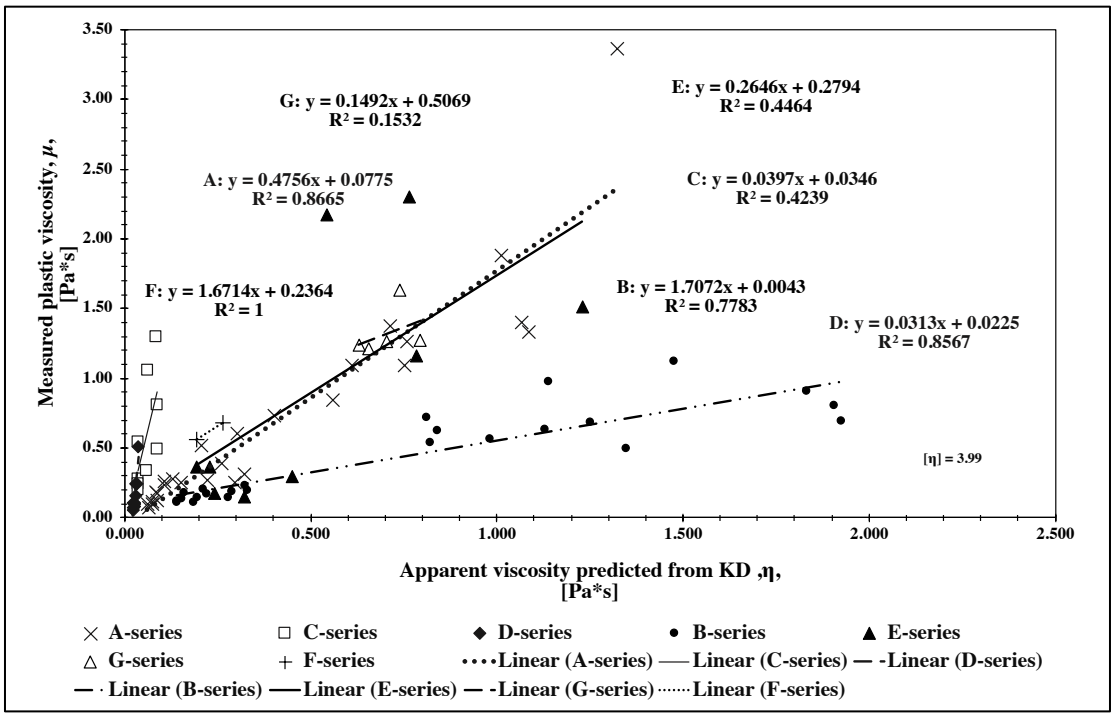

(a)

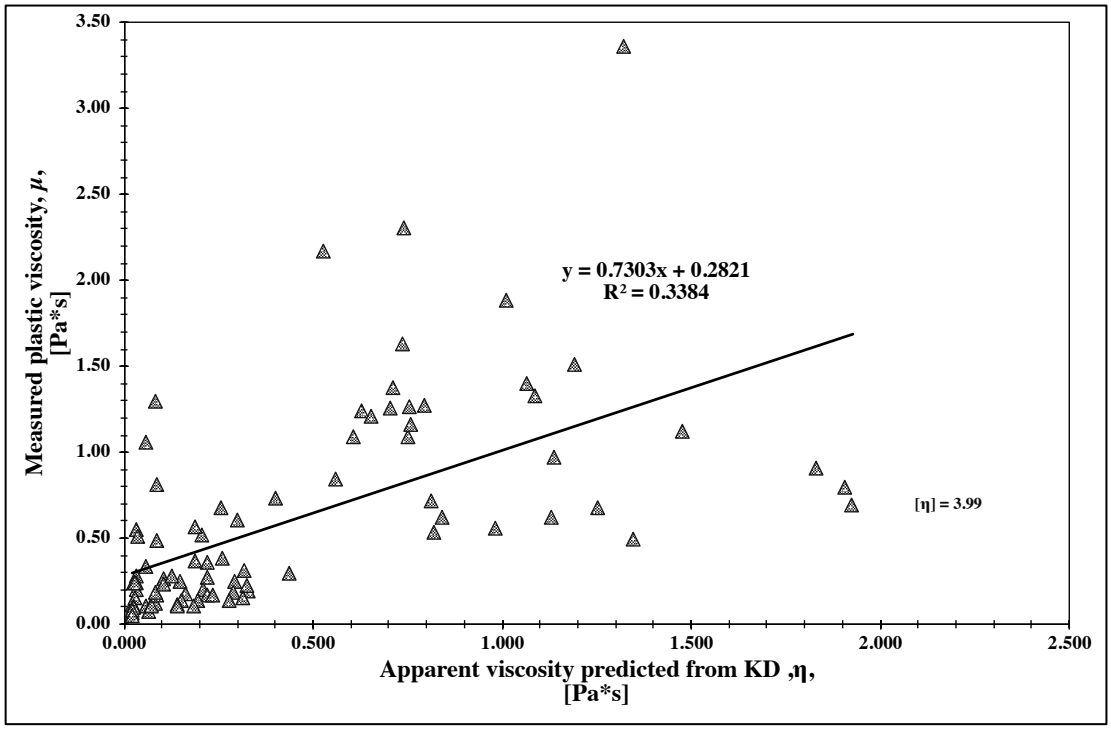

(b)

Figure H 4 The plastic viscosity measured from matrices plotted against the apparent viscosity of pore fluid calculated by the Krieger-Dougherty equation with constant intrinsic viscosity, no silica for (a) each of the series and (b) all the series.

Appendix I: Chong's apparent viscosity

All of the detailed calculation from the Chong's equation (eq.*(10)*) can be found as an online appendix uploaded as an Excel file "Chong viscosity.xlsx" on:
https://www.dropbox.com/s/jrr4ka671ef6qcj/Chong%20viscosity.xlsx?dl=0

Note that the measured plastic viscosity in this Appendix had been taken from Appendix B.

All the online Appendixes are uploaded in the folder "TKT4925 Concrete Technology Master's thesis Appendices – Metathip Sihaklang" on:
https://www.dropbox.com/sh/2b6ybeshelxa0km/AAB0KqYhQlAyVkCcG64TCbCva?dl=0

Table I 1 The apparent viscosity from all the series calculated by the Chong's relative viscosity equation (eq.(10))

Viscosity of excess fluid by the Chong's equation														
A-series									C-series			D-series		
Mix no.	η	μ	Mix no.	η	μ	Mix no.	η	μ	Mix no.	η	μ	Mix no.	η	μ
1	0.206	1.090	10	0.188	0.840	19	0.244	1.370	1	0.029	0.546	1	0.031	0.509
2	0.214	1.260	11	0.214	1.090	20	0.291	1.880	2	0.046	1.057	2	0.021	0.240
3	0.256	1.400	12	0.261	1.330	21	0.320	3.360	3	0.024	0.275	3	0.016	0.108
4	0.044	0.260	13	0.068	0.250	22	0.099	0.520	4	0.022	0.237	4	0.014	0.068
5	0.140	0.310	14	0.091	0.270	23	0.132	0.600	5	0.022	0.200	5	0.025	0.238
6	0.096	0.384	15	0.110	0.250	24	0.157	0.730	6	0.032	0.333	6	0.021	0.153
7	0.031	0.100	16	0.034	0.070	25	0.047	0.180	7	0.052	1.296	7	0.019	0.106
8	0.037	0.110	17	0.037	0.100	26	0.057	0.230	8	0.046	0.810	8	0.019	0.096
9	0.039	0.120	18	0.041	0.170	27	0.066	0.280	9	0.042	0.487	9	0.017	0.080
												10	0.014	0.050
B-series														
Mix no.	η	μ	Mix no.	η	μ	Mix no.	η	μ	Mix no.	η	μ	Mix no.	η	μ
1	0.279	0.717	6	0.462	0.795	11	0.391	0.490	16	0.068	0.134	21	0.106	0.182
2	0.328	0.972	7	0.283	0.532	12	0.466	0.690	17	0.090	0.167	22	0.061	0.104
3	0.357	1.118	8	0.326	0.624	13	0.073	0.174	18	0.121	0.225	23	0.073	0.101
4	0.291	0.619	9	0.444	0.902	14	0.086	0.197	19	0.061	0.115	24	0.100	0.136
5	0.363	0.676	10	0.340	0.559	15	0.124	0.193	20	0.077	0.138			
E-series														
Mix no.	η	μ	Mix no.	η	μ	Mix no.	η	μ	Mix no.	η	μ	Mix no.	η	μ
1	0.178	2.171	10	0.093	0.245	19	0.063	0.372	28	0.076	0.373	37	0.117	0.480
2	0.264	1.157	11	0.060	0.246	20	0.063	0.325	29	0.050	0.286	38	0.132	0.439
3	0.081	0.362	12	0.078	0.173	21	0.065	0.266	30	0.061	0.255	39	0.157	0.363
4	0.085	0.361	13	0.071	0.403	22	0.070	0.184	31	0.060	0.376	44	0.102	1.073
5	0.107	0.169	14	0.074	0.237	23	0.079	0.510	32	0.034	0.406	45	0.139	0.698
6	0.127	0.149	15	0.208	2.300	24	0.080	0.284	33	0.081	0.635	46	0.132	0.396
7	0.069	0.293	16	0.340	1.511	25	0.053	0.363	34	0.086	0.668	47	0.197	0.359
8	0.072	0.209	17	0.051	0.419	26	0.068	0.239	35	0.105	0.811	48	0.169	0.297
9	0.079	0.427	18	0.056	0.216	27	0.067	2.171	36	0.093	0.733			
F-series									G-series					
Mix no.	η	μ	Mix no.	η	μ	Mix no.	η	μ	Mix no.	η	μ	Mix no.	η	μ
1	0.083	0.562	3	0.069	0.587	5	0.087	0.336	1	0.177	1.239	4	0.199	1.258
2	0.100	0.679	4	0.072	0.211	6	0.071	0.330	2	0.226	1.274	5	0.209	1.629
									3	0.184	1.210			

η = Predicted apparent viscosity by the Chong's equation μ = Measured plastic viscosity from the laboratory

Appendix J: The liquid thicknesses

Note that the LT1 in this Appendix had been calculated by Skare in Appendix B, and the LT2 was calculated before in Appendix F.

Table J 1 The values of LT1 and LT2

LT1 and LT2														
A-series									C-series			D-series		
Mix no.	LT1	LT2	Mix no.	LT1	LT2	Mix no.	LT1	LT2	Mix no.	LT1	LT2	Mix no.	LT1	LT2
1	1.228	0.150	10	1.286	0.162	19	1.159	0.129	1	1.202	0.303	1	1.202	0.348
2	1.178	0.146	11	1.247	0.151	20	1.098	0.114	2	1.082	0.229	2	1.279	0.392
3	1.132	0.132	12	1.210	0.138	21	1.043	0.106	3	1.207	0.338	3	1.331	0.463
4	1.506	0.301	13	1.623	0.323	22	1.375	0.226	4	1.209	0.367	4	1.383	0.536
5	1.451	0.274	14	1.578	0.283	23	1.312	0.189	5	1.211	0.371	5	1.297	0.363
6	1.400	0.243	15	1.535	0.245	24	1.254	0.167	6	1.090	0.286	6	1.395	0.421
7	1.773	0.506	16	1.946	0.522	25	1.586	0.369	7	1.062	0.280	7	1.385	0.459
8	1.714	0.437	17	1.895	0.485	26	1.520	0.316	8	1.066	0.243	8	1.466	0.482
9	1.673	0.426	18	1.860	0.460	27	1.476	0.292	9	1.068	0.256	9	1.457	0.505
												10	1.522	0.584

B-series														
Mix no.	LT1	LT2	Mix no.	LT1	LT2	Mix no.	LT1	LT2	Mix no.	LT1	LT2	Mix no.	LT1	LT2
1	1.286	0.142	6	1.210	0.111	11	1.247	0.118	16	1.623	0.336	21	1.535	0.265
2	1.247	0.129	7	1.286	0.139	12	1.210	0.108	17	1.578	0.294	22	1.623	0.367
3	1.210	0.122	8	1.247	0.129	13	1.623	0.316	18	1.535	0.248	23	1.578	0.323
4	1.286	0.137	9	1.210	0.110	14	1.578	0.287	19	1.623	0.351	24	1.535	0.291
5	1.247	0.121	10	1.286	0.132	15	1.535	0.243	20	1.578	0.328			

E-series														
Mix no.	LT1	LT2	Mix no.	LT1	LT2	Mix no.	LT1	LT2	Mix no.	LT1	LT2	Mix no.	LT1	LT2
1	0.880	0.119	10	0.382	0.121	19	0.208	0.088	28	0.216	0.086	37	0.193	0.059
2	0.880	0.101	11	0.353	0.130	20	0.215	0.093	29	0.209	0.095	38	0.193	0.056
3	1.130	0.218	12	0.378	0.126	21	0.209	0.083	30	0.215	0.095	39	0.193	0.051
4	1.105	0.206	13	0.350	0.121	22	0.219	0.087	31	0.208	0.090	44	0.275	0.080
5	1.130	0.189	14	0.376	0.131	23	0.208	0.077	32	0.215	0.132	45	0.275	0.070
6	1.105	0.169	15	0.859	0.112	24	0.218	0.081	33	0.340	0.108	46	0.275	0.069
7	0.352	0.121	16	0.859	0.087	25	0.209	0.092	34	0.194	0.069	47	0.275	0.058
8	0.385	0.136	17	0.209	0.096	26	0.217	0.090	35	0.324	0.092	48	0.971	0.131
9	0.350	0.113	18	0.215	0.099	27	0.208	0.084	36	0.193	0.066			

F-series									G-series					
Mix no.	LT1	LT2	Mix no.	LT1	LT2	Mix no.	LT1	LT2	Mix no.	LT1	LT2	Mix no.	LT1	LT2
1	1.185	0.223	3	0.358	0.075	5	0.389	0.073	1	1.243	0.163	4	1.230	0.155
2	1.166	0.203	4	0.391	0.079	6	0.382	0.081	2	1.240	0.145	5	1.214	0.147
									3	1.237	0.165			

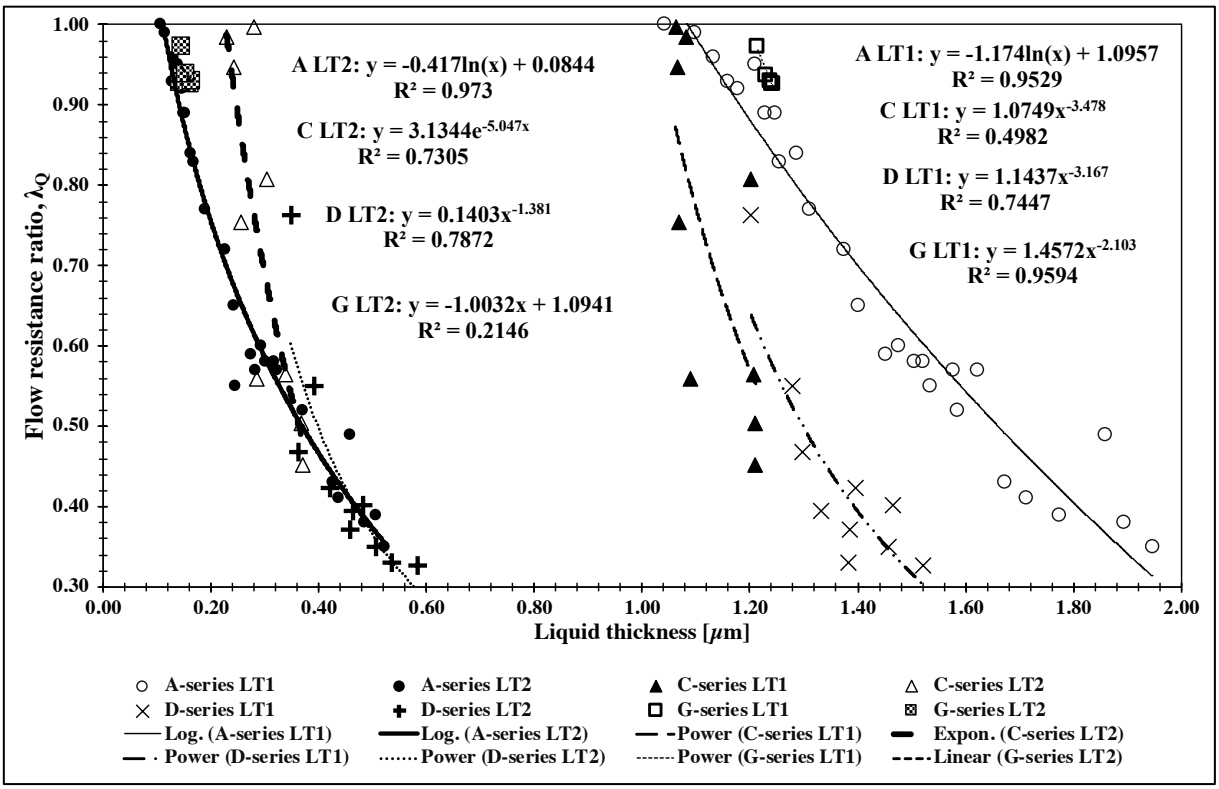

(a)

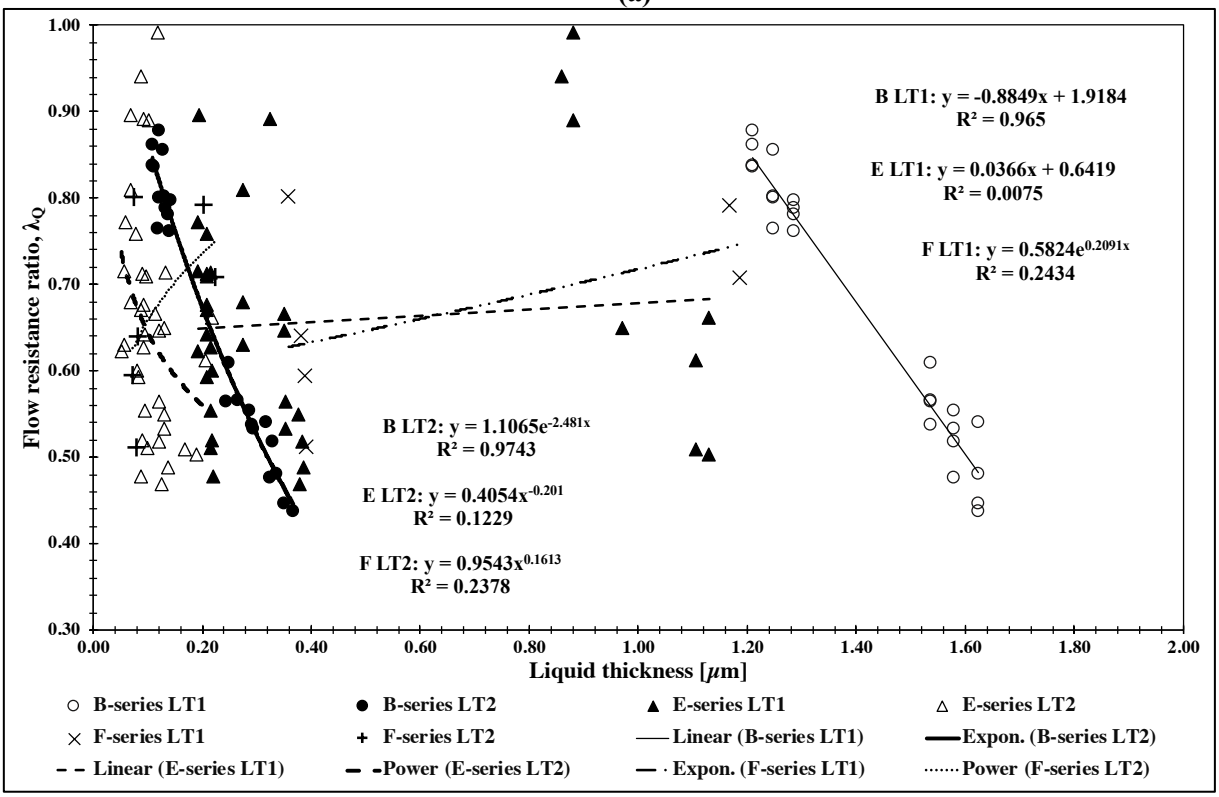

(b)

Figure J 1 The relationships of liquid thicknesses (LT1 and LT2) on flow resistance ratio (λ_Q) from (a) the A-, C-, D- and G-series, and (b) the B-, E- and F-series

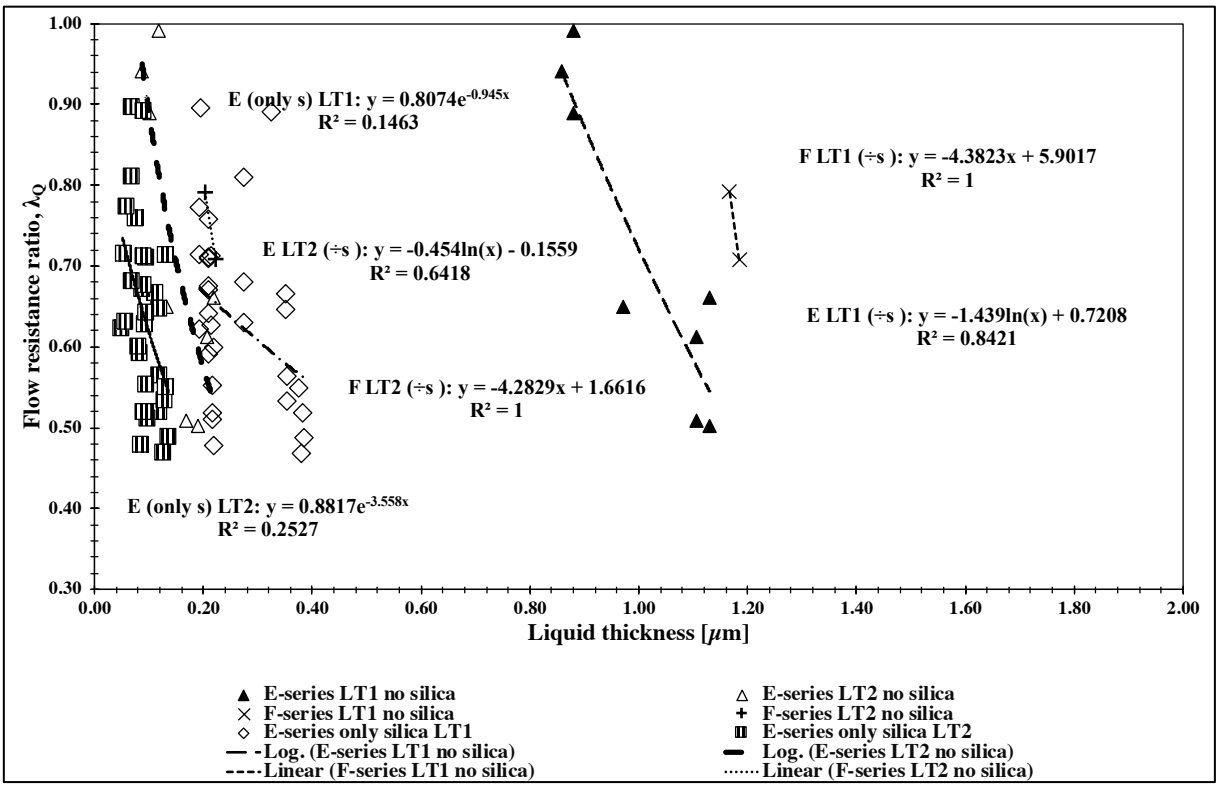

Figure J 2 The relationships of liquid thicknesses (LT1 and LT2) on flow resistance ratio (λ_Q) from the E- and F-series, with and without silica fume

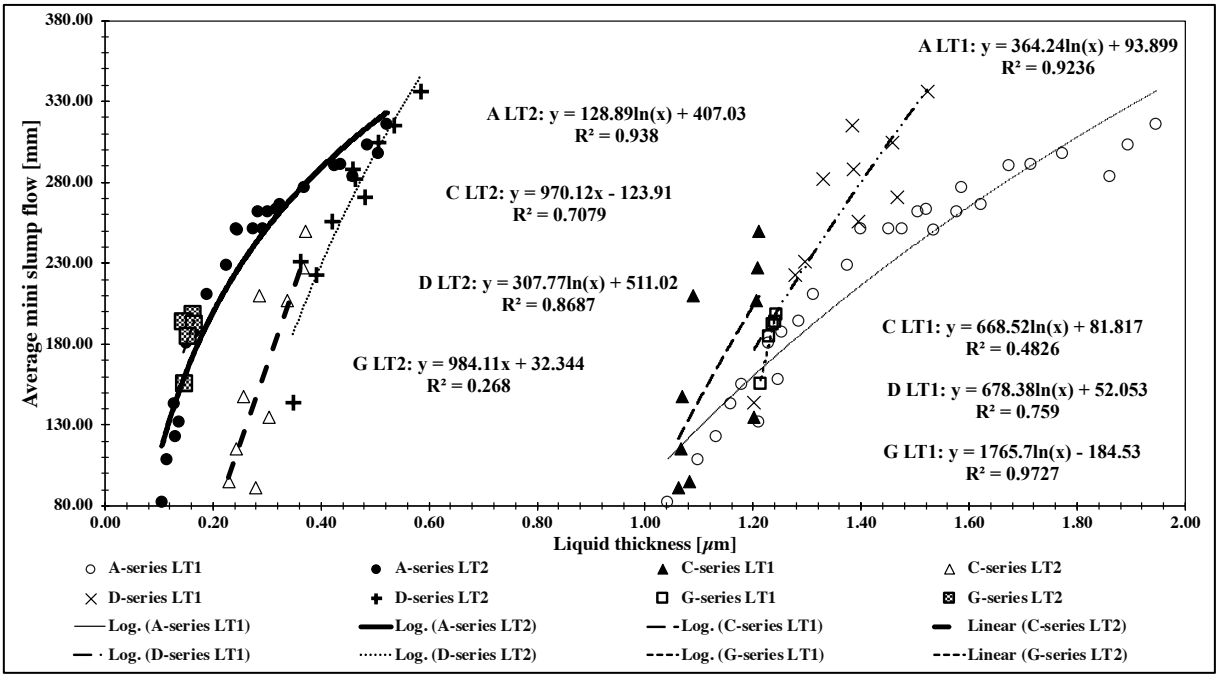

(a)

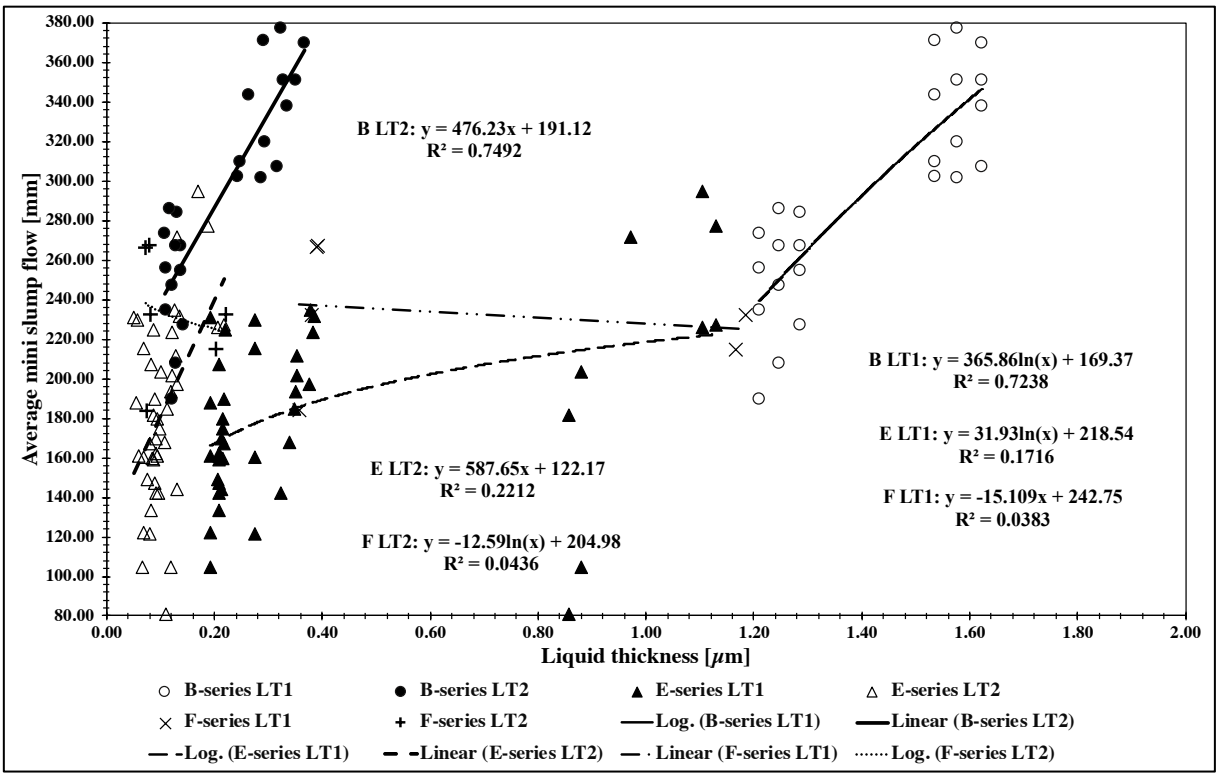

(b)

Figure J 3 The relationships of liquid thicknesses (LT1 and LT2) on average mini slump flow from (a) the A-, C-, D- and G-series, and (b) the B-, E- and F-series

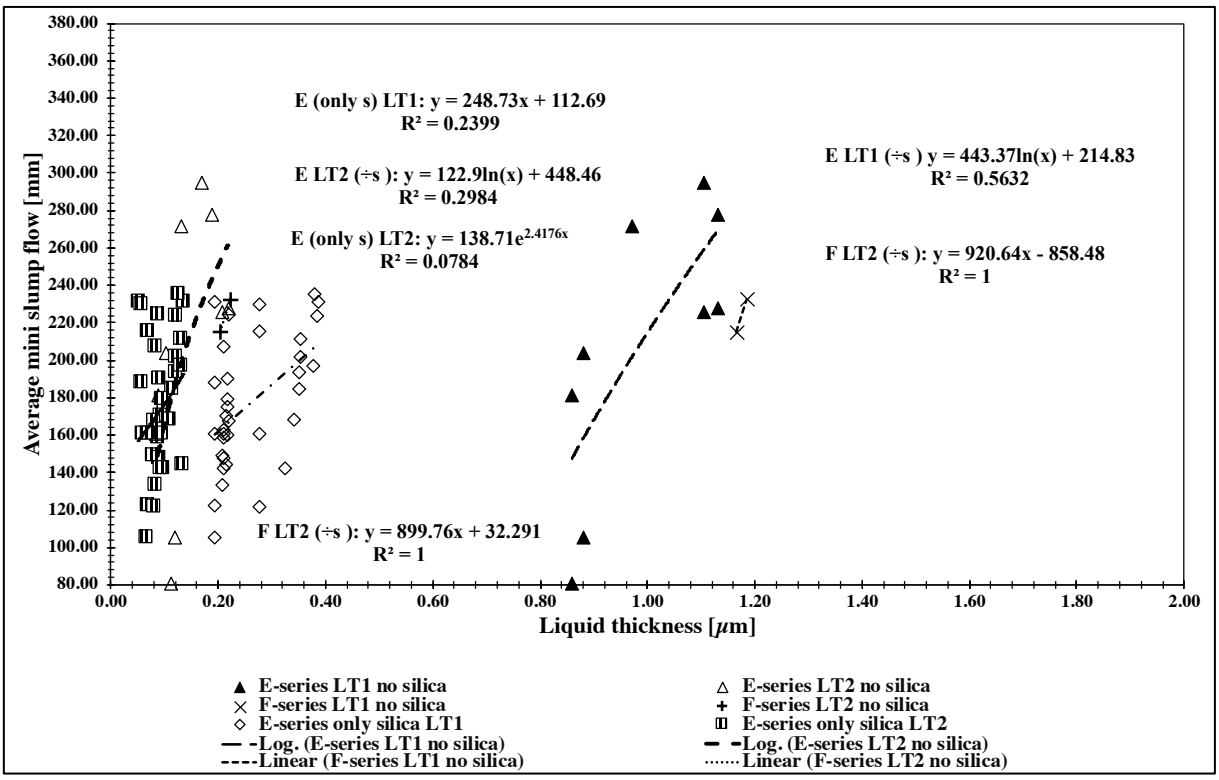

Figure J 4 The relationships of liquid thicknesses (LT1 and LT2) on average mini slump flow from the E- and F-series, with and without silica fume

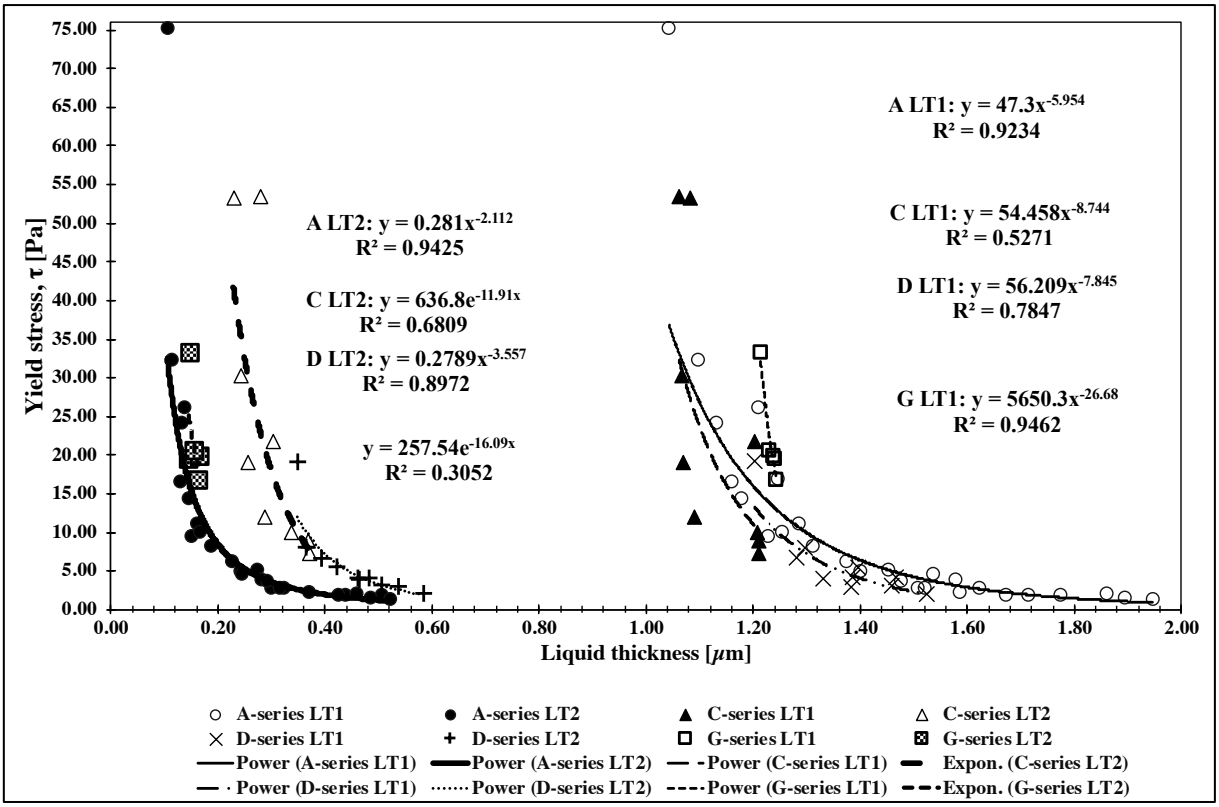

(a)

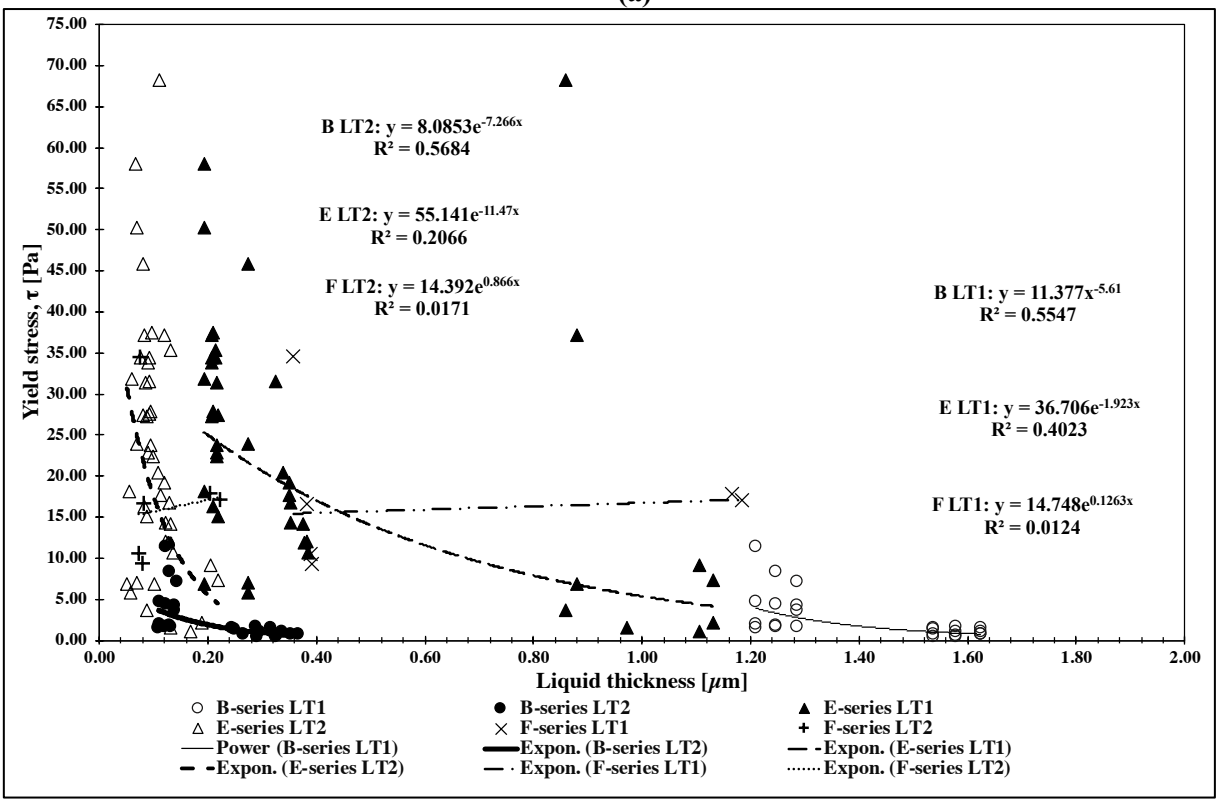

(b)

Figure J 5 The relationships of liquid thicknesses (LT1 and LT2) on yield stress (τ_0) from (a) the A-, C-, D- and G-series, and (b) the B-, E- and F-series

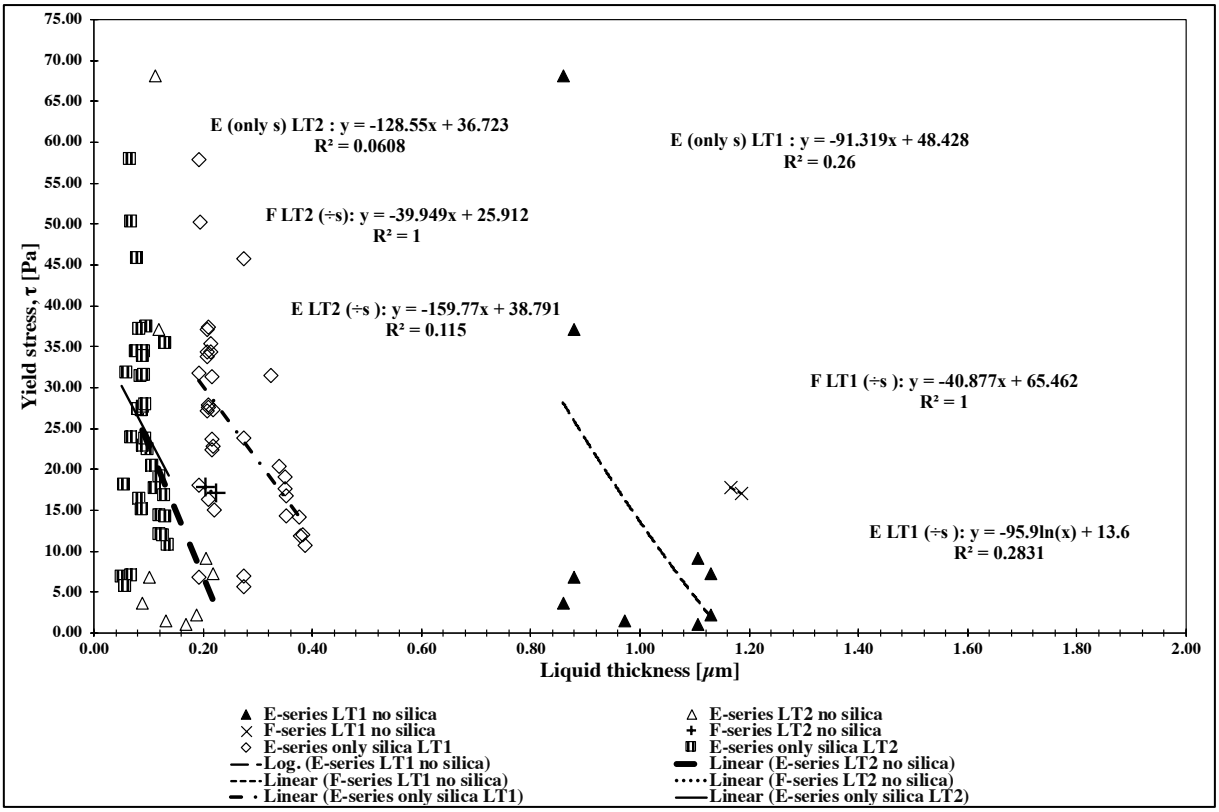

Figure J 6 The relationships of liquid thicknesses (LT1 and LT2) on yield stress (τ_0) from the E- and F-series, with and without silica fume

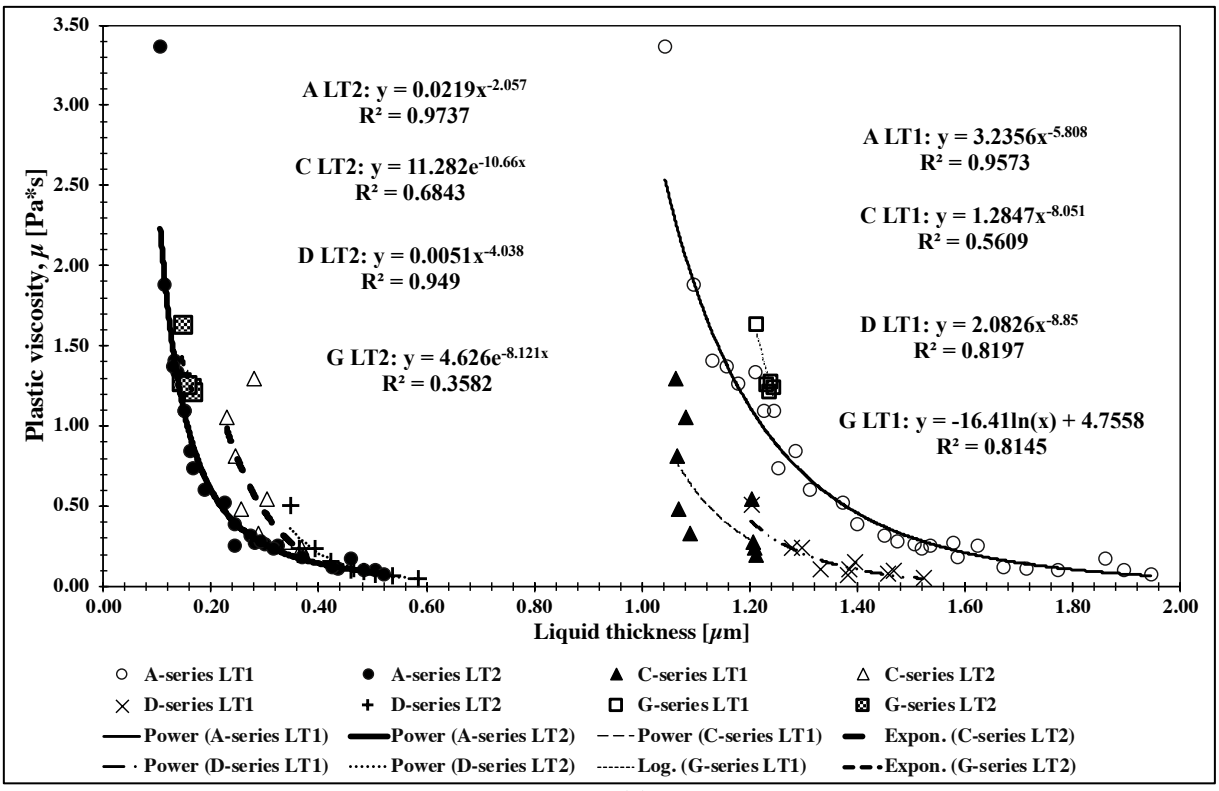

(a)

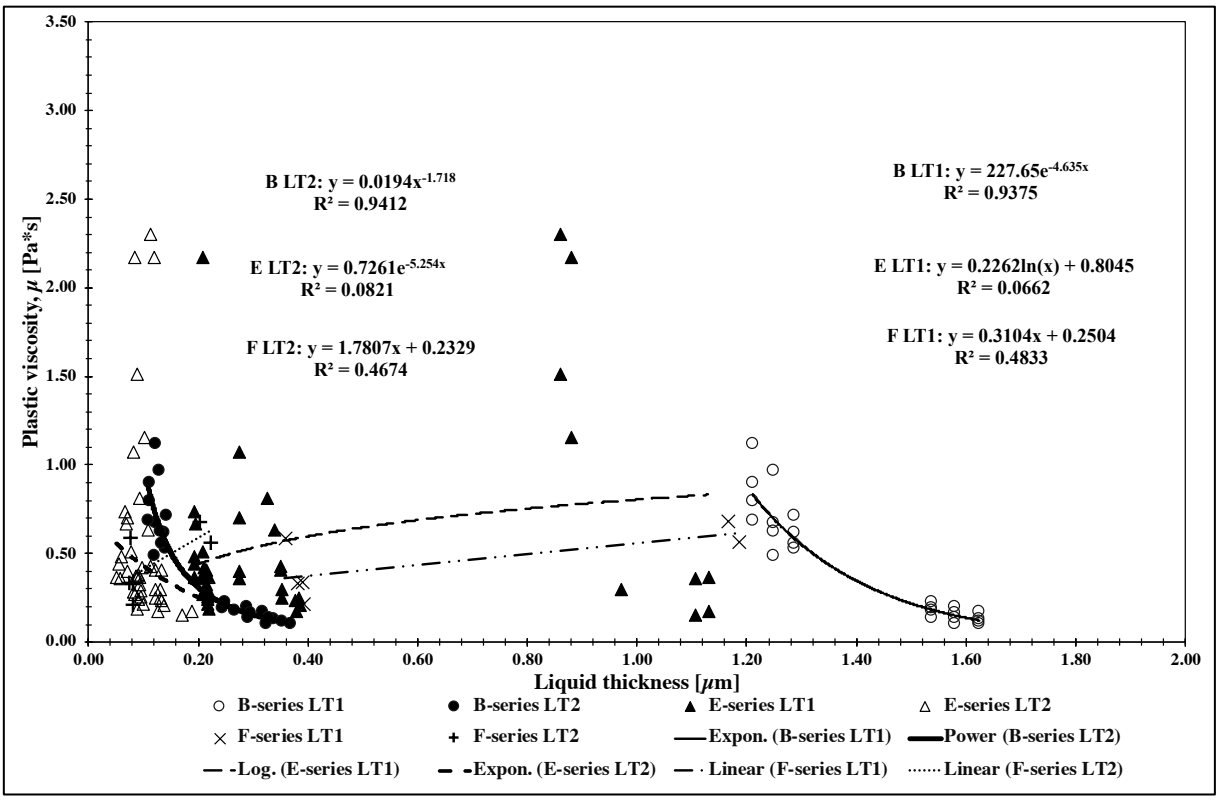

(b)

Figure J 7 The relationships of liquid thicknesses (LT1 and LT2) on plastic viscosity (μ) from (a) the A-, C-, D- and G-series, and (b) the B-, E- and F-series

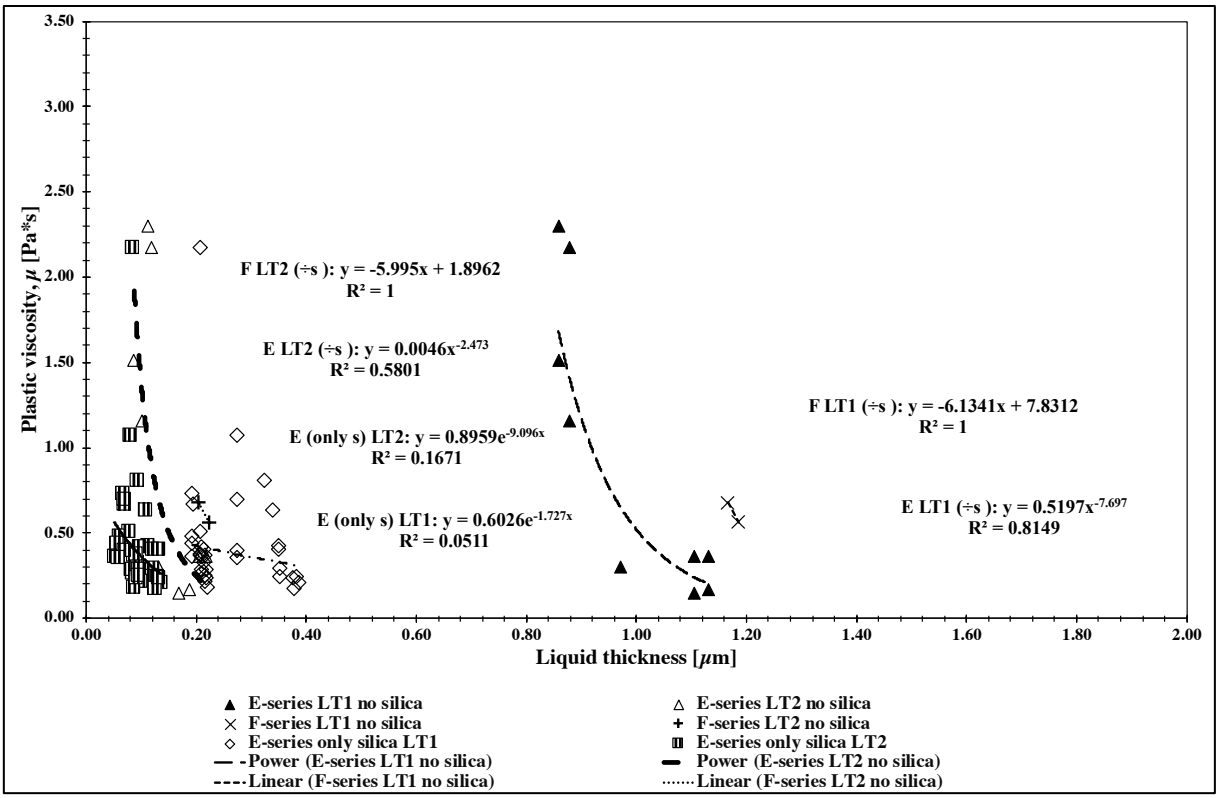

Figure J 8 The relationships of liquid thicknesses (LT1 and LT2) on plastic viscosity (μ) from the E- and F-series, with and without silica fume

Appendix K Mapei, Dynamon SR-N, superplasticizer

See the next pages (3).

MAPEI

Dynamon SR-N

Superplastiserende tilsetningsstoff

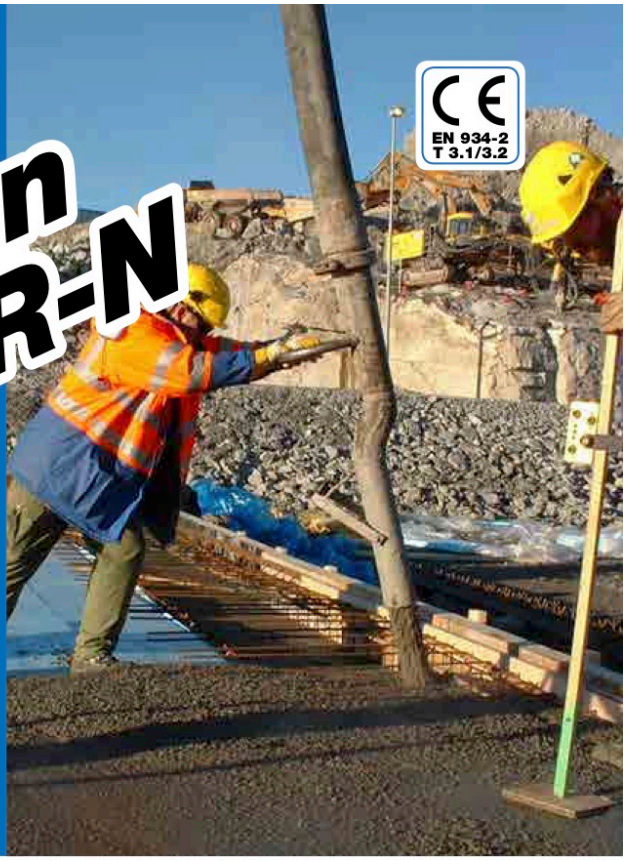

PRODUCT DESCRIPTION
Dynamon SR-N is a high performance superplasticizing admixture based on modified acrylic polymers.
The product is part of the **Dynamon System**, based on the Mapei developed DPP technology (DPP = Designed Performance Polymers) where the properties of the admixture are tailored according to the specific performances required of the concrete.
The **Dynamon System** is developed on the basis of Mapei's own design and production of monomers.

AREAS OF APPLICATION
Dynamon SR-N is a superplasticizing admixture used to improve workability and/or reduce the amount of mixing water.
Dynamon SR-N is a **Dynamon** variant where by normal dosage (0.3 - 1.5 %) a longer pot life (less slump loss) can be achieved than with **Dynamon SX** products.
The product is therefore specially suited for ready-mix concrete production, where the time from mixing to placement is relatively long, e.g. due to long transportation times or requirements for a slow rate of climb. **Dynamon SR-N** nevertheless gives high early strength at normal dosages due to its effective dispersion of the cement All **Dynamon** products are significantly different from conventional sulphonated melamine based and sulphonated naphthalene based superplasticizers, and also from first generation acrylic based polymers in terms of their superior water-reduction. Over-dosing can cause concrete separation. We always recommend the use of trial pours using the actual parameters.

The dosage required to achieve a particular workability will be considerably lower for **Dynamon SR-N** than for previous superplasticizers. In contrast to conventional melamine or naphthalene based admixtures, **Dynamon SR-N** produces the maximum effect regardless of when it is added, but the time of addition can influence the mixing time. If at least 80 % of the mixing water is added before **Dynamon SR-N** the required mixing time will generally be shortest.
It is nevertheless important to perform trials using the actual mixing equipment.

TECHNICAL PROPERTIES
Dynamon SR-N is an aqueous solution of active acrylic copolymers which effectively disperse the cement grains.

<u>This effect can, in principle, be used in three ways:</u>
1. To reduce the amount of mixing water, but at the same time maintain the concrete workability. Lower w/c ratio gives increased strength, reduced permeability and improved durability.
2. To increase workability compared to concrete with the same w/c ratio. The strength remains the same but ease of placement is improved.
3. To reduce both the water and the cement without altering the mechanical strength.
   Through this method it is possible to reduce costs (less cement), shrinkage (less water) and also the risk of temperature gradients due to the lower heat of hydration. This last effect is particularly important for concrete containing a high percentage of cement.

Dynamon SR-N

COMPATIBILITY WITH OTHER PRODUCTS
Dynamon SR-N can be combined with other Mapei admixtures, e.g. set accelerating additives such as **Mapefast SA** and set retarding admixtures, such as **Mapetard R**. The product is also compatible with air entraining admixtures for the production of frost resistant concrete, e.g. **Mapeair L** or **Mapeair 25** (the selection of air entraining admixture depends upon the other components e.g. cement type and aggregate).

DOSAGE
To achieve the desired results (strength, durability, workability, cement reduction) add **Dynamon SR-N** in dosages between 0.3 and 1.5 % of the cement weight.
Increased dosages will also increase the open time (the length of time the concrete is workable).

PACKAGING
Dynamon SR-N is available in 25 liter cans, 200 liter drums, 1000 liter IBC tanks and in tank.

STORAGE
The product must be stored at temperatures between +8 and +35°C, and will retain its properties for at least one year if stored unopened in its original packaging. If the product is exposed to direct sunlight, colour variation may occur, but this will not affect the technical properties of the product.

SAFETY INSTRUCTIONS FOR PREPARATION AND INSTALLATION
Instructions for the safe use of our products can be found on the latest version of the SDS available from our website www.mapei.no

PRODUCT FOR PROFESSIONAL USE

WARNING
Although the technical details and recommendations contained in this product data sheet correspond to the best of our knowledge and experience, all the above - information must, in every case, be taken as merely indicative and subject to confirmation after long-term practical application: for this reason, anyone who intends to use the product must ensure beforehand that it is suitable for the envisaged application: in every case, the user alone is fully responsible for any consequences deriving from the use of the product.

Please refer to the current version of the technical data sheet, available from our web site www.mapei.no

LEGAL NOTICE
The contents of this Technical Data Sheet ("TDS") may be copied into another project-related document, but the resulting document shall not supplement or replace requirements per the TDS in force at the time of the MAPEI product installation.
The most up-to-date TDS can be downloaded from our website www.mapei.no
ANY ALTERATION TO THE WORDING OR REQUIREMENTS CONTAINED OR DERIVED FROM THIS TDS EXCLUDES THE RESPONSIBILITY OF MAPEI.

All relevant references for the product are available upon request and from www.mapei.no

Dynamon SR-N

TECHNICAL DATA (typical values)

PRODUCT IDENTITY	
Appearance:	liquid
Colour:	yellowish brown
Viscosity (Brookfield Viscometer DV-1, LV1, 100rpm at 20±2°C:	low viscosity; < 30 mPa*S
Dry solids content, %:	19.5 ± 1.0
Density, g/cm³:	1.05 ± 0.02
pH:	6.5 ± 1
Chloride content, %:	< 0.05
Alkali content (equiv. Na_2O) %:	< 2.0

CONCRETE PROPERTIES		
As water reducing admixture	Reference	Dynamon SR-N
Quantity of cement kg/m³ (CEM I- 42.5R):	350	350
Admixture dosage (% by weight of cement):	0	1.1
Mass ratio (w/c ratio):	0.50	0.41
Compressive strength (N/mm²):		
- 1 day	26	37
- 7 days	43	56
- 28 days	52	66
As superplasticising admixture	Reference	Dynamon SR-N
Quantity of cement kg/m³ (CEM I- 42.5R):	350	350
Admixture dosage (in % of cement weight):	0	1.1
Mass ratio (w/c ratio):	0.49	0.49
Air content:	2.4	1.9
Workability, mm:		
- slump, 5 min	40	200
- slump, 30 min	30	200
- slump, 60 min	20	210
- slump, 90 min	20	180
- slump flow, 5 min	200	430
- slump flow, 30 min	200	340
- slump flow, 60 min	200	330
- slump flow, 90 min	200	320

6917-07-2017(GB)

MAPEI®

BUILDING THE FUTURE

Appendix L Opaque and transparent characteristics of excess fluid

All the details of characteristics of all the series can be found as an online appendix uploaded as an Excel file “Opaque and transparent characteristics of EF.xlsx” on:

https://www.dropbox.com/s/d4vxeb2rx1oh1af/Opaque%20and%20transparent%20characteristics%20of%20EF.xlsx?dl=0

All the pictures/raw data of each of the mixes can be found in Appendix F.

All the online Appendixes are uploaded in the folder “TKT4925 Concrete Technology Master’s thesis Appendices – Metathip Sihaklang” on:

https://www.dropbox.com/sh/2b6ybeshelxa0km/AAB0KqYhQlAyVkCcG64TCbCva?dl=0

Table L 1 Overview of the characteristics of mixes from B-, E- and F-series, with an overview of SP-dosage and pozzolans content for each mix.

Characteristics of EF										
Mix no.	**B-series**	**Mix no.**	**B-series**	**Mix no.**	**B-series**	**Mix no.**	**B-series**	**Mix no.**	**B-series**	
1	O	**6**	O	**11**	O	**16**	O	**21**	O	
2	O	**7**	O	**12**	O	**17**	O	**22**	O	
3	O	**8**	O	**13**	O	**18**	O	**23**	O	
4	O	**9**	O	**14**	O	**19**	O	**24**	O	
5	O	**10**	O	**15**	O	**20**	O			
Mix no.	**E-series**	**Mix no.**	**E-series**	**Mix no.**	**E-series**	**Mix no.**	**E-series**	**Mix no.**	**E-series**	
1	T	**10**	O	**19**	O*	**28**	O	**37**	O	
2	O	**11**	O	**20**	O	**29**	O	**38**	O*	
3	O	**12**	O	**21**	O*	**30**	O	**39**	O	
4	T	**13**	O	**22**	O	**31**	O	**44**	O	
5	O	**14**	O	**23**	O	**32**	O	**45**	O	
6	O*	**15**	O	**24**	O	**33**	O	**46**	O	
7	O*	**16**	O	**25**	O	**34**	O	**47**	O	
8	O	**17**	O	**26**	O	**35**	T	**48**	O	
9	O*	**18**	O*	**27**	O	**36**	O*			
Mix no.	**F-series**	**Mix no.**	**F-series**		**Color code**					
1	O*	**4**	O			SP≥1		Fly ash + Silica		
2	O*	**5**	O			Silica		Silica +SP≥1		
3	O	**6**	O			Fly ash		SP≥1+Fly ash+Silica		
						Fly ash +SP≥1				
O=Opaque				**T=Transparent**			**O*=Almost transparent**			

Appendix M Repeatability of A6, B22, E39 and E47

The full calculations of the repeatability and differences of the maximum packing (ϕ_{max}), the kinematic viscosity and the dynamic viscosity can be found as an online appendix uploaded on: **https://www.dropbox.com/s/lja4z4pzeskqtih/Repeatability%20of%20A6%20B22%20E39%20E47.xlsx?dl=0**

All the online Appendixes are uploaded in the folder "TKT4925 Concrete Technology Master's thesis Appendices – Metathip Sihaklang" on: **https://www.dropbox.com/sh/2b6ybeshelxa0km/AAB0KqYhQlAyVkCcG64TCbCva?dl=0**

Table M 1 The repeatability and differences in maximum packing, kinematic viscosity and dynamic viscosity of A6, B22, E39 and E47

Series	Mix no.	ϕ_{max}	Kinematic Viscosity (v) (m2/s)	Dynamic viscosity (μ) (mPa.s)	The difference in ϕ_{max}	The difference in Kinematic viscosity (%)	The difference in dynamic viscosity (%)
B	**22***	0.543	1.406E-06	1.428E+00	0.005	3.4%	3.8%
B test	**22***	0.538	1.454E-06	1.482E+00			
E	**39**	0.560	1.310E-06	1.333E+00	0.002	5.5%	5.7%
E test	**39**	0.558	1.382E-06	1.408E+00			
E	**47**	0.553	1.302E-06	1.340E+00	0.002	6.8%	5.7%
E test	**47**	0.554	1.390E-06	1.416E+00			
A	**6**	0.551	1.219E-06	1.230E+00	0.003	3.6%	3.4%
A test	**6**	0.548	1.175E-06	1.188E+00			

*The paste of B22 was not well packed after centrifugation

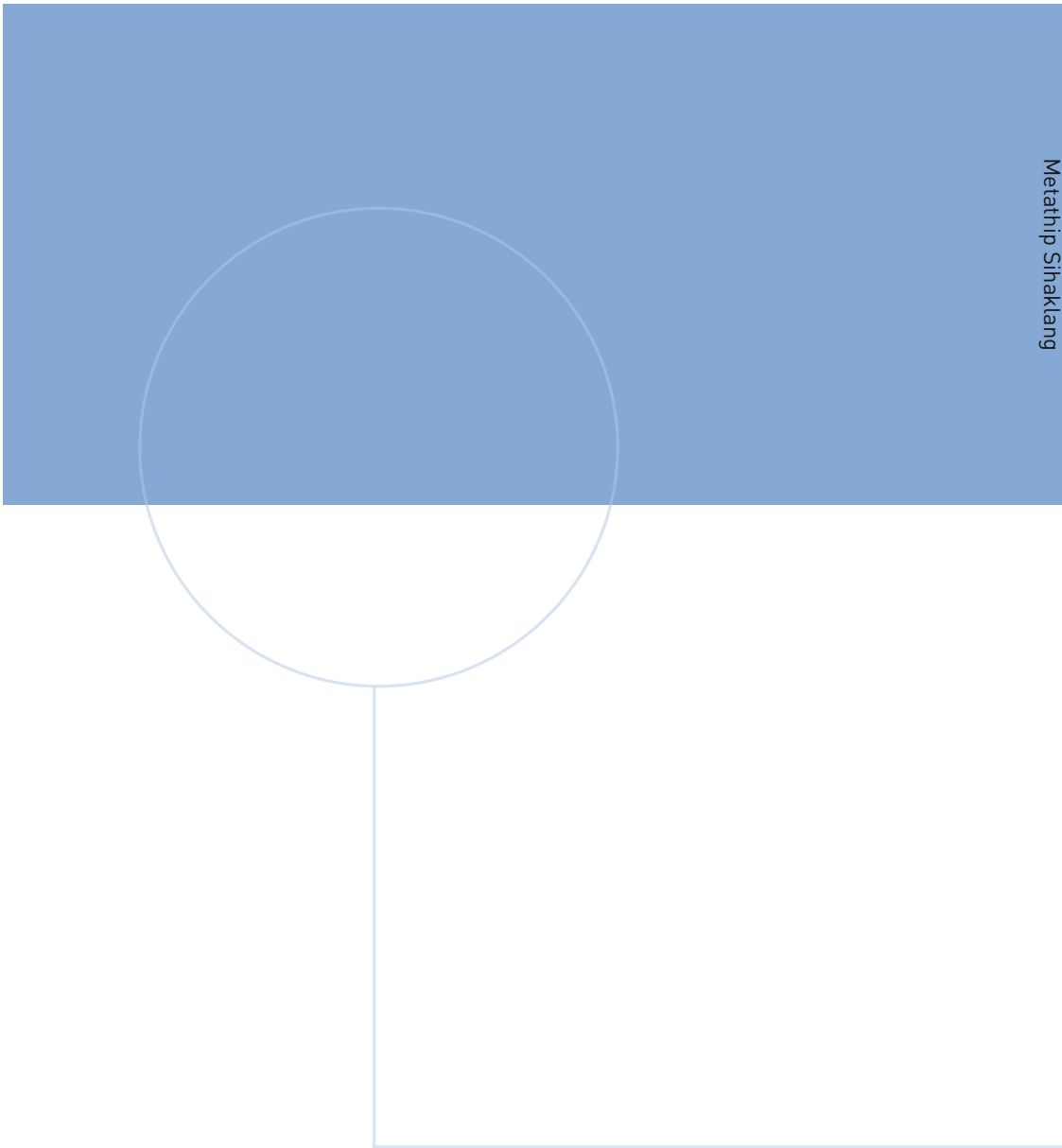

Metathip Sihaklang

NTNU
Norwegian University of
Science and Technology